CHARGED PARTICLE ENERGY TRANSFER FOR PARALLEL AND CONCENTRIC CYLINDRICAL NANOTUBES

by

Antonios Balassis

A dissertation submitted to the Graduate Faculty in Physics in partial fulfillment of the requirements for the degree of Doctor of Philosophy, The City University of New York

2006

UMI Number: 3232039

ProQuest Information and Learning Company
300 North Zeeb Road
P.O. Box 1346
Ann Arbor, MI 48106-1346

This manuscript has been read and accepted for the Graduate Faculty in Physics in satisfaction of the dissertation requirement for the degree of Doctor of Philosophy.

	G. Gumbs
Date	Chair of Examining Committee
	S. Catto
Date	Executive Officer
	L. Cohen
	L. Massa
	L. Deych
	V. Fessatidis
	Supervisory Committee

THE CITY UNIVERSITY OF NEW YORK

Abstract

CHARGED PARTICLE ENERGY TRANSFER FOR PARALLEL AND CONCENTRIC CYLINDRICAL NANOTUBES

by

Antonios Balassis

Adviser: Distinguished Professor Godfrey Gumbs

This dissertation is mainly concerned with three topics : (1) the separation of the particle-hole and plasmon excitation contributions to the energy transfer when a moving charged particle interacts with a cylindrical nanotube; (2) the demonstration of a plasmon instability for a multi-wall nanotube or a pair of parallel nanotubes; and (3) the image potential for multi-wall nanotubes. We consider nanotubes embedded in a dielectric material. The electrons on a single cylindrical nanotube form a free electron gas confined to the surface of an infinitely long cylinder. We employ self-consistent field theory given in terms of Laplace's equation along with the linear response formalism to calculate the collective plasma excitations on a single-wall nanotube. We obtain their frequency-dependence on the linear wave vector along the axis of the nanotube. The plasma dispersion relation is calculated for intrasubband and intersubband transitions, where each subband is labeled by an angular momentum quantum number. We generalize our formalism to coaxial and parallel tubules. In addition we determine the way in which the collective modes are affected by the electrostatic interaction between the tubules. Making use of these results, we calculate the rate of transfer

of energy between the plasma modes and charged particle moving parallel to the axis of the tubule. The frictional force due to the electrostatic interaction of the charged particle with the electrons on the surface of the nanotube is calculated using the inverse dielectric function. The energy loss of the charged particle to single particle and plasmon excitations is calculated. We demonstrate that the plasmon excitations for coaxial and parallel tubules may become unstable and radiate energy. The velocities of the charged particle for which the instabilities occur are identified by examining the plasmon dispersion relating and matching where the phase velocity of a plasmon excitation equals the velocity of the impinging particle. We calculate the image potential for a single-wall and a double-wall nanotube. This image potential has bound states which depend on the angular momentum quantum number around the axis of the tubule. We examine the way in which these bound states can be influenced when there are two coaxial tubules.

Acknowledgments

A long journey has come to an end successfully. This would not be possible without the help of few people that guided me and supported me to walk on the paths of physics.

I gratefully acknowledge the help offered from my advisor, Professor Godfrey Gumbs. Without his devotion in physics, his patient guidance and the many discussions that we had, my research would not have been completed. He believed that I could finish successfully this dissertation and he helped me to overcome many of the obstacles that I encountered in my studies with his enlightening advise.

The supervisory committee with their questions helped me immensely to improve and clarify many points of my dissertation. Professor Sultan Catto offered me his help and encouragement whenever I needed it, I really thank him for his kindness.

I would like to thank the Physics Department at Hunter College for their hospitality and for providing me with resources and funding while I was a graduate student. I would also like to express my sincerest thanks to the State Scholarship Foundation of Greece (I.K.Y) for the important financial support that offered me.

I am deeply indebted to my wife, Maria, and my two children, Katerina and Niko. They supported me emotionally and my thoughts were always with them

during the many periods of our separation. They embraced me with patience and love which were key in helping me to finish this project. This dissertation is dedicated to them.

My mother instilled in me the value of a good education. I took her advise and i make it this far. The role she played in my life will always be remembered and cherished.

Contents

List of Figures

Chapter 1

INTRODUCTION AND BACKGROUND

Carbon nanotubes were discovered in 1991 by the Japanese Sumio Iijima of NEC [1]. Soon after their discovery they attracted the interest of physicists, chemists and engineers because of their exceptional electrical and mechanical properties. The field is growing very fast and looks very promising. We can think of them as a normal graphene sheet (a honeycomb lattice) rolled up in a cylinder. The radius of the cylinder is a few nanometers and the length is of the order of micrometers. Because of the different ways that the graphene sheet can be rolled to a cylinder (chirality), carbon nanotubes can have different electronic structures and they can be metallic, semiconducting or insulators [2]. In the semiconducting nanotubes the energy gap depends on their radius. It is well known that carbon nanotubes can be modeled as quasi-1D systems. Their dielectric functions depend on the longitudinal wave number, the frequency and angular momentum of the elementary excitations. They also depend on geometrical factors such as their radius and the chiral angle. In a first approximation we can study the plasma excitations on a nanotube if we use a simple model that describes its electronic

properties. We assume that the electrons lying on a single cylindrical nanotube consist a free electron gas which is distributed uniformly to the surface of an infinitely long cylinder (since the length of the nanotube is much more larger than its radius). At $T = 0$ K such an electron gas is completely described by its surface density and the radius of the tubule.

According to Landau Fermi liquid theory [3] such an interacting system of fermions can be described in terms of almost free quasiparticles or elementary excitations. These quasiparticles behave like particles that carry energy $\epsilon = \hbar\omega$ and momentum $\mathbf{p} = \hbar\mathbf{q}$. Their energy is connected to their momentum through a dispersion relation $\omega = \omega(\mathbf{q})$. They are well defined and they can be safely used to describe the interacting system as long as they have a lifetime (quasiparticles can interact with each other and with impurities) which is shorter than the electron-electron scattering relaxation time but large enough so that they have a well defined energy and momentum. This is the case of the low temperature limit where there are only few such excitations. For the non-interacting electron gas the only possible elementary excitations are particles and holes. When though the electron-electron interaction is taken into account a new kind of elementary excitation appears which is called plasmon. The name comes from the fact that plasmon represents the quantum of collective charge oscillations. It has large lifetime when it carries small momentum $\hbar\mathbf{q}$ (or equivalently when it has long wavelength) and at metallic densities its energy (for low momentum) is few eV. The dispersion relation of plasmons depends on the dimensionality of the considered system.

We will use the semiclassical approximation to treat the electron gas in externally applied fields when we calculate plasmon dispersions. This means that we will use a classical approximation for externally applied potentials $U(\mathbf{r}, t)$ and a quantum mechanical (second quantization) approach for the electron gas on

the nanotubes. The semiclassical approximation is valid when the externally applied field is weak and its frequency is low. In this case linear response theory is applicable. Within the random phase approximation (RPA), first introduced by Bohm and Pines [4], the total field experienced by the electrons is approximated by the sum of the external and the induced potential. This is equivalent to use the Hartree approximation in determining the response of the electron gas to lowest order in the externally applied potential. In our calculations we use the dielectric formalism, introduced by Martin and Schwinger [5], employing the inverse dielectric function to incorporate the effects of the external field and of the electron-electron interaction.

We consider that the electron gas is immersed in a uniform positive background (jellium model). The electrons are interacting through a spin and time independent Coulomb potential which we denote by $V(\mathbf{r}_1 - \mathbf{r}_2)$. In the presence of an external time-dependent potential $U(\mathbf{r}_1, t_1)$ the electron system is described by the Hamiltonian

$$\begin{aligned} \hat{H}(\mathbf{r}_1, t_1) &= \hat{H}_{\rm eb} + \int d\mathbf{r}_1 \hat{\psi}^\dagger(\mathbf{r}_1) \left(-\frac{\hbar^2}{2m} \nabla^2 \right) \hat{\psi}(\mathbf{r}_1) \\ &+ \frac{1}{2} \int d\mathbf{r}_1 \int d\mathbf{r}_2 \hat{\psi}^\dagger(\mathbf{r}_1) \hat{\psi}^\dagger(\mathbf{r}_2) V(\mathbf{r}_1 - \mathbf{r}_2) \hat{\psi}(\mathbf{r}_2) \hat{\psi}(\mathbf{r}_1) \\ &+ \int d\mathbf{r}_1 \hat{\psi}^\dagger(\mathbf{r}_1) U(\mathbf{r}_1, t_1) \hat{\psi}(\mathbf{r}_1) \ , \end{aligned} \tag{1.1}$$

where $\hat{H}_{\rm eb}$ is the interaction energy of the electron with the positive background, $\hat{\psi}$ and $\hat{\psi}^\dagger$ are the field operators. The background potential is a one particle-operator and can be considered as a time-independent potential added to the external potential $U(\mathbf{r}_1, t_1)$ to give the external potential $U'(\mathbf{r}_1, t_1) = \hat{H}_{\rm eb} + U(\mathbf{r}_1, t_1)$. For the uniform electron gas that we study $\hat{H}_{\rm eb}$ is a c number. The effect of the externally applied field $U(\mathbf{r}_1, t_1)$ is to change the initially uniform electron density, i.e., the material becomes polarized. There is a density perturbation (or induced charge density) and an induced potential associated to this polarization. For

the description of our system we use the single particle thermal Green's function G(1,2). It satisfies the equation of motion

$$\left[i\hbar\frac{\partial}{\partial t_1}+\frac{\hbar^2\nabla_1^2}{2m}-U'(1)\right]G(1,2)=\delta(1,2)-i\int d3v(1,3)G_2(1,3;2,3^+)\ . \quad (1.2)$$

In this notation $v(1,3)=V(\mathbf{r}_1-\mathbf{r}_3)\delta(t_1-t_3)$ is the Coulomb potential due to the electron-electron interaction, and G_2 is the two particle Green's function for the interacting system which describes the response of the electron gas to processes involving two particles. We note from the last equation that $G(1,2)$ can be considered as a functional of the external field $U(1)$ (since $\hat{H}_{\rm eb}$ is a c number). In the case that there is no interaction between the electrons, i.e.,when $v(1,3)=0$, the solution is the non-interacting electron Green's function which is denoted by $G_0(1,2)$. Integrating Eq. (1.2) we find that the integral equation which should be solved to find the Green's function is

$$G(1,2)=G_0(1,2)+i\int d3\int d4G_0(1,4)v(4,3)G_2(4,3;2,3^+)\ . \quad (1.3)$$

In the Hartree-Fock approximation we neglect the two particle correlations and G_2 can be written as

$$G_2(4,3;2,3^+)=G(4,2)G(3,3^+)-G(4,3)G(3,2)\ . \quad (1.4)$$

Equation (1.3) then becomes

$$G(1,2)=G_0(1,2)+i\int d3\int d4G_0(1,4)v(4,3)\left[G(4,2)G(3,3^+)-G(4,3)G(3,2)\right]\ , \quad (1.5)$$

and is diagrammatically given in Fig. (1.1) using Feynman diagrams. The first term in the square brackets of the right side of Eq. (1.5) is the Hartree or direct term which describes the interaction of an electron with the mean local potential created by the average electron density $n(3)=-iG(3,3^+)$. The second term in the same bracket is the exchange or Fock term and describes the correction

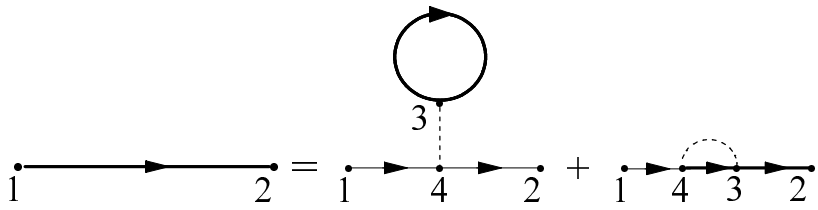

Figure 1.1: The Feynman diagrams for the Hartree-Fock approximation to the interacting electron propagator (thick arrow). A thin arrow represents the non-interacting propagator while a dotted line represents the Coulomb interaction between the electrons. The closed loop represents the average electron density.

to the Hartree term because of a nonlocal potential that originates from the indistinguishability of the electrons. In addition this term cancels the interaction of a particle with itself. We have to note that in the Hartree-Fock approximation one does not have to assume that the interaction is weak like in the case of perturbation theory. Equation (1.5) is a self-consistent integral equation. To find the first order approximation in the interaction potential $v(4,3)$ (perturbation expansion) we have to replace the term in the square brackets of the right hand side by

$$G_2(4,3;2,3^+) = G_0(4,2)G_0(3,3^+) - G_0(4,3)G_0(3,2) \ . \tag{1.6}$$

We know that the Hartee approximation gives satisfactory results for long-range potentials (like the Coulomb potential that we use) because in this case the effect of the exchange term is less important (see for example [6]). Using only the Hartree term of Eq. (1.6) into Eq. (1.2) we obtain the equation of motion of the single particle Green's function in the Hartree approximation

$$\left[i\hbar\frac{\partial}{\partial t_1} + \frac{\hbar^2\nabla_1^2}{2m^*} - V(1) \right] G(1,2) = \delta(1-2) \ . \tag{1.7}$$

The effective potential $V(1)$ (total potential due to the external and the induced

potential) in this approximation is

$$V(1) = U'(1) - i \int d3v(1,3)G(3,3^+) \ , \tag{1.8}$$

or

$$V(1) = U(1) + \hat{H}_{\rm eb} + \int d3v(1,3)n(3) \ . \tag{1.9}$$

The electron-background interaction potential has the form

$$\hat{H}_{\rm eb} = - \int d3v(1,3)n_0(3) \ , \tag{1.10}$$

where $n_0(3)$ is the positive background density which is equal to the equilibrium density of the electron gas. Therefore Eq. (1.10) becomes

$$V(1) = U(1) + \int d3v(1,3)\rho(3) \ , \tag{1.11}$$

where $\rho(3) = n(3) - n_0(3)$ is the perturbation of the electrons density. The second term of the right side of Eq. (1.11) describes an induced shielding potential

$$V_{\rm ind}(1) = \int d3v(1,3)\rho(3) \ , \tag{1.12}$$

created by the external potential U in the case of an interacting electron gas. This term is zero when $U(1) = 0$, since in this case we have a uniform electron gas, i.e., $n(3) = n_0(3)$. The most general linear relation in between the external potential and the total potential can be expressed as [5]

$$V(1) = \int d2\, \varepsilon^{-1}(1,2)U(2) \ , \tag{1.13}$$

where $\varepsilon^{-1}(1,2)$ is the inverse dielectric function of the electron gas. This equation can also be used to define the inverse dielectric function as

$$\varepsilon^{-1}(1,2) \equiv \frac{\delta V(1)}{\delta U(2)} \ . \tag{1.14}$$

Using Eq. (1.11) in Eq. (1.14) we find that the inverse dielectric function is given by the integral equation

$$\varepsilon^{-1}(1,2) = \delta(1-2) + \int d3\, v(1,3)\frac{\delta\rho(3)}{\delta U(2)} \ , \tag{1.15}$$

or using the chain rule for functional derivatives

$$\varepsilon^{-1}(1,2) = \delta(1-2) + \int d3 \int d4\, v(1,3)\chi(3,4)\varepsilon^{-1}(4,2) \ , \tag{1.16}$$

where

$$\chi(3,4) \equiv \frac{\delta\rho(3)}{\delta V(4)} = \frac{\delta n(3)}{\delta V(4)} = -i\frac{\delta G(3,3^+)}{\delta V(4)} \ , \tag{1.17}$$

is the density perturbation response function (or polarization function). It describes the response of the electron gas to the effective potential. To a first approximation we can use in place of $G(3,3^+)$ the non-interacting single particle Green's function $G_0(3,3^+)$ and use for the functional derivative $\delta G_0(3,3^+)/\delta V(4)$ the result (see for example [7])

$$\frac{\delta G_0(3,3^+)}{\delta V(4)} = G_0(3,4)G_0(4,3^+) \ . \tag{1.18}$$

Equation (1.16) then becomes

$$\varepsilon^{-1}(1,2) = \delta(1-2) + \int d3 \int d4\, v(1,3)\chi_0(3,4)\varepsilon^{-1}(4,2) \ , \tag{1.19}$$

where

$$\chi_0(3,4) = -iG_0(3,4)G_0(4,3^+) \ , \tag{1.20}$$

is the polarization function of the non-interacting electron gas. Equation (1.19) is the RPA equation for the inverse dielectric function. It is a result obtained by linearize the Hartree approximation in the external field U. Using the analytic expressions of the thermal Green's functions we find that

$$\begin{aligned} \chi_0(3,4) &= -2i\theta(t_3-t_4)\sum_{\nu,\nu'}[f_0(\epsilon_{\nu'}) - f_0(\epsilon_\nu)] \\ &\times \ \psi_\nu(\mathbf{r}_3)\psi^*_{\nu'}(\mathbf{r}_3)\psi^*_\nu(\mathbf{r}_4)\psi_{\nu'}(\mathbf{r}_4)e^{-i(\epsilon_\nu-\epsilon_{\nu'})(t_3-t_4)} \ , \end{aligned} \tag{1.21}$$

where $\theta(t_3-t_4)$ is the Heaviside step function and $\psi_\nu(\mathbf{r}_j)$ are single particle eigenfunctions of the non-interacting electron gas.

The electron density perturbation $\rho(1)$ can be found in this approximation as

$$\rho(1) = \int d2 \frac{\delta\rho(1)}{\delta V(2)} V(2) = -i\int d2 \frac{\delta G_0(1,1^+)}{\delta V(2)} V(2) \ , \tag{1.22}$$

or using Eqs. (1.18) and (1.20)

$$\rho(1) = \int d2\chi_0(1,2)V(2) \ . \tag{1.23}$$

The direct dielectric function ε can be defined as

$$\varepsilon(1,2) \equiv \frac{\delta U(1)}{\delta V(2)} \ , \tag{1.24}$$

and is related to the inverse dielectric function through the equation

$$\int d3\, \varepsilon(1,3)\varepsilon^{-1}(3,2) = \delta(1-2) \ . \tag{1.25}$$

Using Eq. (1.19) along with Eq. (1.25) we find that in the RPA the dielectric function is given by

$$\varepsilon(1,2) = \delta(1-2) - \int d3v(1,3)\chi_0(3,2) \ . \tag{1.26}$$

The polarizability $\alpha(1,2)$ of the electron gas can be defined through the equation

$$\varepsilon(1,2) = \delta(1-2) + 4\pi\alpha(1,2) \ , \tag{1.27}$$

so that

$$4\pi\alpha(1,2) = -\int d3v(1,3)\chi(3,2) \ . \tag{1.28}$$

In the case of a solid-state plasma the electrons move about in a solid ionic background. We can take into account the effect of the lattice on the electron gas by using the effective mass m^* of the electron (instead of the free electron mass) and the dielectric constant ε_b of the lattice. The ionic background reduces both the external potential $U(1)$ and the Coulomb potential $v(1,2)$ by the lattice dielectric constant ε_b. Therefore Eq. (1.11) becomes

$$V(1) = \frac{1}{\varepsilon_b}\left[U(1) + \int d3v(1,3)\rho(3)\right] \ , \tag{1.29}$$

and the RPA inverse and direct dielectric functions are given respectively by

$$\varepsilon^{-1}(1,2) = \frac{1}{\varepsilon_b}\left[\delta(1-2) + \int d3 \int d4\, v(1,3)\chi_0(3,4)\varepsilon^{-1}(4,2)\right] \ , \tag{1.30}$$

$$\varepsilon(1,2) = \varepsilon_b\left[\delta(1-2) - \frac{1}{\varepsilon_b}\int d3v(1,3)\chi_0(3,2)\right] \ . \tag{1.31}$$

From the last equation we find that if we express the background dielectric constant as $\varepsilon_b = 1 + \alpha_b$, where α_b is the background polarizability we have

$$4\pi\alpha(1,2) = \varepsilon(1,2) - \delta(1-2) = \alpha_b\delta(1-2) - \int d3v(1,3)\chi(3,2) \ , \tag{1.32}$$

as an expression for the RPA polarizability of the electron gas.

It is very useful to Fourier transform the above derived equations in the momentum-frequency space. For convenience we consider that the electron gas is translational invariant in time and in all three directions of space. Equation (1.31) then becomes

$$\varepsilon(\mathbf{q},\omega) = \varepsilon_b \left[1 - \frac{1}{\varepsilon_b} v(\mathbf{q})\chi_0(\mathbf{q},\omega)\right] \ . \tag{1.33}$$

From the definition of the dielectric function, Eq. (1.24), we find that

$$U(1) = \int d2\, \varepsilon(1,2)V(2) \ , \tag{1.34}$$

or after taking the Fourier transform

$$U(\mathbf{q},\omega) = V(\mathbf{q},\omega)\varepsilon(\mathbf{q},\omega) \ , \tag{1.35}$$

where $V(\mathbf{q},\omega) = U(\mathbf{q},\omega) + V_{\text{ind}}(\mathbf{q},\omega)$. Therefore Eq. (1.35) becomes

$$\varepsilon(\mathbf{q},\omega)V_{\text{ind}}(\mathbf{q},\omega) = \left[1 - \varepsilon(\mathbf{q},\omega)\right] U(\mathbf{q},\omega) \ . \tag{1.36}$$

From this equation we see that if $\varepsilon(\mathbf{q},\omega) = 0$ then $V_{\text{ind}}(\mathbf{q},\omega)$ can be nonzero when $U(\mathbf{q},\omega)$ is zero. This means that electron density oscillations can exist in the system without the existence of an external driving potential. Hence, the condition for the existence of self-sustained collective charge oscillations (plasmons) is

$$\varepsilon(\mathbf{q},\omega) = \varepsilon_b \left[1 - \frac{1}{\varepsilon_b} v(\mathbf{q})\chi_0(\mathbf{q},\omega)\right] = 0 \ , \tag{1.37}$$

from which the plasmons dispersion equation $\omega = \omega(\mathbf{q})$ can be found.

The polarization function gives information about the energy absorbed by the electron gas when it interacts with an externally applied electric field $\mathbf{E}$ [8]. The power dissipation per unit volume at point ($\mathbf{r}$,t) is given by $w = \mathbf{J}\cdot\mathbf{E} = \sigma\,|\mathbf{E}|^2$, for convenience we assume that our system is translational invariant, and therefore the total energy dissipated by the electron gas is given by the real part of

$$E = \int d\mathbf{r} \int dt \mathbf{J}(\mathbf{r},\mathbf{t})\cdot\mathbf{E}(\mathbf{r},\mathbf{t}) = \frac{1}{V}\sum_{\mathbf{q}} \int \frac{d\omega}{2\pi}\,|\mathbf{E}(\mathbf{q},\omega)|^2\,\sigma(\mathbf{q},\omega)\ . \tag{1.38}$$

The conductivity is connected to the polarization through the equation

$$\sigma(\mathbf{q},\omega) = i\frac{\omega}{q^2}\chi(\mathbf{q},\omega)\ , \tag{1.39}$$

so the real part of the conductivity is given by

$$\Re e\,\sigma(\mathbf{q},\omega) = -\frac{\omega}{q^2}\Im m\,\chi(\mathbf{q},\omega)\ , \tag{1.40}$$

which shows that energy can be dissipated by the electron gas if $\Im m\,\chi(\mathbf{q},\omega) \neq 0$. In the case of the non-interacting electron gas the incoming energy can be absorbed by the creation of electron-hole pairs (or single particle excitations). The area in $(\mathbf{q},\omega)$ space where $\Im m\,\chi(\mathbf{q},\omega) \neq 0$ defines the particle-hole region. Outside this area momentum and energy conservation is not satisfied, therefore energy can not be absorbed through single particle excitations. In the case though of the interacting electron gas a second mechanism of energy absorption exists, the excitation of plasmon modes. If the plasmon dispersion curve is outside the particle-hole region then the plasmon has long lifetime. If though the curve enters in the electron-hole continuum then the plasmon decays, i.e., it has a short lifetime. This case is known as Landau damping.

In the case of a nanotube of radius R lying along the z-axis, there is translational symmetry along the z direction and azimuthal symmetry around the z-axis. The single particle eigenfunctions and energy eigenvalues for electrons on

the surface of the nanotube that can be used in Eq. (1.21) have the form (we assume periodic boundary conditions along the z-axis)

$$\psi_\nu(\mathbf{r}) = \frac{e^{ik_z z}}{\sqrt{L_z}} \frac{e^{il\phi}}{\sqrt{2\pi}} P(\rho) \ , \qquad P^2(\rho) = \frac{\delta(\rho - R)}{\rho} \ , \tag{1.41}$$

$$\epsilon_\nu = \frac{\hbar^2 k_z^2}{2m^*} + \frac{\hbar^2 l^2}{2m^* R^2} \ , \tag{1.42}$$

where $P(\rho)$ comes from the confinement of the wave function ψ_ν along the radial direction, and $\nu = \{k_z, l\}$ is a composite index characterizing the electron eigenstates in terms of the quantum numbers $k_z = 2n\pi/L_z$ and l $(n, l = 0, \pm 1, \pm 2, \ldots)$. The Fourier transform of Eq. (1.21) with respect to t leads to

$$\chi_0(\mathbf{r}_3, \mathbf{r}_4, \omega) = 2 \sum_{\nu,\nu'} \frac{f_0(\epsilon_{\nu'}) - f_0(\epsilon_\nu)}{\hbar\omega + \epsilon_{\nu'} - \epsilon_\nu + i0^+} \psi_\nu(\mathbf{r}_3) \psi^*_{\nu'}(\mathbf{r}_3) \psi^*_\nu(\mathbf{r}_4) \psi_{\nu'}(\mathbf{r}_4) \ , \tag{1.43}$$

and if in addition we Fourier transform with respect to z and ϕ we obtain

$$\chi_L(\rho_1, \rho_2, q_z, \omega) = -\frac{1}{2\pi} \chi_L(q_z, \omega) \frac{\delta(\rho_1 - R)}{\rho_1} \frac{\delta(\rho_2 - R)}{\rho_2} \ , \tag{1.44}$$

where $\chi_L(q_z, \omega)$ is defined by

$$\chi_L(q_z, \omega) = 2 \sum_{l=-\infty}^{\infty} \int_{-\infty}^{\infty} \frac{dk_z}{2\pi} \frac{f_0(\epsilon_{k_z,l}) - f_0(\epsilon_{k_z - q_z, l-L})}{\hbar\omega + \epsilon_{k_z - q_z, l-L} - \epsilon_{k_z,l} + i0^+} \ , \tag{1.45}$$

and it is the Lindhard polarization function for the non-interacting electron gas on the nanotube. In this notation $q_z = k_z - k'_z$ and $L = l - l'$ is the linear and angular momentum transfer respectively between two electrons interacting through the Coulomb potential. The integration can be done analytically when $T = 0$ K and the results for the real and imaginary parts of this function are given in Appendix B along with some useful properties. In order to find the plasmon dispersion relation we Fourier transform Eq. (1.31) and we have

$$\varepsilon_L(\rho_1, \rho_2, q_z, \omega) = \varepsilon_b \left[\frac{\delta(\rho_1 - \rho_2)}{\rho_1} + \frac{1}{2\pi\varepsilon_b} u_L(\rho_1, R, q_z) \chi_L(q_z, \omega) \frac{\delta(\rho_2 - R)}{\rho_2} \right] \ , \tag{1.46}$$

where $u_L(\rho_1, \rho_2, q_z)$ is the Fourier transform of the Coulomb interaction energy in cylindrical coordinates. Since the electron gas is confined to the surface of the cylinder, there is a density response to an external perturbation only when ρ_1 and ρ_2 are equal to R. In this case, the delta function on the right side of Eq.(1.46) factors out and the dispersion equation becomes

$$\varepsilon_L(q_z, \omega) \equiv 1 + \frac{1}{2\pi\varepsilon_b} u_L(R, R, q_z)\chi_L(q_z, \omega) = 0 \ . \tag{1.47}$$

Chapter 2

PLASMA EXCITATIONS ON NANOTUBES

The transport properties of arrays of carbon nanotubes may be understood by studying their plasmon excitation spectrum. Lin and Shung [9] calculated the plasmon spectrum in a single cylindrical tubule and in a system of several co-axial cylindrical tubules. Gumbs and Aĭzin [10] calculated the plasmon excitations in a linear array of aligned multishell nanotubes using the RPA. Que [11] has presented a detailed study of plasmons in bundles of nanotubes. Other authors [12]-[18] have also reported some interesting results on intersubband and intrasubband plasmons in single-wall and multi-wall carbon nanotubes. There has also been considerable theoretical and experimental work on the plasmon excitations of low-dimensional systems [19]. Several authors have investigated the linear response of nanotubes of various radii which is related to their crossover from one dimensionality to another [20]-[22].

We start our study by first looking to the case of a single nanotube. This will provide us with the appropriate formalism and understanding required to move into more complex configurations of nanotubes.

2.1 Single particle and collective modes for one tubule

We first consider a single wall cylindrical nanotube of radius R and we take its axis of symmetry to be the z-axis. The nanotube is filled with a material of dielectric constant ε_1 inside and is surrounded by a material of dielectric constant ε_2. An electron confined on the surface of this nanotube is described by the eigenfunctions and energy eigenvalues given by Eqs. (1.41) and (1.42). We note from (1.42) that for a specific value of k_z, the azimuthal quantum number l can assume different values, i.e., we can have different energy subbands.

We assume that the electron gas on the surface of the cylinder is perturbed by an external probe (for example a charged moving particle) and then is left alone to evolve in time. The induced potential produced by the redistribution of the electron density is given by the solution of the Laplace equation $\nabla^2\Phi = 0,\ \rho \neq R$ along with the appropriate boundary conditions. We expand in Fourier series the induced potential by writing

$$\Phi(\rho, \phi, z, \omega) = \sum_{q_z, L} e^{iq_z z} e^{iL\phi} \Phi_L(\rho, q_z, \omega) \ , \tag{2.1}$$

and we substitute it in Laplace equation to obtain the radial differential equation

$$\frac{1}{\rho}\frac{\partial}{\partial\rho}\left[\rho\frac{\partial\Phi_L\left(\rho, q_z, \omega\right)}{\partial\rho}\right] - \left(q_z^2 + \frac{L^2}{\rho^2}\right)\Phi_L\left(\rho, q_z, \omega\right) = 0, \quad \rho \neq R \ . \tag{2.2}$$

The solutions of this equation are the modified Bessel functions $I_L(q_z\rho)$ and $K_L(q_z\rho)$. Taking into account the requirements that at the origin the solutions should be finite and that at large distances should fall to zero we have

$$\Phi_{1,L}(\rho, q_z, \omega) = C_{1,L}(q_z, \omega) I_L(q_z\rho) \ , \ \rho < R \tag{2.3}$$

$$\Phi_{2,L}(\rho, q_z, \omega) = C_{2,L}(q_z, \omega) K_L(q_z\rho) \ , \ \rho > R \ . \tag{2.4}$$

The boundary conditions for these solutions regard the continuity of the potential Φ and of the electric displacement vector $\mathbf{D} = \varepsilon\mathbf{E} = -\varepsilon\boldsymbol{\nabla}\Phi$ on the surface of the

cylinder

$$C_{1,L}(q_z,\omega)I_L(q_zR) = C_{2,L}(q_z,\omega)K_L(q_zR)\ , \tag{2.5}$$

$$\begin{aligned}(\mathbf{D_2}-\mathbf{D_1})\cdot\hat{\mathbf{n}}_{21}\big|_{\rho=R} &= 4\pi\sigma(R,\phi,z,\omega) \quad \text{or}\\ \varepsilon_1\frac{\partial\Phi_{1,L}}{\partial\rho}-\varepsilon_2\frac{\partial\Phi_{2,L}}{\partial\rho}\bigg|_{\rho=R} &= 4\pi\sigma(R,\phi,z,\omega)\ ,\end{aligned} \tag{2.6}$$

where $\hat{\mathbf{n}}_{21} = \hat{\boldsymbol{\rho}}$ is the unit vector perpendicular to the tubule's surface with direction from medium 1 to medium 2 (that is from the inside of the tubule to its outside) and σ is the induced surface charge density which also can be written as

$$\sigma(\phi,z,\omega)=\sum_{q_z,L}e^{iq_zz}e^{iL\phi}\sigma_L(q_z,\omega)\ .$$

The boundary condition given by Eq. (2.6) can now be expressed in the form

$$q_z\left[\varepsilon_1C_{1,L}(q_z,\omega)I'_L(q_zR)-\varepsilon_2C_{2,L}(q_z,\omega)K'_L(q_zR)\right]=4\pi\sigma_L(q_z,\omega)\ , \tag{2.7}$$

where the primes indicate derivatives with respect to the argument.

The induced electron charge density $\rho_{\rm e}$ is given by (Appendix A)

$$\rho_{\rm e}(\mathbf{r},\omega)=-e\rho(\mathbf{r},\omega)=-e\sum_{\nu,\nu'}<\nu\mid\hat{\varrho}_1(\mathbf{r},\omega)\mid\nu'>\psi^*_{\nu'}(\mathbf{r})\psi_\nu(\mathbf{r})\ , \tag{2.8}$$

where $\rho(\mathbf{r},\omega)$ is the induced particle density. In the lowest order of perturbation theory we have

$$<\nu\mid\hat{\varrho}_1(\mathbf{r},\omega)\mid\nu'>=2e\,\frac{f_0(\epsilon_\nu)-f_0(\epsilon_{\nu'})}{\hbar\omega+\epsilon_{\nu'}-\epsilon_\nu+i0^+}<\nu\mid\Phi(\mathbf{r},\omega)\mid\nu'>\ . \tag{2.9}$$

In this notation $f_0(\epsilon_\nu)$ is the Fermi-Dirac equilibrium distribution function. Substitution of Eqs. (1.41), (2.1) and (2.9) in Eq. (2.8) gives

$$\rho_{\rm e}(\rho,\phi,z,\omega)=-\frac{e^2}{2\pi R}\sum_{q_z,L}e^{iq_z}e^{iL\phi}\chi_L(q_z,\omega)\Phi_L(R,q_z,\omega)\delta(\rho-R)\ , \tag{2.10}$$

where $\chi_L(q_z,\omega)$ is the density response function for a single nanotube given by Eq. (1.45). From Eq. (2.10) we can deduce, since $\rho_{\rm e}(\mathbf{r},\omega)=\sigma(\phi,z,\omega)\delta(\rho-R)$, that

$$\sigma_L(q_z,\omega)=-\frac{e^2}{2\pi R}\,\chi_L(q_z,\omega)\Phi_L(R,q_z,\omega)\ . \tag{2.11}$$

We can now solve the set of Eqs. (2.5), (2.7) with $\sigma_L(q_z,\omega)$ given by Eq. (2.11) for the unknown coefficients $C_{1,L}(q_z,\omega)$ and $C_{2,L}(q_z,\omega)$. For non-zero solutions the condition

$$\varepsilon_L(q_z,\omega) = 1 + \alpha_L(q_z,\omega) = 0 \tag{2.12}$$

should be satisfied, where $\alpha_L(q_z,\omega)$ is the nanotube's polarizability function

$$\alpha_L(q_z,\omega) = \frac{2e^2 I_L(q_z R) K_L(q_z R)}{\varepsilon_1 + (\varepsilon_1 - \varepsilon_2) q_z R I_L(q_z R) K'_L(q_z R)}\, \chi_L(q_z,\omega)\ , \tag{2.13}$$

and $\varepsilon_L(q_z,\omega)$ is the dielectric function. When the condition given by Eq. (2.12) is satisfied the induced potential is non-vanishing although the external driving potential does not exist. Equation (2.12) describes the propagation of charge collective excitations on the surface of the nanotube, i.e., it is the plasmon dispersion equation. It is a generalization of the result given by Lin and Shung [9] to the case when the background dielectric constant is not uniform and it reduces to the well-known dispersion formula of plasmon in a 2D electron gas [23] when the radius is taken to be infinite. Our calculation yields in addition the dispersion equation of Arista and Fuentes [24] for a cylindrical cavity ($\varepsilon_1 = 1$ and $\chi_L(q_z,\omega) = 0$), which is $\varepsilon_1 + (\varepsilon_1 - \varepsilon_2) q_z R I_L(q_z R) K'_L(q_z R) = 0$.

Taking the limit $q_z R \to 0$ (long wavelength limit) and using the results of Appendix C, we find that the frequency of the highest plasmon mode for $L = 0$ is given by (in this notation n is the linear electron density)

$$\omega^2 \approx -\frac{2e^2 n}{m^* \varepsilon_2} q_z^2 \ln\left(\frac{q_z R}{2}\right) \left[1 + \frac{1}{2}\left(1 - \frac{\varepsilon_1}{\varepsilon_2}\right)(q_z R)^2 \ln\left(\frac{q_z R}{2}\right)\right]^{-1}\ . \tag{2.14}$$

For our numerical calculations we consider the case of a nanotube with $R = 11$ Å, $E_F = 0.6$ eV, $m^* = 0.25 m_e$ (m_e is the electron's mass) embedded in a background of dielectric constant $\varepsilon_1 = \varepsilon_2 = \varepsilon_b = 2.4$. This choice corresponds to simulating a graphene tubule. Equation (2.12) becomes in this case

$$\varepsilon_L(q_z,\omega) = 1 + \frac{2e^2}{\varepsilon_b} I_L(q_z R) K_L(q_z R) \chi_L(q_z,\omega) = 0\ . \tag{2.15}$$

For the chosen values of R and E_F we have that there are only five occupied subbands, i.e $|l| \leq 2$ (see Eqs. (B.5), (B.9) of Appendix B). The calculation of the polarization function has been done for $T = 0$ K. This is a good approximation since for our electron gas $T_F \simeq 7,000$ K. In Fig. 2.1 we plot the particle-hole excitations which is the only mechanism for the absorption of energy from a non-interacting electron gas when this interacts with an external electrostatic potential. These excitations satisfy the condition

$$\Im m\ [1 + a_L(q_z, \omega)] = \Im m\, \chi_L(q_z, \omega) \neq 0\ . \tag{2.16}$$

We plot in Fig. 2.2 the plasmon dispersion relation, Eq. (2.15), when $L = 0$ (intrasubband plasmons), for two nanotubes of the same $E_F = 0.6$ eV but of different radii (and therefore different number of occupied subbands), $R_1 = 11$ Å and $R_2 = 15$ Å. The small values of R implies that we deal with a quasi-1D system [13]. As R increases the nanotube behaves more like a 2D system. We see that for $L = 0$ we have three acoustic modes, one for each value of $|l|$. In Fig. 2.3 we plot the $L = 1$ and $L = 2$ plasmon excitations (intersubband plasmons). From this figure we note that for $L \geq 1$ we have not only acoustic but in addition optical modes. Using Eq. (2.14) we find an analytic expression for the plasmon dispersion when $L = 0$ and $\varepsilon_1 = \varepsilon_2 = \varepsilon_b$

$$\omega^2 \approx \frac{2e^2 n}{m^* \epsilon_b}\, q_z^2 |\ln(\frac{q_z R}{2})|\ . \tag{2.17}$$

The plasmon dispersion for a 2D electron gas in the same limit is $\omega^2 \propto q$ [26]. Equation (2.17) has a structure similar to that of the long wavelength limit dispersion for plasmons in quantum wires [27].

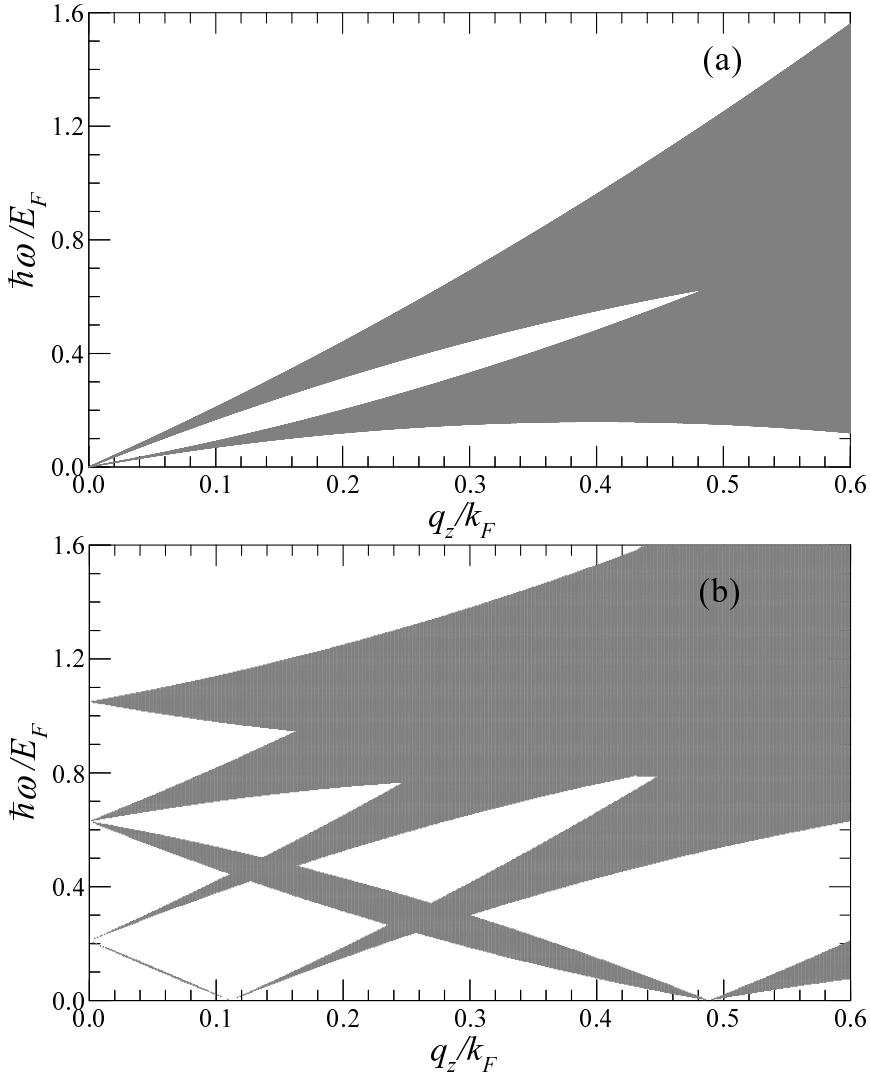

Figure 2.1: Particle-hole region for a single nanotube of $R = 11$ Å, $E_F = 0.6$ eV, when (a) $L = 0$ and (b) $L = 1$.

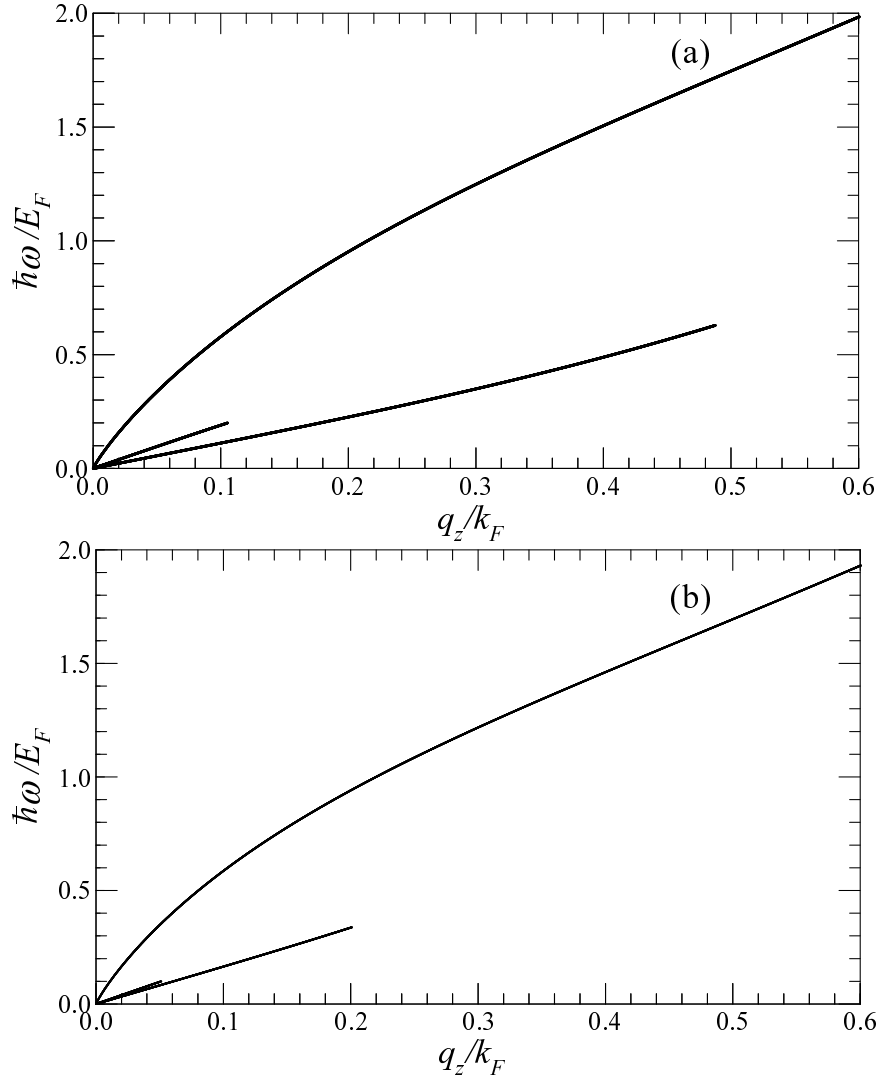

Figure 2.2: Plasmon dispersion for $L = 0$ when (a) $R = 11$ Å and (b) $R = 15$ Å.

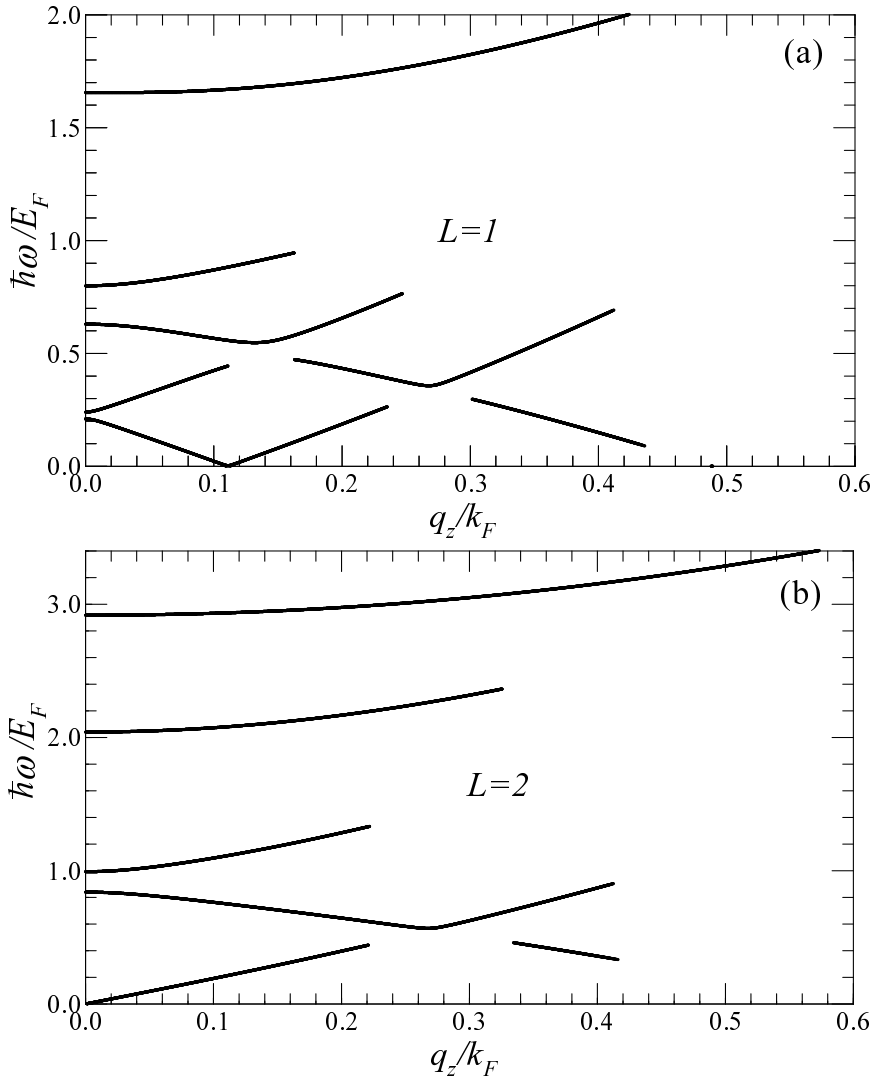

Figure 2.3: Plasmon dispersion for a single nanotube of $R = 11$ Å when (a) $L = 1$ and (b) $L = 2$.

2.2 Concentric tubules

We now consider a system of $N > 1$ concentric nanotubes of radius R_j ($j = 1, 2, \ldots, N$). The eigenstates for an electron confined to move on the $j - th$ tubule have in this case the form

$$\psi_{j\nu}(\mathbf{r}) = \frac{e^{ik_z z}}{\sqrt{L_z}} \frac{e^{il\phi}}{\sqrt{2\pi}} P_j(\rho) \ , \tag{2.18}$$

where $P_j^2(\rho) = \delta(\rho - R_j)$, and the energy eigenvalues have the same form as before. The inverse dielectric function ε^{-1} is given by the RPA integral equation (Eq. (1.19))

$$\varepsilon^{-1}(1,2) = \frac{1}{\varepsilon_b}\, \delta^4(1-2) + \frac{1}{\varepsilon_b} \int d^4 3 \int d^4 4\, v(1-4)\, \chi(4,3)\, \varepsilon^{-1}(3,2) \ , \tag{2.19}$$

where $1 = (\mathbf{r_1}, t_1)$ is a space-time point, v is the Coulomb interaction potential, ε_b is the background dielectric constant, and χ is the response function of the electron gas. We Fourier transform with respect to z and ϕ to obtain

$$\begin{aligned} \varepsilon_L^{-1}(\rho_1, \rho_2, q_z, \omega) &= \frac{1}{\varepsilon_b} \frac{\delta(\rho_1 - \rho_2)}{\rho_1} + \frac{1}{\varepsilon_b} \int d\rho_3\, \rho_3 \int d\rho_4\, \rho_4\, u_L(\rho_1, \rho_4, q_z) \\ &\times \chi_L(\rho_4, \rho_3, q_z, \omega)\, \varepsilon_L^{-1}(\rho_3, \rho_2, q_z, \omega) \ , \end{aligned} \tag{2.20}$$

where

$$u_L(\rho_1, \rho_4, q_z) = 4\pi e^2 I_L(q_z \rho_<) K_L(q_z \rho_>) \ , \tag{2.21}$$

is the Fourier transform of the Coulomb interaction energy in cylindrical coordinates [25]. We substitute in the last equation the Fourier transform of $\chi_L(\rho_4, \rho_3, q_z, \omega)$

$$\chi_{j,l}(\rho_4, \rho_3, q_z, \omega) = -\frac{1}{2\pi} \sum_{j=1}^{N} \chi_{j,L}(q_z, \omega) \frac{\delta(\rho_3 - R_j)}{\rho_3} \frac{\delta(\rho_4 - R_j)}{\rho_4} \ , \tag{2.22}$$

and we obtain

$$\begin{aligned} \varepsilon_L^{-1}(\rho_1, \rho_2, q_z, \omega) &= \frac{1}{\varepsilon_b} \frac{\delta(\rho_1 - \rho_2)}{\rho_1} - \frac{1}{2\pi\varepsilon_b} \sum_{j=1}^{N} \chi_{j,L}(q_z, \omega) \\ &\times u_L(\rho_1, \rho_4 = R_j, q_z)\, \varepsilon_L^{-1}(\rho_3 = R_j, \rho_2, q_z, \omega) \ . \end{aligned} \tag{2.23}$$

In this equation $\chi_{j,L}(q_z,\omega)$ is the polarization function of the j-th nanotube given by

$$\chi_{j,L}(q_z,\omega) = 2\sum_{l=-\infty}^{\infty}\int_{-\infty}^{\infty}\frac{dk_z}{2\pi}\frac{f_0(\epsilon_{j,k_z,l}) - f_0(\epsilon_{j,k_z-q_z,l-L})}{\hbar\omega + \epsilon_{j,k_z-q_z,l-L} - \epsilon_{j,k_z,l} + i0^+} \ . \tag{2.24}$$

We multiply both sides of Eq. (2.23) by $\rho_1 R_{j'}^2(\rho_1)$ and we integrate with respect to ρ_1, the result is

$$\begin{aligned}\varepsilon_L^{-1}(\rho_1 = R_{j'},\rho_2,q_z,\omega) &= \frac{1}{\varepsilon_b}\frac{\delta(\rho_2 - R_{j'})}{\rho_2} - \frac{1}{2\pi\varepsilon_b}\sum_{j=1}^{N}\chi_{j,L}(q_z,\omega) \\ &\times\ u_L(R_j,R_{j'},q_z)\,\varepsilon_L^{-1}(\rho_3 = R_j,\rho_2,q_z,\omega)\ ,\end{aligned} \tag{2.25}$$

which can be also written in the form

$$\sum_{j=1}^{N}\left[\delta_{jj'} + \frac{1}{2\pi\varepsilon_b}\chi_{j,L}(q_z,\omega)u_L(R_j,R_{j'},q_z)\right]\varepsilon_L^{-1}(\rho = R_j,\rho_2,q_z,\omega) = \frac{1}{\varepsilon_b}\frac{\delta(\rho_2 - R_{j'})}{\rho_2}\ . \tag{2.26}$$

Equation (2.26) for fixed L represents a set of N equations with unknown the N quantities $\varepsilon_L^{-1}(\rho = R_j,\rho_2,q_z,\omega)$. We call $A_L(q_z,\omega)$ the matrix with elements

$$A_{L,jj'}(q_z,\omega) = \delta_{jj'} + \frac{1}{2\pi\varepsilon_b}\chi_{j',L}(q_z,\omega)u_L(R_j,R_{j'},q_z)\ , \tag{2.27}$$

and $A_L^{-1}(q_z,\omega)$ the inverse. The solutions of Eq.(2.26) are given by

$$\varepsilon_L^{-1}(\rho = R_j,\rho_2,q_z,\omega) = \frac{1}{\varepsilon_b}\sum_{j'=1}^{N}A_{L,jj'}^{-1}(q_z,\omega)\frac{\delta(\rho_2 - R_{j'})}{\rho_2}\ , \tag{2.28}$$

and substituting them into Eq. (2.23) we find that the Fourier transform of the inverse dielectric function for a system of N concentric nanotubes is given by

$$\begin{aligned}\varepsilon_L^{-1}(\rho_1,\rho_2,q_z,\omega) &= \frac{1}{\varepsilon_b}\frac{\delta(\rho_1 - \rho_2)}{\rho_1} - \frac{1}{2\pi\varepsilon_b^2}\sum_{j,j'=1}^{N}\frac{\delta(\rho_2 - R_{j'})}{\rho_2} \\ &\times\ \chi_{j,L}(q_z,\omega)u_L(\rho_1,R_j,q_z)\,A_{L,jj'}^{-1}(q_z,\omega)\ .\end{aligned} \tag{2.29}$$

The singularities of this function give the plasmon dispersion modes for each value of L. Since the matrix $A_L^{-1}(q_z,\omega)$ is proportional to $1/\det A_L(q_z,\omega)$ these singularities are given by the solutions of the equation

$$\det A_L(q_z,\omega) = 0\ . \tag{2.30}$$

We study the case $N = 2$. The matrix $A_L(q_z, \omega)$ has then the form

$$A_L(q_z,\omega) = \begin{pmatrix} \varepsilon_{1,L}(q_z,\omega) & \dfrac{\chi_{2,L}(q_z,\omega)u_L(R_1,R_2,q_z)}{2\pi\varepsilon_b} \\ \dfrac{\chi_{1,L}(q_z,\omega)u_L(R_1,R_2,q_z)}{2\pi\varepsilon_b} & \varepsilon_{2,L}(q_z,\omega) \end{pmatrix} , \quad (2.31)$$

where

$$\varepsilon_{j,L}(q,\omega) = 1 + \frac{2e^2}{\epsilon_b} I_L(q_z R_j) K_L(q_z R_j) \chi_{1,L}(q_z,\omega) , \quad (2.32)$$

is the dielectric function of the j-th tubule. In Fig. 2.4 we plot the plasmon dispersion equation when $L = 0$ for the case that there is no interaction between the two tubules. In this case $u_L(R_1, R_2, q_z) = 0$ and the non-diagonal matrix elements of $A_L(q_z, \omega)$ are zero. The plasmons dispersion curve is the combination of the plasmons dispersion curves of a single nanotube of radius $R_1 = 11$ Å and of a single nanotube of radius $R_2 = 15$ Å, i.e., it is the combination in one plot of Figs. 2.2(a) and (b). In Fig. 2.5 we plot the plasmon dispersion, Eq. (2.30), for the case of non-zero interaction when $L = 0$ and $L = 1$. We used for the numerical calculation the same $E_F = 0.6$ eV for both nanotubes. For these

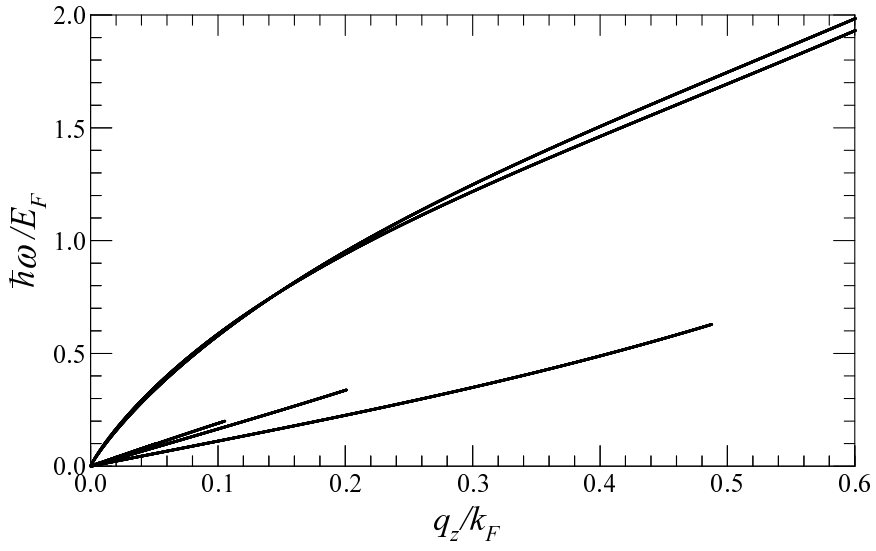

Figure 2.4: Plasmon dispersion for two non-interacting nanotubes when $L = 0$.

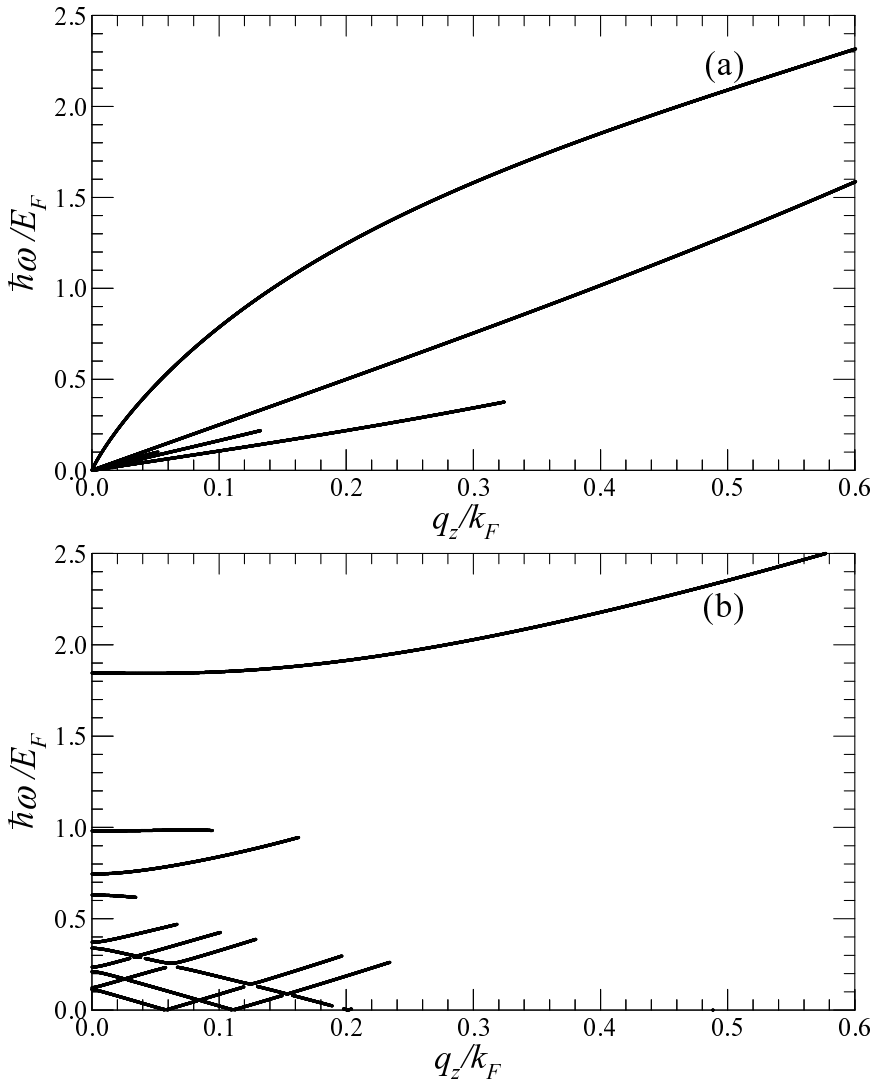

Figure 2.5: Plasmon dispersion for two concentric interacting nanotubes when (a) $L = 0$ and (b) $L = 1$.

values of E_F,R_1,R_2, each tubule has five occupied subbands. We clearly see by comparing Fig. 2.4 to Fig. 2.5(a) that the intertubular interaction is stronger for the high energy acoustic modes, causing their total separation.

One can obtain closed-form analytic expressions for the frequencies of the two highest plasmon modes in the long wavelength limit. Assuming that $q_z R_2 \ll 1$, our calculations show that these frequencies are given by

$$\omega_{\pm}^2 \approx \frac{q_z^2}{2}\left[\overline{\gamma}^{(1)}\left|\ln\left(\frac{q_z R_1}{2}\right)\right| + \overline{\gamma}^{(2)}\left|\ln\left(\frac{q_z R_2}{2}\right)\right|\right]$$
$$\pm \frac{q_z^2}{2}\left\{\left[\overline{\gamma}^{(1)}\left|\ln\left(\frac{q_z R_1}{2}\right)\right| - \overline{\gamma}^{(2)}\left|\ln\left(\frac{q_z R_2}{2}\right)\right|\right]^2 + 4\overline{\gamma}^{(1)}\overline{\gamma}^{(2)}\left|\ln\left(\frac{q_z R_1}{2}\right)\right|^2\right\}^{1/2}, \quad (2.33)$$

where $\overline{\gamma}^{(j)} = \dfrac{2e^2}{\varepsilon_b m^*}\overline{n}_j$ is expressed in terms of the linear density $\overline{n}_j$ on the nanotube of radius R_j. In fact, for Fermi energy E_F on the j-th tubule, we have at $T = 0$ K

$$\overline{n}_j = \frac{2}{\pi}\sum_{l=-S_j}^{S_j}\sqrt{\frac{2m^* E_F}{\hbar^2} - \frac{l^2}{R_j^2}}\,, \quad (2.34)$$

where S_j is the highest occupied subband level. This result shows that the number of electrons occupying each subband depends on the radius of the tubule. If the electron density is the same on each of the two co-axial nanotubes so that $\overline{\gamma}^{(1)} = \overline{\gamma}^{(2)} \equiv \overline{\gamma}$, then we have in the long wavelength limit

$$\omega_+ \approx q_z\left|\frac{\overline{\gamma}}{2}\ln\left(\frac{q_z^2}{4}R_2\left(R_1 + R_2\right)\right)\right|^{1/2}, \quad \omega_- \approx q_z\left[\frac{\overline{\gamma}}{2}\ln\left(\frac{R_2}{R_1}\right)\right]^{1/2}. \quad (2.35)$$

These results show that ω_- depends linearly on wave number q_z. In contrast to the constant phase velocity in the long wavelength limit for the ω_--mode, the dispersion relation for the ω_+-mode shows that its phase velocity has a logarithmic dependence on wave number.

2.3 Parallel tubules

We turn our attention to a system of two nanotubes with their axes parallel to the z direction. The axis of one of the nanotubes is at $x = 0$ with radius R_1 and the other at $x = a$ with radius R_2 on the x axis with $a > R_1 + R_2$. In the absence of tunneling between the nanotubes, the wavefunction for an electron on the j-th nanotube ($j = 1, 2$) is given by

$$< \mathbf{r} \mid j\nu >= \frac{e^{ik_z z}}{\sqrt{L_z}} \Psi_{jl} \left(\boldsymbol{\rho} - (j-1)a\hat{e}_x \right), \quad \Psi_{jl}(\boldsymbol{\rho}) = \frac{e^{il\phi}}{\sqrt{2\pi}} \frac{P_j(\rho)}{\sqrt{\rho}} \ , \tag{2.36}$$

with $\nu = \{k_z, l\}$ and $P_j^2(\rho) = \delta(\rho - R_j)$. The energy spectrum has the form of Eq. (1.42)

$$\epsilon_{j,\nu} = \frac{\hbar^2 k_z^2}{2m^*} + \frac{\hbar^2 l^2}{2m^* R_j^2} \ . \tag{2.37}$$

The equation of motion of the density matrix operator is

$$\imath\hbar \frac{\partial \hat{\varrho}}{\partial t} = [\hat{H}, \hat{\varrho}] \ , \tag{2.38}$$

where $\hat{H} = \hat{H}_0 - e\Phi$ is the Hamiltonian of the electron on the surface of the cylinder, $\hat{H}_0$ is the free electron Hamiltonian and Φ is the induced potential. The potential Φ satisfies Poisson's equation

$$\nabla^2 \Phi(\mathbf{r}) = \frac{4\pi e}{\varepsilon_b} \rho(\mathbf{r}) \ , \tag{2.39}$$

where ε_b is the uniform background dielectric constant, and $\rho(\mathbf{r})$ is the induced electron density. We use linear response theory (Appendix A) to calculate the induced particle density as

$$\rho(\mathbf{r}, \omega) = \sum_{j,j'} \sum_{\nu,\nu'} < \mathbf{r} \mid j\nu >< j\nu \mid \hat{\varrho}_1(\mathbf{r}, \omega) \mid j'\nu' >< j'\nu' \mid \mathbf{r} > \ , \tag{2.40}$$

where

$$< j\nu \mid \hat{\varrho}_1(\mathbf{r}, \omega) \mid j'\nu' >= 2e \, \frac{f_0(\epsilon_{j\nu}) - f_0(\epsilon_{j'\nu'})}{\hbar\omega + \epsilon_{j'\nu'} - \epsilon_{j\nu}} < j\nu \mid \Phi(\mathbf{r}, \omega) \mid j'\nu' > \ , \tag{2.41}$$

and we express the induced potential as $\Phi(\mathbf{r}) = \frac{1}{V}\sum_{\mathbf{q}'}\Phi(\mathbf{q}')e^{i\mathbf{q}'\cdot\mathbf{r}}$. Then Eq. (2.40) becomes

$$\begin{aligned}\rho(\mathbf{r}) &= \frac{2e}{V}\sum_{j,j'}\sum_{\nu,\nu'}\frac{f_0(\epsilon_{j\nu})-f_0(\epsilon_{j'\nu'})}{\hbar\omega+\epsilon_{j'\nu'}-\epsilon_{j\nu}} < \mathbf{r} \mid j\nu >< j'\nu' \mid \mathbf{r} > \\ &\times \sum_{\mathbf{q}'}\Phi(\mathbf{q}') < j\nu \mid e^{i\mathbf{q}'\cdot\mathbf{r}} \mid j'\nu' > , \end{aligned} \tag{2.42}$$

or by taking Fourier transform with respect to $\mathbf{r}$

$$\begin{aligned}\rho(\mathbf{q}) &= \frac{2e}{V}\sum_{j,j'}\sum_{\nu,\nu'}\frac{f_0(\epsilon_{j\nu})-f_0(\epsilon_{j'\nu'})}{\hbar\omega+\epsilon_{j'\nu'}-\epsilon_{j\nu}} < j'\nu' \mid e^{-i\mathbf{q}\cdot\mathbf{r}} \mid j\nu > \\ &\times \sum_{\mathbf{q}'}\Phi(\mathbf{q}') < j\nu \mid e^{i\mathbf{q}'\cdot\mathbf{r}} \mid j'\nu' > \ . \end{aligned} \tag{2.43}$$

The matrix elements $< j\nu \mid e^{i\mathbf{q}\cdot\mathbf{r}} \mid j'\nu' >$ with wave functions $< \mathbf{r} \mid j\nu >$ given by Eq. (2.36) can be calculated using the Jacobi-Anger expansion of a plane wave in cylindrical waves

$$e^{izcos\theta} = \sum_{m=-\infty}^{+\infty} i^m J_m(z)e^{im\theta} \ . \tag{2.44}$$

The result is

$$< j\nu \mid e^{i\mathbf{q}\cdot\mathbf{r}} \mid j'\nu' >= \delta_{jj'}\delta_{k_z-k'_z,q_z}e^{i(j-1)q_xa}e^{-im\theta}i^m J_m(q_\perp R_j) \ , \tag{2.45}$$

where $J_m(z)$ is the Bessel function of the first kind, $m = l - l'$ is the angular momentum transfer, $\mathbf{q}_\perp = (q_x, q_y)$ and θ is the angle between $\mathbf{q}_\perp$ and $\hat{e}_x$. Substituting Eq. (2.45) into Eq. (2.43), we obtain after some algebra

$$\begin{aligned}\rho(\mathbf{q}) &= \frac{2e}{V}\sum_{k_z}\sum_{l,m=0,\pm1,\pm2,\cdots}\sum_{j=1,2}\frac{f_0(\epsilon_{j,k_z,l})-f_0(\epsilon_{j,k_z-q_z,l-m})}{\hbar\omega+\epsilon_{j,k_z-q_z,l-m}-\epsilon_{j,k_z,l}}e^{im\theta}J_m\left(q_\perp R_j\right) \\ &\times e^{-i(j-1)q_xa}\sum_{q'_xq'_y}e^{i(j-1)q'_xa}\Phi\left(q'_x,q'_y,q_z\right)J_m\left(q'_\perp R_j\right)\left(\frac{q'_x-iq'_y}{q'_\perp}\right)^m \ . \end{aligned} \tag{2.46}$$

Taking the Fourier transform of Eq. (2.39) we have $\Phi(\mathbf{q}) = -4\pi e\rho(\mathbf{q})/\varepsilon_b q^2$. Using this relation in Eq. (2.46), we obtain

$$\rho(\mathbf{q}) = -\frac{4\pi e^2}{\varepsilon_b}\sum_{j,m}\chi_{j,m}(q_z,\omega)e^{-i(j-1)q_xa}J_m\left(q_\perp R_j\right)U_{j,m}(q_z)\left(\frac{q_x+iq_y}{q_\perp}\right)^m \ , \tag{2.47}$$

where $\chi_{j,m}(q_z,\omega)$ is the density response function of the j-th nanotube given by Eq.(2.24), and

$$U_{j,m}(q_z) = \frac{1}{L_x L_y}\sum_{q_x,q_y} e^{i(j-1)q_x a}\frac{\delta n(q_x,q_y,q_z)}{q_x^2+q_y^2+q_z^2} J_m\left(q_\perp R_j\right)\left(\frac{q_x - iq_y}{q_\perp}\right)^m \ . \qquad (2.48)$$

Here, L_x and L_y are normalization lengths. Substituting the expression for $\rho(\mathbf{q})$ given in Eq. (2.47) into Eq. (2.48), we obtain

$$\sum_{j'=1}^{2}\sum_{m'=-\infty}^{\infty}\left[\delta_{jj'}\delta_{mm'} + \frac{2e^2}{\varepsilon_b}\chi_{j',m'}(q_z,\omega)V_{j'm',jm}(q_z,a)\right]U_{j',m'}(q_z) = 0 \ , \qquad (2.49)$$

where

$$V_{j'm',jm}(q_z,a) = i^{(m'-m)}\int_0^\infty dq_\perp \frac{q_\perp}{q_\perp^2+q_z^2} J_m(q_\perp R_j)J_{m'}(q_\perp R_{j'})J_{m'-m}\left((j-j')q_\perp a\right). \qquad (2.50)$$

We have explicitly

$$\begin{aligned} &\left[1+\frac{2e^2}{\varepsilon_b}I_m(q_z R_1)K_m(q_z R_1)\chi_{1,m}(q_z,\omega)\right]U_{1,m}(q_z) \\ + \ &\frac{2e^2}{\epsilon_b}\sum_{m'}\chi_{2,m'}(q_z,\omega)\overline{V}^*_{m',m}\left(q_z,R_1,R_2;a\right)U_{2,m'}(q_z) = 0 \ , \end{aligned} \qquad (2.51)$$

$$\begin{aligned} &\frac{2e^2}{\epsilon_b}\sum_{m'}\chi_{1,m'}(q_z,\omega)\overline{V}_{m,m'}\left(q_z,R_1,R_2;a\right)U_{1,m'}(q_z) \\ + \ &\left[1+\frac{2e^2}{\varepsilon_b}I_m(q_z R_2)K_m(q_z R_2)\chi_{2,m}(q_z,\omega)\right]U_{2,m}(q_z) = 0 \ , \end{aligned} \qquad (2.52)$$

where

$$\overline{V}_{m,m'}(q_z,R_1,R_2;a) \equiv i^{(m'-m)}\int_0^\infty dq_\perp \ q_\perp \frac{J_{m'-m}(q_\perp a)J_m(q_\perp R_2)J_{m'}(q_\perp R_1)}{q_\perp^2+q_z^2} \ . \qquad (2.53)$$

The set of linear equations (2.49) and (2.52) have nontrivial solutions provided the determinant of the coefficient matrix of $\{U_{1,m}(q_z), U_{2,m}(q_z)\}$ is zero. Thus modes with different values of m on the two nanotubes are in general coupled to each other. Since $\overline{V}_{m,m'}(q_z,R_1,R_2;a) \to 0$ in the limit $a \to \infty$, this matrix is

diagonal when $a \gg R_1, R_2$ and the dispersion equation reduces to the result for isolated nanotubes

$$\prod_m \varepsilon_{1,m}(q,\omega)\,\varepsilon_{2,m}(q,\omega) = 0 \ , \tag{2.54}$$

where $\varepsilon_{j,m}(q,\omega)$ is given by Eq. (2.32). The beauty of equations (2.49) and (2.52) is that they automatically give the Coulomb interaction on the two nanotubes as well as between the pair of nanotubes.

The simplest case of interest occurs when the only allowed transitions are the $m = 0$. Then the dispersion equation becomes

$$\begin{aligned} & \left[1 + \frac{1}{2\pi\varepsilon_b} u_0(R_1, R_1, q_z)\chi_{1,0}(q_z,\omega)\right]\left[1 + \frac{1}{2\pi\varepsilon_b} u_0(R_2, R_2, q_z)\chi_{2,0}(q_z,\omega)\right] \\ - & \left[\frac{4\pi e^2}{\varepsilon_b}\overline{V}_{0,0}(q_z, R_1, R_2; a)\right]^2 \chi_{1,0}(q_z,\omega)\chi_{2,0}(q_z,\omega) = 0 \ , \end{aligned} \tag{2.55}$$

where $u_0(R_j, R_j', q_z)$ is given by Eq. (2.21). If we take $R_1 = R_2 = R$, and use a result in [28] we have

$$\overline{V}_{0,0}(q_z, R, R; a) = I_0^2(q_z R) K_0(q_z a) \ . \tag{2.56}$$

Using the low-frequency, long wavelength approximation for the polarization function (Appendix C) $\chi_{j,m=0}(q_z,\omega) \approx -\dfrac{n_j q_z^2}{m^*\omega^2}$, where n_j is the linear electron density on the j-th nanotube, a straightforward calculation shows that in the long wavelength limit $q_z a \ll 1$, we obtain two modes above the particle-hole mode region with frequency $\omega_\pm$ given by

$$\begin{aligned} \omega_\pm^2 &\approx \frac{e^2}{\varepsilon_b}\frac{q_z^2}{m^*}(n_1+n_2)\left|\ln\left(\frac{q_z R}{2}\right)\right| \\ &\pm \frac{2e^2}{\varepsilon_b}\frac{q_z^2}{m^*}\left\{\frac{1}{4}(n_1-n_2)^2\left|\ln\left(\frac{q_z R}{2}\right)\right|^2 + n_1 n_2\left|\ln\left(\frac{q_z a}{2}\right)\right|^2\right\}^{1/2} \ . \end{aligned} \tag{2.57}$$

If the two nanotubes are identical with $n_1 = n_2 = n$, we have

$$\omega_-^2 \approx \frac{2e^2}{\varepsilon_b}\frac{q_z^2}{m^*} n \ln(\frac{a}{R}) \tag{2.58}$$

$$\omega_+^2 \approx \frac{2e^2}{\varepsilon_b}\frac{q_z^2}{m^*} n \ln(\frac{q_z^2 a R}{4}) \ . \tag{2.59}$$

Thus, the coupling between the single-nanotube modes of frequency ω_1 (say) given by Eq. (2.17) lifts their degeneracy to give modes of frequency $\omega_\pm$ so that $\omega_- < \omega_1 < \omega_+$. The high-frequency quasi-optical ω_+ mode corresponds to in-phase longitudinal electron density oscillations along the axes of the nanotubes. The low-frequency quasi-acoustic ω_- mode is an out-of-phase collective excitation of the carriers on the two nanotubes and is linear in q_z. In Fig. 2.6 we plot the plasmon dispersion relation Eq.(2.55) for two identical nanotubes of radius $R = 11$ Å separated by a distance $a = 25$ Å. All calculations were carried out at zero temperature. We used for E_F, m^* and ε_b the same values that we used in the case of the plasmons on a single nanotube. For the values of the parameters chosen, in each nanotube there are only five subbands occupied by electrons corresponding to $l = 0, \pm 1, \pm 2$. Only the part of the plasmon spectrum which is undamped is shown in this figure. There are three plasmons branches for a single nanotube corresponding to $|l| = 0, 1, 2$. For the pair of nanotubes the degeneracy is lifted by the Coulomb interaction. However splitting is so small for the lower

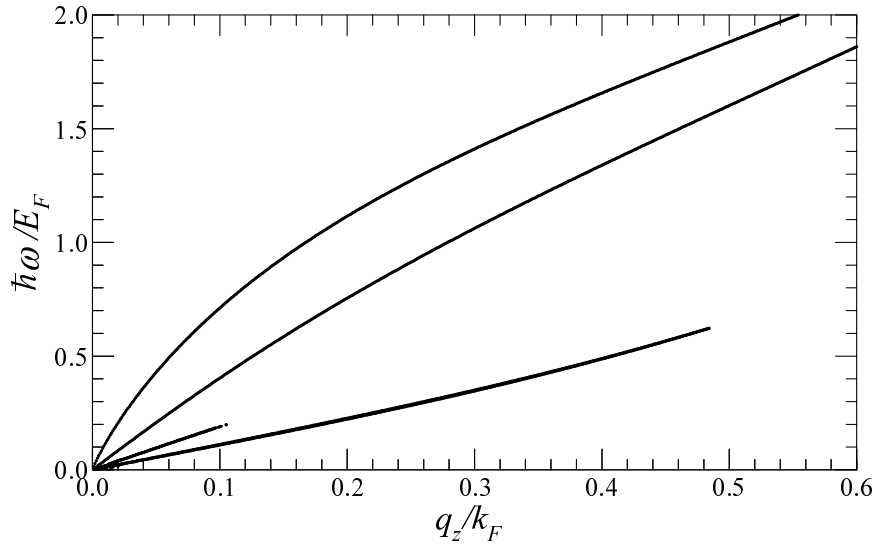

Figure 2.6: Plasmon dispersion for two identical parallel nanotubes of radius R=11 Å separated by a distance a=25 Å when $m = 0$.

branches compared with the higher frequency modes that we cannot distinguish between the lowest modes.

Chapter 3

ENERGY TRANSFER IN NANOTUBES

Over the years, there have been several papers devoted to the theory of electron energy loss spectroscopy(EELS) [29]-[38]. These works were concerned with EELS for films, the two dimensional electron gas (2DEG) and nanowires. Most recently, there have been several papers dealing with the theory of EELS for cylindrical nanotubes and cylindrical cavities. However, the published work so far [39]-[45] does not fully compare the contributions from plasmons and single particle excitations for nanotubes. This scattering problem deserves some attention and will be the subject of this chapter. We will present a model and theory within the RPA for EELS in cylindrical nanotubes. The solid metallic cylinder is a special case which is obtained when the polarization function is set equal to infinity. However, this latter model does not allow the contributions to energy loss from individual subbands to be analyzed. Our model provides a way of separating and calculating the plasmon and particle-hole contributions.

3.1 Energy loss on a single wall nanotube

We assume that a particle of mass m and charge Q moves with velocity $\mathbf{v} = v\hat{z}$ parallel to the axis of the nanotube (of radius R) with impact parameter $\rho_0 > R$, i.e., we take the particle to move outside the cylinder. The position vector of the particle at any time t is given by $\mathbf{r}_0 = (\rho_0, \phi_0, z_0 = vt)$.

The total electrostatic potential Φ at any point of space for any time t satisfies Poisson equation

$$\nabla^2\Phi_1(\rho,\phi,z,t) = 0\ , \quad \rho < R \tag{3.1}$$

$$\nabla^2\Phi_2(\rho,\phi,z,t) = -\frac{4\pi Q}{\varepsilon_2}\delta(\mathbf{r}-\mathbf{r}_0)\ , \quad \rho > R\ , \tag{3.2}$$

along with the boundary conditions

$$\Phi_1(\rho = R,\phi,z,\omega) = \Phi_2(\rho = R,\phi,z,\omega) \tag{3.3}$$

$$(\mathbf{D}_2 - \mathbf{D}_1)\cdot\hat{\mathbf{n}}_{21}\big|_{\rho=R} = 4\pi\sigma(R,\phi,z,\omega)\ , \tag{3.4}$$

where σ is the induced surface charge density and $\hat{\mathbf{n}}_{21} = \hat{\boldsymbol{\rho}}$ (see also Eq. (2.6)).

The solution Φ_1 of Eq. (3.1) can be Fourier expanded as

$$\Phi_1(\rho,\phi,z,t) = \frac{Q}{\pi\varepsilon_1}\sum_{L=-\infty}^{\infty} e^{iL(\phi-\phi_0)}\int_{-\infty}^{\infty} dq_z e^{iq_z(z-vt)}C_L^<(q_z)I_L(q_z\rho)\ , \tag{3.5}$$

and from this we find

$$\Phi_1(\rho,\phi,z,\omega) = \frac{2Q}{\varepsilon_1}\sum_{L=-\infty}^{\infty} e^{iL(\phi-\phi_0)}\int_{-\infty}^{\infty} dq_z C_L^<(q_z)I_L(q_z\rho)\delta(\omega - q_z v)\,. \tag{3.6}$$

The potential Φ_2 can be written using superposition as

$$\Phi_2(\rho,\phi,z,t) = \frac{Q}{\varepsilon_2|\mathbf{r}-\mathbf{r_0}(t)|} + \Phi_{\rm ind}^>(\rho,\phi,z,t)\ , \tag{3.7}$$

where $Q/|\mathbf{r}-\mathbf{r_0}(t)|$ is the potential of the moving charged particle and $\Phi_{\rm ind}^>$ is the potential due to the induced surface charge density (a solution of Laplace equation

for $\rho > R$). We can write these electric potentials in cylindrical coordinates as

$$\frac{Q}{|\mathbf{r}-\mathbf{r_0}(t)|} = \frac{Q}{\pi}\sum_{L=-\infty}^{\infty} e^{iL(\phi-\phi_0)}\int_{-\infty}^{\infty} dq_z e^{iq_z(z-vt)} I_L(q_z\rho_<)K_L(q_z\rho_>)\ , \tag{3.8}$$

$$\Phi^{>}_{\rm ind}(\rho,\phi,z,t) = \frac{Q}{\pi\varepsilon_2}\sum_{L=-\infty}^{\infty} e^{iL(\phi-\phi_0)}\int_{-\infty}^{\infty} dq_z e^{iq_z(z-vt)} C^{>}_L(q_z)K_L(q_z\rho)\ , \tag{3.9}$$

where $\rho_<(\rho_>)$ is the smaller(larger) of ρ and ρ_0. Therefore Eq. (3.7) can be written as

$$\begin{aligned}\Phi_2(\rho,\phi,z,t) &= \frac{Q}{\pi\varepsilon_2}\sum_{L=-\infty}^{\infty} e^{iL(\phi-\phi_0)}\int_{-\infty}^{\infty} dq_z e^{iq_z(z-vt)}\left[I_L(q_z\rho_<)K_L(q_z\rho_>)\right.\\ &+ \left. C^{>}_L(q_z)K_L(q_z\rho)\right]\ ,\end{aligned} \tag{3.10}$$

or

$$\begin{aligned}\Phi_2(\rho,\phi,z,\omega) &= \frac{2Q}{\varepsilon_2}\sum_{L=-\infty}^{\infty} e^{iL(\phi-\phi_0)}\int_{-\infty}^{\infty} dq_z e^{iq_z z}\left[I_L(q_z\rho_<)K_L(q_z\rho_>)\right.\\ &+ \left. C^{>}_L(q_z)K_L(q_z\rho)\right]\delta(\omega-q_z v)\,.\end{aligned} \tag{3.11}$$

The induced charge density can be found in this case by substituting Eqs. (3.6), (3.10), (3.11) into the boundary conditions Eqs. (3.3), (3.4) and following the steps of Sec. 2.1, Eqs. (2.8) through (2.11). We find in this way that

$$\begin{aligned}\rho(\mathbf{r},\omega) &= -\frac{Qe^2}{\pi R\varepsilon_1}\,\delta(\rho-R)\sum_{L=-\infty}^{\infty} e^{iL(\phi-\phi_0)}\int_{-\infty}^{\infty} dq_z e^{iq_z z}\\ &\times\ \chi_L(q_z,\omega)C^{<}_L(q_z)I_L(q_zR)\delta(\omega-q_z v)\ ,\end{aligned} \tag{3.12}$$

and that the induced surface charge density is given by

$$\begin{aligned}\sigma(R,\phi,z,\omega) &= -\frac{Qe^2}{\pi R\varepsilon_1}\sum_{L=-\infty}^{\infty} e^{iL(\phi-\phi_0)}\int_{-\infty}^{\infty} dq_z e^{iq_z z}\chi_L(q_z,\omega)\\ &\times\ C^{<}_L(q_z)I_L(q_zR)\delta(\omega-q_z v)\,.\end{aligned} \tag{3.13}$$

The boundary conditions Eqs. (3.3), (3.4) can now be written using the expressions found for Φ_1,Φ_2 and σ as

$$\varepsilon_2 C^{<}_L(q_z)I_L(q_zR) = \varepsilon_1\left[I_L(q_zR)K_L(q_z\rho_0) + C^{>}_L(q_z)K_L(q_zR)\right]\ , \tag{3.14}$$

$$C_L^<(q_z)I_L'(q_zR) - C_L^>(q_z)K_L'(q_zR) = K_L(q_z\rho_0)I_L'(q_zR) \\ -\frac{2e^2}{\varepsilon_1 q_z R}\chi_L(q_z,\omega=q_zv)C_L^<(q_z)I_L(q_zR)\,. \tag{3.15}$$

The solutions of the set of Eqs. (3.14) and (3.15) are given by the expressions

$$C_L^<(q_z) = \frac{\varepsilon_1 K_L(q_z\rho_0)}{D_L(q_z,\omega=q_zv)}\ , \tag{3.16}$$

$$\begin{aligned} C_L^>(q_z) &= -\left[2e^2 I_L(q_zR)\chi_L(q_z,\omega=q_zv) + q_zR(\varepsilon_1-\varepsilon_2)I_L'(q_zR)\right] \\ &\times \frac{K_L(q_z\rho_0)I_L(q_zR)}{D_L(q_z,\omega=q_zv)}\ , \end{aligned} \tag{3.17}$$

with

$$D_L(q_z,\omega) = \varepsilon_1 + (\varepsilon_1-\varepsilon_2)q_zRI_L(q_zR)K_L'(q_zR) + 2e^2\chi_L(q_z,\omega)I_L(q_zR)K_L(q_zR)\ , \tag{3.18}$$

or

$$D_L(q_z,\omega) = \left[\varepsilon_1 + (\varepsilon_1-\varepsilon_2)q_zRI_L(q_zR)K_L'(q_zR)\right]\left[1+\alpha_L(q_z,\omega)K_L(q_zR)\right]\ , \tag{3.19}$$

where

$$\alpha_L(q_z,\omega) = \frac{2e^2 I_L(q_zR)K_L(q_zR)}{\varepsilon_1 + (\varepsilon_1-\varepsilon_2)q_zRI_L(q_zR)K_L'(q_zR)}\chi_L(q_z,\omega)\ , \tag{3.20}$$

is the polarizability function of the electron gas, and $\varepsilon_L(q_z,\omega) = 1+\alpha_L(q_z,\omega)$ is the dielectric function (see also Eqs.(2.12) and (2.13)).

We can now find the induced potential because of the charge density fluctuations on the surface of the cylinder. For $\rho > R$ using Eq. (3.9) and Eq. (3.17) we find

$$\begin{aligned} \Phi_{\rm ind}^>(\mathbf{r},t) &= -\frac{Q}{\pi\varepsilon_2}\sum_{L=-\infty}^{\infty} e^{iL(\phi-\phi_o)}\int_{-\infty}^{\infty} dq_z e^{iq_z(z-vt)}K_L(q_z\rho)K_L(q_z\rho_0)I_L(q_zR) \\ &\times \left[\frac{1}{K_L(q_zR)}\frac{\alpha_L(q_z,\omega)}{1+\alpha_L(q_z,\omega)} + q_zR(\varepsilon_1-\varepsilon_2)\frac{I_L'(q_zR)}{D_L(q_z,\omega)}\right]_{\omega=q_zv}\ , \end{aligned} \tag{3.21}$$

while for $\rho < R$ using Eq. (3.5) and Eq. (3.16) we obtain (since $\Phi_1(\mathbf{r},t) = \Phi_{\rm ind}^<(\mathbf{r},t)$)

$$\Phi_{\rm ind}^<(\mathbf{r},t) = \frac{Q}{\pi}\sum_{L=-\infty}^{\infty} e^{iL(\phi-\phi_0)}\int_{-\infty}^{\infty} dq_z e^{iq_z(z-vt)}\frac{I_L(q_z\rho)K_L(q_z\rho_0)}{D_L(q_z,\omega=q_zv)}\ . \tag{3.22}$$

The force applied to the moving charged particle from the induced charge density on the surface of the nanotube is therefore given by

$$\mathbf{F} = -Q\boldsymbol{\nabla}\Phi^{>}_{\rm ind}(\mathbf{r})|_{\mathbf{r}=(\rho_0,\phi_0,z_0=vt)} \ , \tag{3.23}$$

and the rate of energy loss can be calculated as

$$\frac{dW}{dt} = \mathbf{F}\cdot\mathbf{v} = -Q\,v\frac{\partial\Phi^{>}_{\rm ind}(\rho,\phi,z,t)}{\partial z}\bigg|_{\mathbf{r}=(\rho_0,\phi_0,z_0=vt)} . \tag{3.24}$$

We then obtain

$$\begin{aligned}\frac{dW}{dt} &= \frac{2Q^2}{\pi}v\sum_{L=-\infty}^{\infty}\int_0^\infty dq_z q_z K_L^2(q_z\rho_0)\frac{I_L(q_zR)}{K_L(q_zR)} \\ &\times \frac{1}{\varepsilon_1 + q_zR(\varepsilon_1-\varepsilon_2)I_L(q_zR)K_L'(q_zR)}\,\Im m\left[\frac{1}{\varepsilon_L(q_z,\omega=q_zv)}\right] .\end{aligned} \tag{3.25}$$

This result generalizes that obtained by Arista and Fuentes [24] for a cylindrical cavity which corresponds to neglecting the response function $\chi_L(q_z,\omega)$ for the electron gas on the surface of the cylinder. Equation (3.25) includes contributions to the total energy loss from all possible linear momentum transfers q_z along the axis of the nanotube and all transitions (angular momentum transfers) L within and between different subbands. However, only excitations of frequencies $\omega = q_zv$ can contribute to the stopping power. The imaginary part of the Fourier transform of the dielectric function $\varepsilon_L(q_z,\omega)$ enters the energy loss formula. This means that we can separate the contributions to Eq. (3.25) from plasmons and particle-hole excitations in a similar way to that done by Horing, Tso and Gumbs [38] in calculations of the stopping power of a 2D sheet of electron gas, if we express

$$\varepsilon_L(q_z,\omega) = \varepsilon_{1,L}(q_z,\omega) + i\varepsilon_{2,L}(q_z,\omega) \ , \tag{3.26}$$

$$\frac{1}{\varepsilon_L(q_z,\omega)} = \frac{-\varepsilon_{2,L}(q_z,\omega)}{\varepsilon^2_{1,L}(q_z,\omega)+\varepsilon^2_{2,L}(q_z,\omega)} \ , \tag{3.27}$$

where $\varepsilon_{1,L}(q_z,\omega)$ and $\varepsilon_{2,L}(q_z,\omega)$ are the real and imaginary parts respectively of $\varepsilon_L(q_z,\omega)$. The imaginary part function in Eq. (3.25) is multiplied by a kinematical

factor depending on the impact parameter, momentum transfer and velocity v which can be adjusted experimentally. There is a contribution from the integrand whenever either

(a) $\varepsilon_{2,L}(q_z, \omega = q_z v) = \Im m\, \alpha_L(q_z, q_z v) \neq 0$ or

(b) $\varepsilon_{1,L}(q_z, \omega = q_z v) = 0$ and $\varepsilon_{2,L}(q_z, \omega = q_z v) = 0$.

When case (a) applies we have Landau damping and the particle-hole region (see Fig. 2.1) contributes to the energy loss. In case (b) though, the dispersion equation for plasmon excitations is satisfied on the surface of the cylinder and the plasmons make a contribution. In this case we use Dirac's identity

$$\lim_{\varepsilon \to 0^+} \frac{\varepsilon}{x^2 + \varepsilon^2} = \pi \delta(x) \tag{3.28}$$

and we find that Eq.(3.25) becomes

$$\begin{aligned} \left.\frac{dW}{dt}\right|_{\text{plasmons}} &= -2Q^2 v \sum_{L=-\infty}^{\infty} \int_0^{\infty} dq_z q_z \frac{\delta\left(\omega - q_z v\right)}{\left|d\varepsilon_{1,L}(q_z, \omega)/d\omega\right|_{\omega=\omega_L(q_z)}} K_L^2(q_z \rho_0) \\ &\times \frac{I_L(q_z R)}{K_L(q_z R)} \frac{1}{\varepsilon_1 + q_z R(\varepsilon_1 - \varepsilon_2) I_L(q_z R) K_L'(q_z R)} \ , \end{aligned} \tag{3.29}$$

where $\omega_L(q_z)$ is the solution of $\varepsilon_L(q_z, \omega) = 0$, i.e., it represents the plasmon dispersion curves. In the case that the charged particle moves parallel to the axis of the tubule at distance ρ_0 with $\rho_0 < R$, the induced potential, charge density and stopping power can be obtained in a similar way. The results are given in Appendix D.

We have calculated the total rate of loss of energy from all subband transitions at $T = 0$ K, as described by Eqs.(3.25) and (D.3). We simulated a graphene tubule by choosing, as we did in Sec. 2.1, $\varepsilon_1 = \varepsilon_2 = 2.4$, $m^* = 0.25 m_e$, $R = 11$ Å and $E_F = 0.6$ eV. We included all the transitions with $|L| \leq 10$ in calculating dW/dt. There are only five subbands occupied by electrons corresponding to $l = 0, \pm 1, \pm 2$. Our results are presented in Figs. 3.1 and 3.2 as functions of v/v_F,

where the Fermi velocity $v_F = 918.88$ km/s. In Fig. 3.1(a), the charged particle travels along the axis of the tubule ($\rho_0 = 0$). Here, the plasmon contribution to the rate of loss of energy is larger than that from single-particle excitations except in the low-velocity limit. For fast moving particles, only plasmons play a role. For both curves, dW/dt initially increase with v but then decreases after reaching a maximum. Therefore the dominant contribution to the energy loss comes from those excitations whose phase velocities lies close to where the maximum occurs. We examined where this peak occurs for each term in the sum over L. Our calculations show that for fixed ρ_0, the rate of loss of energy has a peak for each value of L contributing to the sum in Eq.(3.25). When the charged particle moves along the axis of the nanotube, only the $L = 0$ transitions contribute. This is explained by the behavior of the Bessel function $I_L(q_z\rho_0)$. However, when the particle trajectory is not along the axis of the cylinder, terms with $L \neq 0$ contribute. The peak position is not the same for each value of L. This accounts for the peaks in the total energy loss dW/dt and is elaborated on below for both plasmon and particle-hole modes for a chosen ρ_0. As a matter of fact, the lowest subband transitions corresponding to $L = 0, 1, 2$ mainly contribute to the total stopping power when $\rho_0 \neq 0$.

In Fig. 3.1(b), we chose $\rho_0 = 5$ Å so that the charged particle trajectory is almost halfway between the axis and the surface of the cylinder. Comparing these results with those in Fig. 3.1(a), the particle-hole mode contribution increases for $v \ll v_F$. In Fig. 3.2(a), we chose $\rho_0 = 10$ Å. For this case when the charged particle trajectory is close to the surface of the cylinder, the energy loss due to particle-hole excitations surpasses that from plasmons for all values of the charged particle velocity, except when $v \approx 1.8v_F$. Both the plasmon and single-particle contributions are increased when the charged particle trajectory is closer to the cylinder surface. In Fig. 3.2(b), it is shown that as ρ_0 is increased with the

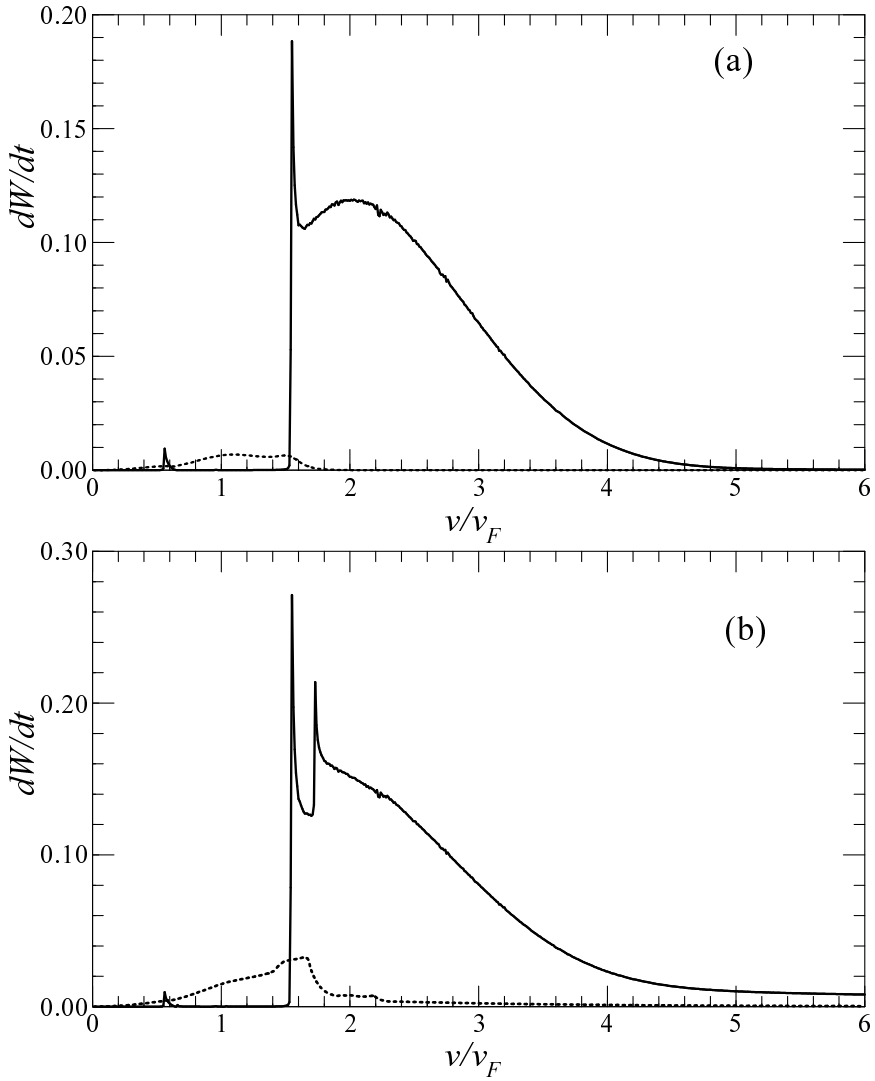

Figure 3.1: The energy loss for plasmon (solid lines) and particle-hole modes (dotted lines) as a function of the charged particle velocity parallel to the axis of the cylinder when (a) $\rho_0 = 0$ Å and (b) $\rho_0 = 5$ Å. The energy loss is expressed in units of $e^2 k_F^2 v_F$.

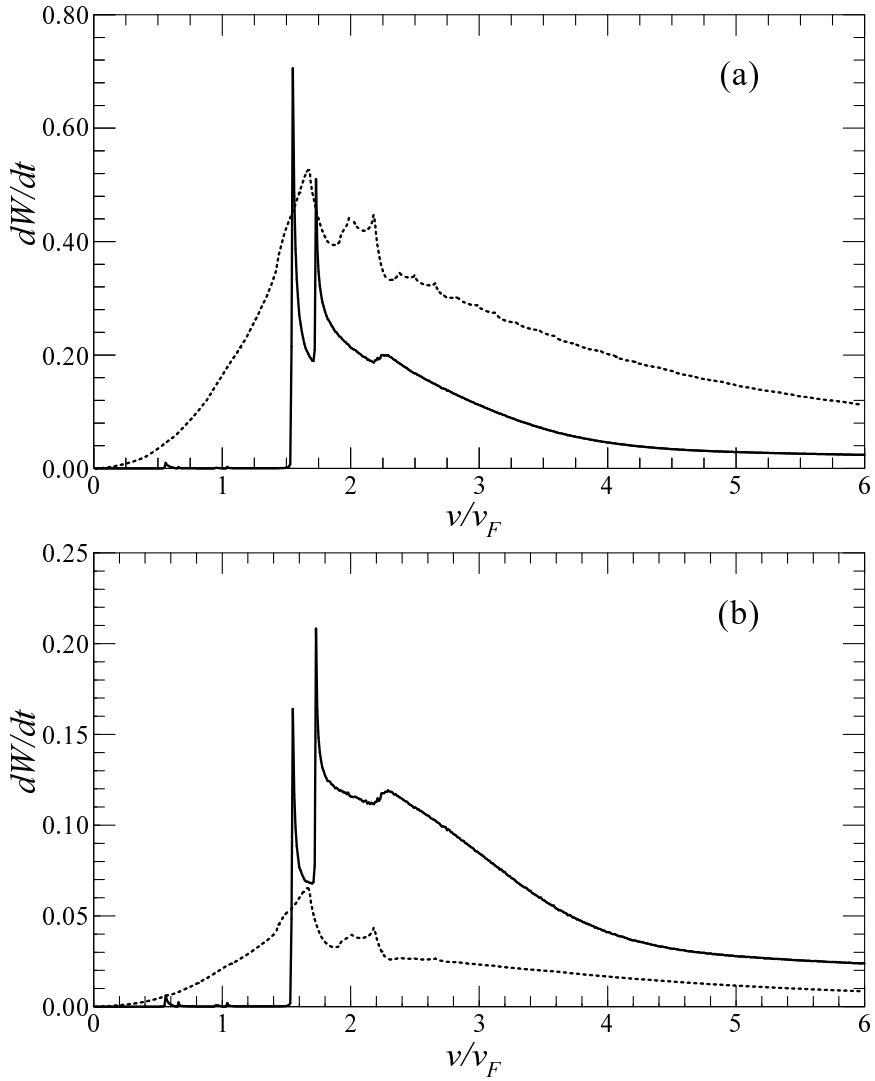

Figure 3.2: The energy loss for plasmon (solid lines) and particle-hole modes (dotted lines) as a function of the charged particle velocity parallel to the axis of the cylinder when (a) $\rho_0 = 10$ Å and (b) $\rho_0 = 15$ Å. The energy loss is expressed in units of $e^2 k_F^2 v_F$.

particle trajectory outside the cylinder, the plasmon contribution to the energy loss is larger than that of the single particle. Our calculations shown that when the charged particle trajectory is at the same distance from the surface either inside or outside the cylinder, there is a small difference in dW/dt. The small difference is due to the asymmetry of the induced potential with respect to the cylindrical surface.

In Fig. 3.3, we plot the contributions to the stopping power from the lowest subbands $L = 0, \pm 1, \pm 2$ when the charged particle distance from the axis of the cylinder is $\rho_0 = 15$ Å. Fig. 3.3(a) is the contribution from plasmon excitations, whereas Fig. 3.3(b) shows the stopping power of particle-hole modes. In Fig. 3.3(a), the $L = 0$ subband is larger than any intersubband transition producing plasmons excitations. In fact, the contribution from plasmons excitations decreases with increasing value of L. However, Fig. 3.3(b) shows that the $|L| = 1$ and $|L| = 2$ subband contributions to the stopping power from particle-hole excitations exceed that from the $L = 0$ subband. The contributions from higher subbands decreases with increasing L. Each curve in Fig. 3.3 has a peak at a value of velocity which shifts to the right as L is increased. Similar results were obtained when the ρ_0 value was changed and the charged particle trajectory was either inside or outside the nanotube.

The numerical results in Fig. 3.1 show that there is a sudden increase in the stopping power of plasmon excitations for specific values of charged particle velocity. The highest threshold value is at $v = 1.55 v_F$ regardless of the chosen impact parameter ρ_0. To explain these characteristics, we have plotted in Fig. 3.4 the three acoustic plasmon modes obtained by solving Eq.(2.12). These plasmons have Landau damping when they enter the particle-hole mode regions which are not shown in Fig. 3.4. This explains why each mode only exists over a range of frequency and wave vector. Only when the plasmon frequency satisfies $\omega = q_z v$

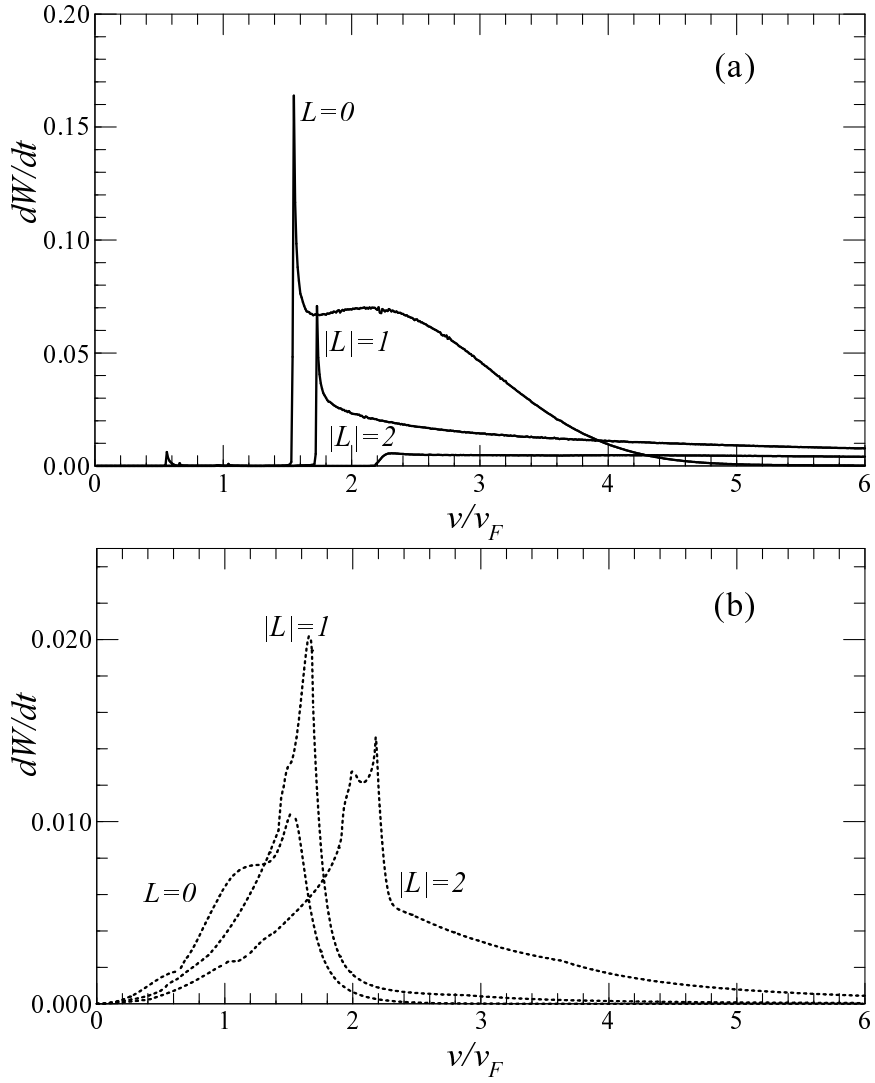

Figure 3.3: The contributions to the stopping power for Fig. 3.2(b) from (a) plasmon and (b) particle-hole excitations for subband transitions L. dW/dt is expressed in the same unit as in Figs. 3.1 and 3.2.

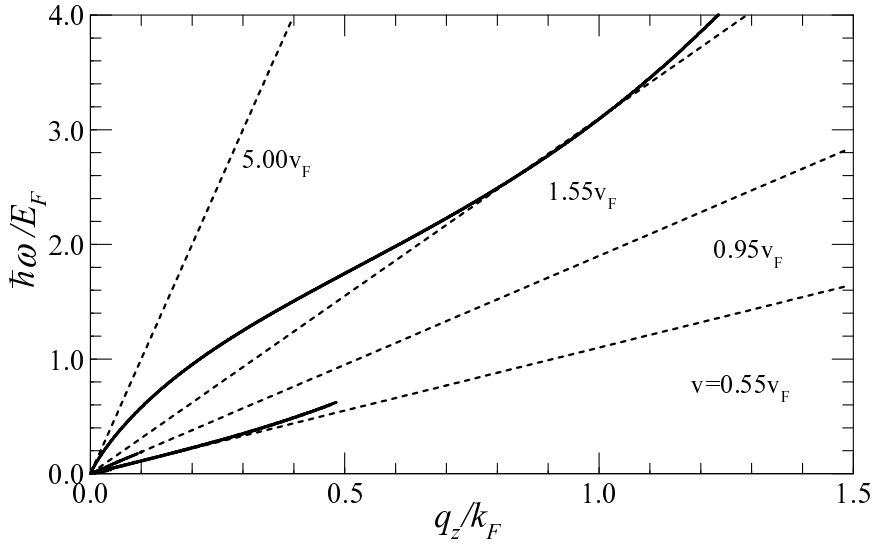

Figure 3.4: The $L = 0$ plasmon excitation energies for a single wall nanotube of $R = 11$ Å. The dashed lines are $\omega = q_z v$, i.e., $\hbar\omega/E_F = 2(q_z/k_F)(v/v_F)$.

we find that there is a contribution to the energy loss. The slope of this straight line increases with v, demonstrating that there is a range of values of charged particle speed below which the stopping power is negligible. The small value of dW/dt for $v \ll v_F$ comes from a narrow region when the excitation energy satisfies $\hbar\omega/E_F \ll 1$. Our numerical calculations clearly show that there is a threshold contribution coming from the plasmon modes whenever the straight line $\omega = q_z v$ just touches the plasmon branches. That is, the plasmon modes start contributing when the $\omega = q_z v$ straight line crosses the lowest plasmon branch. The threshold for the lowest mode corresponds to a speed $v = 0.55 v_F$. This mode gives a small peak in our energy loss plots at the particle velocity. According to Fig. 3.4, the middle plasmon branch contributes when the speed of the charged particle is $v = 0.95 v_F$. The contribution to the energy loss from this mode is small as can be deduced from Fig. 3.4. Finally, when the charged particle speed lies in the range $1.55 v_F < v < 5.00 v_F$, the most energetic plasmon branch contributes. When this branch starts to contribute, we have the high peak in our

energy loss plots at the threshold speed $v = 1.55v_F$. There is a single-particle excitation region below the lowest acoustic plasmon branch which leads to energy loss to these excitations at low charged particle velocity.

3.2 Energy transfer on concentric tubules

We now formulate a theory for the energy-transfer for a charged particle moving parallel to the axis of a multi-walled nanotube consisting of $N > 1$ coaxial nanotubes. The tubules are of radius $R_1, R_2, \ldots, R_N$ and their common axis lies along the z-axis. The velocity of the moving charged particle is $\mathbf{v} = v\hat{z}$ and its position vector is $\mathbf{r}_0 = (\rho_0, \phi_0, z_0 = vt)$.

The total electrostatic potential and the induced charge density at any space-time point $1 = (\mathbf{r}_1, t_1)$ are given respectively by

$$V(1) = \int d^4 2 \; \varepsilon^{-1}(1,2) U(2) \; , \tag{3.30}$$

$$\rho(1) = -\frac{\varepsilon_b}{4\pi e} \nabla_1^2 \left[V(1) - \frac{1}{\varepsilon_b} \; U(1) \right] \; , \tag{3.31}$$

where ε_b is the background dielectric constant and $U(\mathbf{r}, t) = Q/|\mathbf{r} - \mathbf{r}_0(t)|$ is the potential produced by the moving charged particle given by Eq. (3.8). We Fourier transform Eq. (3.30) with respect to the z, ϕ and t variables and we obtain

$$\begin{aligned} V(1) = \int d\rho_2 \rho_2 \int \frac{dq_z}{2\pi} \int \frac{d\omega}{2\pi} e^{i(q_z z_1 - \omega t_1)} \frac{1}{2\pi} \sum_L e^{iL\phi_1} \\ \times \; \varepsilon_L^{-1}(\rho_1, \rho_2, q_z, \omega) U_L(\rho_2, q_z, \omega) \, . \end{aligned} \tag{3.32}$$

According to Eq. (3.8) we can write the potential $U(2)$ as

$$U(\rho_2, \phi_2, z_2, t_2) = \frac{Q}{e^2} \int_{-\infty}^{\infty} \frac{dq_z}{2\pi} e^{iq_z(z_2 - vt_2)} \frac{1}{2\pi} \sum_{L=-\infty}^{\infty} e^{iL\phi_2} u_L(\rho_0, \rho_2, q_z) \; , \tag{3.33}$$

where $u_L(\rho_1, \rho_2, q_z)$ had defined before in Eq. (2.21) and for convenience we choose $\phi_0 = 0$. We therefore obtain from the last equation that

$$U_L(\rho_2, q_z, \omega) = \frac{2\pi Q}{e^2} u_L(\rho_0, \rho_2, q_z) \delta(\omega - q_z v) \; , \tag{3.34}$$

and Eq. (3.32) becomes

$$V(1) = \frac{Q}{e^2}\int d\rho_2\rho_2 \int \frac{dq_z}{2\pi} e^{iq_z(z_1-vt_1)}\frac{1}{2\pi}\sum_L e^{iL\phi_1} \times u_L(\rho_0,\rho_2,q_z)\varepsilon_L^{-1}(\rho_1,\rho_2,q_z,\omega=q_zv)\ , \tag{3.35}$$

where the inverse dielectric function $\varepsilon_L^{-1}(\rho_1,\rho_2,q_z,\omega)$ for the concentric nanotubes is given by Eq. (2.29). We can now find that if we substitute Eqs. (3.33) and (3.35) into Eq. (3.31) the induced charge density $\rho(1)$ at any space-time point is given by

$$\begin{aligned}\rho(1) = -\frac{Q\varepsilon_b}{4\pi e^3}\int_{-\infty}^{\infty}\frac{dq_z}{2\pi}e^{iq_z(z_1-vt_1)}\frac{1}{2\pi}\sum_{L=-\infty}^{\infty}e^{iL\phi_1} \\ \times\left\{\int_0^\infty d\rho_2\rho_2 u_L(\rho_0,\rho_2,q_z)\left[-q_z^2-\frac{m^2}{\rho_1^2}+\frac{1}{\rho_1}\frac{\partial}{\partial\rho_1}\left(\rho_1\frac{\partial}{\partial\rho_1}\right)\right]\right. \\ \left.\times\,\varepsilon_L^{-1}\left(\rho_1,\rho_2,q_z,\omega=q_zv\right)+\frac{4\pi e^2}{\varepsilon_b}\frac{\delta\left(\rho_1-\rho_0\right)}{\rho_1}\right\}.\end{aligned} \tag{3.36}$$

The force and the energy loss that the moving charged particle experiences are $\mathbf{F} = e\int d^31\rho(1)\boldsymbol{\nabla}_1V(1)$ and $dW/dt = \mathbf{F}\cdot\mathbf{v} = F_zv$ respectively. We find for the z-component of this force

$$\begin{aligned}F_z = \frac{Q^2\varepsilon_b}{16\pi^3e^4}i\int_0^\infty d\rho_1\rho_1\int_0^\infty dq_zq_z\sum_{L=-\infty}^{\infty}\left\{\frac{4\pi e^2}{\varepsilon_b}\frac{\delta(\rho_1-\rho_0)}{\rho_1}\right. \\ \left.-\int_0^\infty d\rho_2\rho_2u_L(\rho_0,\rho_2,q_z)\left[q^2+\frac{m^2}{\rho_1^2}-\frac{1}{\rho_1}\frac{\partial}{\partial\rho_1}\left(\rho_1\frac{\partial}{\partial\rho_1}\right)\right]\varepsilon_L^{-1}(\rho_1,\rho_2,q_z,\omega=q_zv)\right\} \\ \times\int_0^\infty d\rho_3\rho_3u_L(\rho_0,\rho_3,q_z)\varepsilon_L^{-1}(\rho_1,\rho_3,-q_z,\omega=-q_zv)\,.\end{aligned} \tag{3.37}$$

The q_z-integral for the second term in curly bracket on the right hand side of Eq. (3.37) vanishes because the integrand is an odd function of q_z. This can be proven if we use the following symmetry properties of the inverse dielectric function

$$\varepsilon_L^{-1}(\rho_1,\rho_2,q_z,\omega) = \varepsilon_L^{-1}(\rho_1,\rho_2,-q_z,\omega)\ , \tag{3.38}$$

$$\Re e\left[\varepsilon_L^{-1}(\rho_1,\rho_2,q_z,\omega)\right] = \Re e\left[\varepsilon_L^{-1}(\rho_1,\rho_2,-q_z,\omega)\right]\ , \tag{3.39}$$

$$-\Im m\left[\varepsilon_L^{-1}(\rho_1,\rho_2,q_z,\omega)\right] = \Im m\left[\varepsilon_L^{-1}(\rho_1,\rho_2,q_z,-\omega)\right]\ . \tag{3.40}$$

Therefore Eq. (3.37) becomes

$$F_z = \frac{Q^2}{4\pi^2 e^2} i \int_{-\infty}^{\infty} dq_z q_z \sum_{L=-\infty}^{\infty} \int_0^{\infty} d\rho_3 \rho_3 u_L(\rho_0, \rho_3, q_z) \times \varepsilon_L^{-1}(\rho_1 = \rho_0, \rho_3, q_z, \omega = -q_z v) \ , \tag{3.41}$$

or expressing $\varepsilon_L^{-1}(\rho_1, \rho_2, q_z, \omega)$ in terms of its real and imaginary parts and using Eqs. (2.29), (3.38) we finally obtain

$$F_z = -\frac{Q^2}{4\pi^3 e^2 \varepsilon_b^2} \sum_{L=-\infty}^{\infty} \int_0^{\infty} dq_z q_z \sum_{j,j'=1}^{N} u_L(\rho_0, R_j, q_z) u_L(\rho_0, R_{j'}, q_z) \times \Im m \left[\chi_{j,L}(q_z, \omega = q_z v) A^{-1}_{L,jj'}(q_z, \omega = q_z v) \right] \ , \tag{3.42}$$

and from this we have for the rate of loss of energy

$$\frac{dW}{dt} = -\frac{Q^2 v}{4\pi^3 e^2 \varepsilon_b^2} \sum_{L=-\infty}^{\infty} \int_0^{\infty} dq_z q_z \sum_{j,j'=1}^{N} u_L(\rho_0, R_j, q_z) u_L(\rho_0, R_{j'}, q_z) \times \Im m \left[\chi_{j,L}(q_z, \omega = q_z v) A^{-1}_{L,jj'}(q_z, \omega = q_z v) \right] . \tag{3.43}$$

The matrix elements $A_{L,jj'}(q_z, \omega)$ are given by Eq. (2.27).

We want now to analyze the contribution to the energy loss formula Eq. (3.43) of the two possible types of excitations that are possible in our model for the electron gas. For this purpose we write

$$A^{-1}_{L,jj'}(q_z, \omega) = \frac{C_{L,jj'}(q_z, \omega)}{\det A_L(q_z, \omega)} \ , \tag{3.44}$$

$$\det A_L(q_z, \omega) = A_{1,L}(q_z, \omega) + i A_{2,L}(q_z, \omega) \ , \tag{3.45}$$

where $A_{1,L}(q_z, \omega)$, $A_{2,L}(q_z, \omega)$ represent the real and imaginary part of $\det A_L(q_z, \omega)$ respectively. Equation (3.43) then can be written as

$$\frac{dW}{dt} = -\frac{Q^2 v}{4\pi^3 e^2 \varepsilon_b^2} \sum_{j,j'=1}^{N} \sum_{L=-\infty}^{\infty} \int_0^{\infty} u_L(\rho_0, R_j, q_z) u_L(\rho_0, R_{j'}, q_z) \times \left\{ \Re e \left[\frac{1}{\det A_L(q_z, \omega)} \right] \Im m \left[\chi_{j,L}(q_z, \omega) C_{L,jj'}(q_z, \omega) \right] + \Im m \left[\frac{1}{\det A_L(q_z, \omega)} \right] \Re e \left[\chi_{j,L}(q_z, \omega) C_{L,jj'}(q_z, \omega) \right] \right\} \Bigg|_{\omega = q_z v} . \tag{3.46}$$

We study the simplest case that $N = 2$, i.e., a system of two concentric nanotubes. If $A_{2,L}(q_z, \omega) \neq 0$ then we have according to Eq. (3.46) loss of the energy of the particle due to particle-hole excitations. If $A_{2,L}(q_z, \omega) = 0$ and $A_{1,L}(q_z, \omega) \neq 0$ then there is no energy loss. In the case though that $A_{2,L}(q_z, \omega) = 0$ and $A_{1,L}(q_z, \omega) = 0$ we have energy loss due to the plasmons excitations. Using the fact that $A_{2,L}(q_z, \omega) = 0 \Rightarrow \Im m\left[\chi_{j,L}(q_z, \omega)\right] = 0$ we rewrite Eq. (3.46) in this case as

$$\left.\frac{dW}{dt}\right|_{\text{plasmons}} = \frac{Q^2 v}{4\pi^2 e^2 \varepsilon_b^2} \sum_{j,j'=1}^{2} \sum_{L=-\infty}^{\infty} \int_0^{\infty} dq_z q_z u_L(\rho_0, R_j, q_z) u_L(\rho_0, R_{j'}, q_z) \times \frac{\delta\left(\omega - \omega_L(q_z)\right)}{\left|dA_{1,L}(q_z, \omega)/d\omega\right|_{\omega = q_z v}} \Re e\left[\chi_{j,L}(q_z, \omega) C_{L,jj'}(q_z, \omega)\right]|_{\omega = q_z v} \,, \quad (3.47)$$

where $\omega_L(q_z)$ represents the plasmon excitations dispersion for fixed L, i.e., the solutions of the equation $\det A_L(q_z, \omega) = 0$. For the case of study($N = 2$) the matrix $C_L(q_z, \omega)$ has the form

$$C_L(q_z, \omega) = \begin{pmatrix} \varepsilon_{2,L}(q_z, \omega) & \dfrac{-\chi_{2,L}(q_z, \omega) u_L(R_1, R_2, q_z)}{(2\pi)^2 \varepsilon_b} \\ \dfrac{-\chi_{1,L}(q_z, \omega) u_L(R_1, R_2, q_z)}{(2\pi)^2 \varepsilon_b} & \varepsilon_{1,L}(q_z, \omega) \end{pmatrix} , \quad (3.48)$$

where $\varepsilon_{j,L}(q_z, \omega)$ is the single nanotube dielectric function. The double sum $\sum_{j,j'}$ of Eqs. (3.46) and (3.47) can be split as $\sum_{j,j'} = \sum_{j=j'} + \sum_{j \neq j'}$. The sum over the diagonal terms ($j = j'$) gives then the energy loss because of the interaction of the particle with each tubule separately (there is no interaction between the 2 tubules). The sum though over the non-diagonal terms ($j \neq j'$) give the energy loss because of the interaction of the particle with the two interacting tubules. We note that the non-diagonal matrix elements of the matrix $C_L(q_z, \omega)$ are proportional to $u_L(R_1, R_2, q_z)$ describing the effect of the interaction between the two tubules. In the case that this interaction is zero (or very small in comparison with interactions $u_L(R_j, R_j, q_z)$ within a tubule) then the matrix $C_L(q_z, \omega)$ becomes diagonal and only the sum $\sum_{j=j'}$ survives, i.e., the particle"feels" two nanotubes that they do not

interact with each other. Because of their importance the numerical results for the power loss in the case of concentric cylinders will be presented and discussed in the next chapter.

3.3 Energy transfer on two parallel tubules

We consider two parallel nanotubes of radii R_1 and R_2 with their axes being parallel to the z-axis and separated by a distance $a > R_1 + R_2$. An electron confined to the surface of the j-th nanotube ($j = 1, 2$) is described by the single particle wavefunctions and energy eigenvalues given by Eqs. (2.36) and (2.37). Using these eigenstates and working in a similar way as in Sec. 2.2 we find that the inverse dielectric function for the two parallel tubules is given by the expression

$$\varepsilon^{-1}(\boldsymbol{\rho}_1, \boldsymbol{\rho}_2, q_z, \omega) = \frac{1}{\varepsilon_b}\, \delta(\boldsymbol{\rho}_1 - \boldsymbol{\rho}_2) - \frac{2e^2}{\varepsilon_b} \sum_j \sum_{m,m'} \chi_{j,m}(q_z, \omega) \times K_{j,m}(\boldsymbol{\rho}_2, q_z, \omega)\, \omega_{jmm'}(q_z, R_j, \rho_1, a)\, e^{-im'\varphi_1} \ , \qquad (3.49)$$

where

$$\omega_{jmm'}(q_z, R_j, \rho_1, a) \equiv \int_0^\infty dq_\perp \frac{q_\perp}{q_\perp^2 + q_z^2} J_m(q_\perp R_j) J_{m'}(q_\perp \rho_1) J_{m'-m}\left((j-1)\, q_\perp a\right) \ ,$$

$$K_{j,m}\left(\boldsymbol{\rho}_2, q_z, \omega\right) \equiv \int d\boldsymbol{\rho}_3 \Psi^*_{jl}\left(\boldsymbol{\rho}_3\right) \Psi_{jl'}\left(\boldsymbol{\rho}_3\right) \varepsilon^{-1}\left(\boldsymbol{\rho}_3 + (j-1)\, a\hat{e}_x, \boldsymbol{\rho}_2, q_z, \omega\right) \ .$$

The quantities $K_{j,m}\left(\boldsymbol{\rho}_2, q_z, \omega\right)$ can be found from the solution of the set of equations

$$\sum_{j'=1}^{2} \sum_{m'=-\infty}^{\infty} \left[\delta_{jj'}\delta_{mm'} + \frac{2e^2}{\varepsilon_b} \chi_{j',m'}\left(q_z, \omega\right) U_{mm'}(q_z, R_j, R_{j'}, a)\right] K_{j',m'}\left(\boldsymbol{\rho}_2, q_z, \omega\right) = \frac{1}{\varepsilon_b} \Psi^*_{jl}\left(\boldsymbol{\rho}_2 - (j-1)\, a\hat{e}_x\right) \Psi_{jl'}\left(\boldsymbol{\rho}_2 - (j-1)\, a\hat{e}_x\right) \ , \qquad (3.50)$$

with $U_{mm'}$ given by

$$U_{mm'}(q_z, R_j, R_{j'}, a) = \int_0^\infty dq_\perp \frac{q_\perp}{q_\perp^2 + q_z^2} J_m(q_\perp R_j) J_{m'}(q_\perp R_{j'}) J_{m'-m}\left((j-j')\, q_\perp a\right). \qquad (3.51)$$

The dispersion equation for plasmon excitations can be found solving for the poles of $\varepsilon^{-1}(\boldsymbol{\rho}_1, \boldsymbol{\rho}_2, q_z, \omega)$, which are given by the condition $\det A(q_z, \omega) = 0$ where A is the matrix with elements

$$A_{jmj'm'}(q_z, \omega) = \delta_{jj'}\delta_{mm'} + \frac{2e^2}{\varepsilon_b}\chi_{j',m'}(q_z, \omega)\, U_{mm'}(q_z, R_j, R_{j'}, a)\,. \tag{3.52}$$

The same dispersion equation for the plasma modes had been found in Eq. (2.49) using a different way. According to Eq. (3.8) a particle of charge Q moving parallel to the pair of nanotubes with a position vector $\mathbf{r}_0 = (\boldsymbol{\rho}_0, z_0 = vt)$, where v is the speed of the particle, creates an electrostatic potential $U(\mathbf{r}, t)$ at any space-time point $(\mathbf{r}, t)$ which is given by

$$U(\mathbf{r}, t) = \frac{Q}{e^2}\int_{-\infty}^{\infty}\frac{dq_z}{2\pi}\, e^{iq_z(z-vt)}\frac{1}{2\pi}\sum_{m=-\infty}^{\infty} e^{im(\varphi-\varphi_0)}u_m(\rho_0, \rho, q_z)\ , \tag{3.53}$$

where $u_m(\rho_0, \rho, q_z)$ is given by Eq. (2.21). The total potential and the induced charge density at any space-time point 1 are given by Eqs. (3.31) and (3.32) respectively and the force exerted on the moving charged particle because of the induced charge density is $\mathbf{F} = e\int d^4 3\rho(1)\boldsymbol{\nabla}_1 V(1)$. We look again at the z-component of this force which causes frictional loss of the particle's kinetic energy. Our calculation gives for the power loss

$$\begin{aligned}\frac{dW}{dt} = F_z v = \frac{Q^2}{(2\pi)^3 e^2 \varepsilon_s}\, v\int_{-\infty}^{\infty} dq_z i q_z \sum_{j=1}^{2}\sum_{n,m,m'}\chi_{j,m}(q_z, \omega)F_{j,n,m}(\boldsymbol{\rho}_0, q_z, \omega)\\ \times\left\{G_{m,m'}(\boldsymbol{\rho}_0, q_z, a) - 2e^2\sum_{j'=1}^{2}\sum_{s,p}(-1)^s\chi_{j',s}(q_z, -\omega)\right.\\ \left.\times\, F_{j',s,p}(\boldsymbol{\rho}_0, q_z, -\omega)L_{jj',mm',s}(q_z, a)\right\}\ ,\end{aligned} \tag{3.54}$$

where n, m, m', s and p run over all integers, $\omega = q_z v$ and

$$\begin{aligned}F_{j,n,m}(\boldsymbol{\rho}_0, q_z, \omega) &= e^{-in\phi_0}\int d\boldsymbol{\rho}_2 e^{in\phi_2}u_n(\rho_0, \rho_2, q_z)K_{j,m}(\boldsymbol{\rho}_2, q_z, \omega)\ ,\\ G_{m,m'}(\boldsymbol{\rho}_0, q_z, a) &= e^{-im'\phi_0}\int_0^{\infty} dq_\perp q_\perp J_m(q_\perp R_j)J_{m'-m}\left((j-1)\, q_\perp a\right)\\ &\quad\times\int_0^{\infty} d\rho_1\rho_1 J_{m'}(q_\perp\rho_1)u_{m'}(\rho_1, \rho_0, q_z)\ ,\end{aligned}$$

$$L_{jj',mm',s}(q_z,a) = \int_0^\infty dq_\perp \frac{q_\perp}{q_\perp^2+q_z^2} J_m(q_\perp R_j) J_{m'-m}\left((j-1)q_\perp a\right) \\ \times \;\; J_s(q_\perp R'_j) J_{m'+s}\left((j'-1)q_\perp a\right) \;\; .$$

When we take the limit $a \to \infty$ equation (3.54) reduces to the result given by Eq. (3.25) for one nanotube. We assume for convenience that the two nanotubes are identical, i.e., they have the same radius R and the electron gas on each tubule has the same E_F. We look at the simplest case that the angular momentum transfer $m = l - l'$ of the plasmon excitations is 0. The energy loss formula given by (3.54) in this case takes the form

$$\frac{dW}{dt} = -\frac{Q^2}{2\pi^3 {\varepsilon_b}^2}\, v \int_0^\infty dq_z q_z \int_0^\infty dq_\perp \frac{q_\perp}{q_\perp^2+{q_z}^2} J_0(q_\perp R) J_0(q_\perp \rho_0) \\ \times \int_0^{2\pi} d\phi \sum_{n=-\infty}^{+\infty} \sum_{j,j'=1}^{2} J_0\left((j-1)q_\perp a\right) e^{in[\, f_{j'}(\phi)-\phi_0]} u_{nj'}\left(\rho_0, \rho_{j'}(\phi), q_z\right) \\ \times \Im m\left[\chi_0(q_z, \omega = q_z v) A^{-1}_{jj'}(q_z, \omega = q_z v)\right]. \qquad (3.55)$$

The matrix $A_{jj'}(q_z,\omega)$ is given by Eq. (3.52) when we use $m = m' = 0$, and the functions $\rho_{j'}(\phi)$ and $f_{j'}(\phi)$ are given respectively by the expressions

$$\rho_{j'}(\phi) = \arccos\left[R^2 + (j'-1)^2 a^2 + 2aR(j'-1)\cos\phi\right]^{1/2} \;\; , \\ f_{j'}(\phi) = \arcsin\left[\frac{R\sin\phi}{\rho_{j'}(\phi)}\right].$$

The separation of the last factor in Eq. (3.55) into the real and imaginary parts of the determinant of the matrix $A_{jj'}$ again identifies the contributions to the energy loss. We will discuss the numerical results coming from Eq. (3.55) in the next chapter, because of their close connection to the plasma instability.

Chapter 4

PLASMA INSTABILITIES

Following the extensive work on gaseous plasmas [46], there has been a considerable amount of effort devoted to the instabilities created in solid-state plasmas by the transfer of energy from a constant current to spontaneously generated plasmon excitations in solid-state plasmas such as semiconductor heterostructures, like two-dimensional layers and superlattices [47]-[53], as well as parallel quantum wire systems [54]. The interest has been stimulated by the potential applications as an infrared laser source or solid state analogs of traveling-waves amplifiers [50], [55]-[57]. The frequency of the emitted radiation has been estimated in the terahertz range for high mobility AlGaAs/InGaAs heterostructures [55]. In Refs.[48]-[52], direct current driven plasma instabilities were considered when current flowed in either the same or neighboring layer as the plasma excitations. Because of the energy transfer from the current to the plasma excitations, there could be an amplification of the collective modes. In principle, this energy could in turn be converted to electromagnetic radiation. For the 2D and superlattice semiconductor heterostructures, there are estimates of the minimum carrier drift velocity for the instability to occur. However, the challenge has been to have the instability occur at drift velocities which are attainable experimentally.

Since instabilities may arise when the drift velocity of the electrons lies within a range which is determined by the phase velocity for the plasmon modes, we may exploit the results of the two previous chapters to study them.

4.1 Drift velocity thresholds for plasma instabilities on tubules

We consider the effect of applying a uniform electric field to a system of two parallel nanotubes which have the same radius $R_1 = R_2 = R$. For any given wave vector q_z, the modes become unstable by the transfer of energy from the current to the plasma wave. This instability occurs if the drift velocity v_D of the electrons exceeds the phase velocity of a plasma wave branch of frequency ω, i.e., $v_D > \omega/q_z$ [53, 56], but it may have an upper bound, as we show below. We now calculate and study the plasmon excitation spectrum and phase velocity by introducing a drift velocity $v_D^{(l,1)}, v_D^{(l,2)}$ parallel to the axis of the nanotube. This leads to a Doppler shift in the susceptibility. If the current is driven in the j-th nanotube, the dispersion relation in Eq. (2.55) is modified by replacing ω in $\chi_{j,0}(q_z,\omega)$ by $\omega - q_z v_D^{(l,j)}$ for subband l. At the threshold of instability, $\Im m\,(\omega) = 0$ and the modified dispersion equation provides the relation between q_z and the phase velocity v_P for chosen values of the drift velocity. Because of the summation over l in Eq. (2.24) for arbitrary maximum value S_j of $|l|$ among the subbands occupied by electrons in the j-th cylindrical nanotube, it is not possible to obtain a general expression for the threshold boundary curve for the region of current-driven instability. In this regard, let us consider the long wavelength limit and approximate $\Re e\,\chi_{j,L}(q_z,\omega)$, taking account of a drift velocity $v_D^{(l,j)}$ for each subband l on the j-th nanotube. Each subband may have a different drift

velocity. We have (generalizing the result of Appendix C)

$$\Re e\,\chi_{j,L=0}(q_z,\omega) \approx -\frac{q_z^2}{m^*}\sum_{l=-S_j}^{S_j}\frac{n_{lj}}{(\omega - q_z v_D^{(l,j)})^2 - v_{Flj}^2 q_z^2}\ , \tag{4.1}$$

where $n_{lj} = 2k_{Flj}/\pi$ is the linear density for subband l on the j-th nanotube. Substituting this into the dispersion equation (2.55), we obtain (since $R_1 = R_2 = R$)

$$\begin{aligned}
&\left[1 - q_z^2 u_0(R,R,q_z)\sum_{l=0,\pm1,\cdots}\frac{\gamma_l^{(1)}}{\left(\omega - q_z v_D^{(l,1)}\right)^2 - v_{Fl1}^2 q_z^2}\right] \\
&\times\left[1 - q_z^2 u_0(R,R,q_z)\sum_{l=0,\pm1,\cdots}\frac{\gamma_l^{(2)}}{\left(\omega - q_z v_D^{(l,2)}\right)^2 - v_{Fl2}^2 q_z^2}\right] \\
&- V^2 q_z^4\sum_{l=0,\pm1,\cdots}\frac{\gamma_l^{(1)}}{(\omega - q_z v_D^{(l,1)})^2 - v_{Fl1}^2 q_z^2} \\
&\times\sum_{l=0,\pm1,\cdots}\frac{\gamma_l^{(2)}}{\left(\omega - q_z v_D^{(l,2)}\right)^2 - v_{Fl2}^2 q_z^2} = 0\ ,
\end{aligned} \tag{4.2}$$

where $u_0(R,R,q_z) = 4\pi e^2 I_0(q_z R)K_0(q_z R)$, $V = 4\pi e^2 I_0^2(q_z R)K_0(q_z a)$, and $\gamma_l^{(j)} = n_{lj}/2\pi m^* \varepsilon_b$. In this notation $v_{Flj} = \hbar k_{Flj}/m^*$ is the Fermi velocity of the l-th subband of the j-th nanotube. If only the $l = 0$ subband is occupied so that just one term contributes to each sum in Eq. (4.2) and we denote the drift velocity for the $l = 0$ subband on a nanotube by $v_D^{(l=0,j)} = v_D^{(j)}$, we obtain the following equation determining ω,

$$\begin{aligned}
&\left(\Omega^2 - q_z^2\overline{v}_D^2\right)^2 - (\Omega - q_z\overline{v}_D)^2(v_{F2}^2 + \gamma_0^{(2)}u_0)q_z^2 - (\Omega + q_z\overline{v}_D)^2(v_{F1}^2 + \gamma_0^{(1)}u_0)q_z^2 \\
&+ \left[\left(v_{F1}^2 + \gamma_0^{(1)}u_0\right)\left(v_{F2}^2 + \gamma_0^{(2)}u_0\right) - \gamma_0^{(1)}\gamma_0^{(2)}V^2\right]q_z^4 = 0\ ,
\end{aligned} \tag{4.3}$$

where $\Omega \equiv \omega - q_z(v_D^{(1)} + v_D^{(2)})/2$, $\overline{v}_D \equiv (v_D^{(1)} - v_D^{(2)})/2$ and $v_{Fj} = v_{Fl=0,j}$. In general, this is a quartic equation which may have real or complex solutions depending on the values chosen for the relevant variables. If the term linear in Ω is sufficiently small to be neglected, we a have a biquadratic equation

$$\Omega^4 - (A + 2\overline{v}_D^2)q_z^2\Omega^2 + (\overline{v}_D^4 - A\overline{v}_D^2 + B)q_z^4 = 0\ , \tag{4.4}$$

where

$$A = v_{F1}^2 + \gamma_0^{(1)} u_0 + v_{F2}^2 + \gamma_0^{(2)} u_0 \ ,$$
$$B = \left[v_{F1}^2 + \gamma_0^{(1)} u_0 \right] \left[v_{F2}^2 + \gamma_0^{(2)} u_0 \right] - \gamma_0^{(1)} \gamma_0^{(2)} \overline{V}_{0,0}^2 \ , \tag{4.5}$$

with $V_{0,0}$ given by Eq. (2.53). We note that since $q_z R \ll 1$,we have that $u_0(R, R, q_z) > 0$ and therefore $A > 0$. The solutions are

$$\Omega_\pm^2 = \frac{q_z^2}{2} \left\{ \left(A + 2\overline{v}_D^2 \right) \pm \left[\left(A + 2\overline{v}_D^2 \right)^2 - 4 \left(\overline{v}_D^4 - A\overline{v}_D^2 + B \right) \right]^{1/2} \right\} \ . \tag{4.6}$$

Instability of the plasmons occur when $\Omega_\pm^2 < 0$. The solutions $\Omega_\pm^2$ are both real and in addition Ω_+^2 can not be negative. Therefore we demand that $\Omega_-^2 < 0$ which in turn gives that $\overline{v}_D^4 - A\overline{v}_D^2 + B < 0$. From this we find that $\omega_- < q_z \overline{v}_D < \omega_+$ where

$$\omega_\pm^2 = \frac{1}{2} \left(v_{F1}^2 + \gamma_0^{(1)} u_0 + v_{F2}^2 + \gamma_0^{(2)} u_0 \right) q_z^2$$
$$\pm \frac{1}{2} \left\{ \left[\left(v_{F1}^2 + \gamma_0^{(1)} u_0 \right) - \left(v_{F2}^2 + \gamma_0^{(2)} u_0 \right) \right]^2 + 4\gamma_0^{(1)} \gamma^{(2)} \overline{V}_{0,0}^2 \right\}^{1/2} q_z^2 \ , \tag{4.7}$$

correspond to acoustic and optical plasmon mode frequencies which are solutions of Eq. (4.4) when $\overline{v}_D^{(1)} = \overline{v}_D^{(2)} = 0$. In this case Ω_- can be written as $\Omega_- = i|\Omega_-|$ and the time evolution of this mode is proportional to $e^{-i\Omega_- t} = e^{|\Omega_-| t}$ which shows that this collective mode is unstable and grows exponentially (for as long as the linear response theory used is valid) . Equation (4.7) agrees with Eq. (2.57) when $v_{Fj}^2 \ll \gamma_0^{(j)} u_0$ and we assume that the linear density is the same for each nanotube. These analytic results are valid only for the modes above the particle-hole region, therefore they are not Landau damped, and when the instability leads to a decay of the plasmon modes with time. Also, the analytic results for the regions of instability are only valid in the long wavelength limit where the plasmon frequencies are not affected by a drift current. An analytic expression for the stability of the plasmon modes may be obtained for arbitrary density after

some tedious algebra but Eq. (4.4) is sufficient to demonstrate that the plasmon modes can become unstable for two parallel cylindrical nanotubes when there is a relative drift of the carriers in the coupled system. Furthermore, for the special case when the two parallel nanotubes are identical with $v_{F1} = v_{F2}$ and $\gamma_0^{(1)} = \gamma_0^{(2)}$, Eq. (4.3) reduces to a quadratic in Ω^2 and the region of current-driven instability can again be established [54] for this case of a pair of coupled nanotubes when only the lowest subband ($l = 0$) is occupied. If more than one subband is occupied, then we must include terms in the sum in Eq. (4.2) in addition to the $l = 0$ term. Clearly, in this case, we may determine a relation for plasmon instability even for one nanotube since the inter-tubule coupling is not needed to obtain multiple branches. If the $l = 0, \pm 1$ subbands are occupied for a single nanotube, a straightforward calculation shows that the plasmon excitations have frequency determined by

$$\left(\Omega^2 - q_z^2\overline{v}_D^2\right)^2 - (\Omega - q_z\overline{v}_D)^2(v_{F1}^2 + 2\gamma_1 u_0)q_z^2 - (\Omega + q_z\overline{v}_D)^2(v_{F0}^2 + \gamma_0 u_0)q_z^2 + \left[v_{F0}^2 v_{F1}^2 + u_0(v_{F1}^2 + 2v_{F0}^2)\right] q_z^4 = 0 \ , \tag{4.8}$$

where now $\Omega \equiv \omega - q_z(v_D^{(l=0,j=1)} + v_D^{(l=1,j=1)})/2$, $\overline{v}_D \equiv (v_D^{(l=0,j=1)} - v_D^{(l=1,j=1)})/2$, $v_{Fl} = v_{Fl,j=1}$ is the Fermi velocity for the l-th subband and the superscript on γ_l has been omitted for convenience. Again, these analytic results are restricted to the long wavelength limit. However, they imply that there is an instability when the average drift velocity exceeds the phase velocity of the lower of the split plasmon branches above the particle-hole mode region but is bounded above by the phase velocity of the highest plasmon branch. If, in general, the plasmon modes become unstable when the average drift velocity is bounded by the plasmon phase velocity for split plasmon branches, there will be several regions of instability in the pockets of the particle-hole mode region. In Fig. 2.6, we presented the results for the ground ($m = 0$) subband plasmon excitations of two parallel identical nanotubes of radius $R_1 = 11$ Å separated by a distance $a = 25$ Å when there

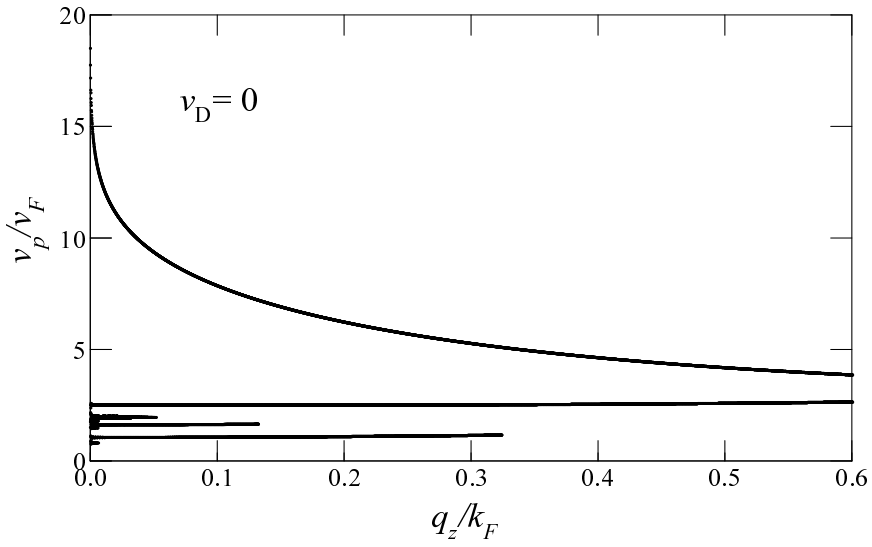

Figure 4.1: The phase velocity v_p of the plasmons shown in Fig. 2.6 as a function of q_z for the case of zero electric field, i.e., when $v_D^{(1)} = v_D^{(2)} = 0$.

is no electric field applied ($v_D^{(1)} = v_D^{(2)} = 0$). In Fig. 4.1 we present the phase velocity corresponding to these plasmons.

In Fig. 4.2(a) we present results showing how the plasmon excitation frequencies of the same nanotubes are modified by a finite value of the drift velocity. We chose $v_D^{(1)} = 0.8v_F$ and $v_D^{(2)} = 0$. Comparing Figs. 2.6 and 4.2(a) we observe that the finite drift velocity does not noticeably affect the optical and acoustic branches when $q_z \ll k_F$ but it does modify the lower modes in this limit. The boundaries of the particle-hole modes are shifted when there is a drift velocity present. The replacement $\omega \to \omega - q_z v_D$ in the dispersion formula leads to a modification of the particle-hole mode boundaries. The resulting undamped plasmons obtained from our numerical calculations which lie outside these new boundaries were plotted. In Fig. 4.2(b) we plotted the phase velocity of the plasmon spectrum of Fig. 4.2(a). the least energetic plasmons have a phase velocity which is less than the Fermi velocity. However the oscillator strengths of these modes are not as large as the high frequency plasmons. Some of the features of the plasmon

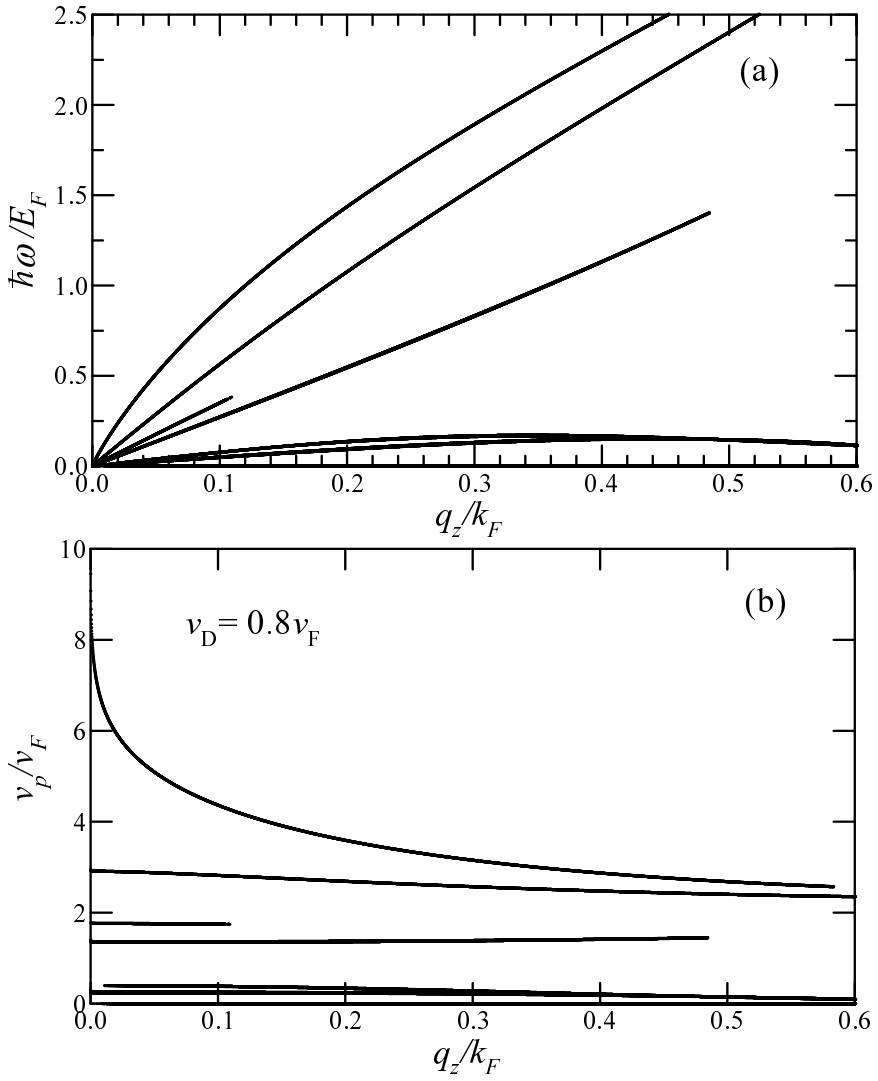

Figure 4.2: (a) The plasmon excitation energy in the ground ($m = 0$) subband for a pair of identical parallel nanotubes with a separation $a = 25$ Å when $v_D^{(1)} = 0.8v_F$ and $v_D^{(2)} = 0$. (b) The phase velocity of the plasmons shown in (a).

spectrum may be verified using the standard electron energy loss technique.

4.2 Plasma instabilities on parallel and concentric tubules

In this section, we present numerical results for the energy transfer and plasmon excitation spectra for a double-wall nanotube and for a pair of single-wall nanotubes whose axes are parallel. The calculations are based on the formulas we derived before in Secs. 3.2 and 3.3. Our results are presented in Figs. 4.3-4.9. In Figs. 4.3-4.4, we plot the plasmon contributions to dW/dt for various impact parameters for chosen R_1 and R_2 of a double-wall nanotube. Figure 4.5 shows the single-particle excitation contribution for the same pair of tubules in Fig. 4.3. There are six plasmon branches, with the highest branch at resonance with the impinging charged particle velocity when its phase velocity is $v = 1.63v_F$, the second highest branch when $v = 1.25v_F$ and subsequent branches as indicated on the plasmon dispersion relation in Fig. 4.6. In this figure, only the plasmon branches which are not Landau damped by the single-particle excitations are given. The abrupt termination of the plasmon modes in Fig. 4.6 arises when the plasmon branches enter the single-particle excitation regions. There are three plasmon branches for each uncoupled tubule, i.e., when the Coulomb interaction between the tubules is neglected. This is the reason why there are six plasmon branches in Fig. 4.6. All of the branches in Fig. 4.6 either have a corresponding peak or dip in Figs. 4.3(a)-(c), but some are too weak to be observed on this scale. Only the second highest branch has a "dip" in the energy transfer spectrum. We were able to identify the peaks and dips in the energy transfer spectrum by drawing the straight lines $\omega = vq_z$ which determine the energy loss contributions. When the slope of the straight line is increased and this line first touches a plasmon

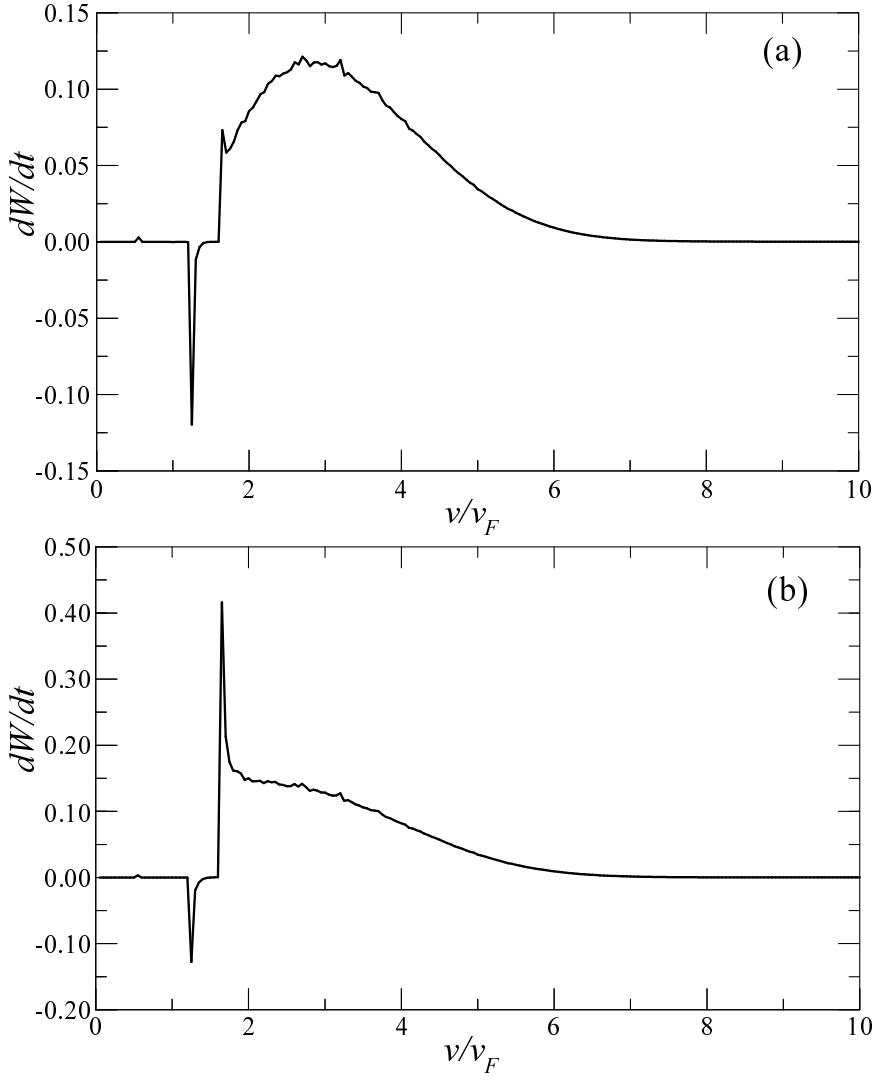

Figure 4.3: The rate of energy transfer when $L = 0$ due to plasmons as a function of the charged particle velocity parallel to the axis of the double-wall nanotube. The energy transfer is expressed in units of $e^2 k_F^2 v_F$ and the velocity in units of v_F. In this notation, $k_F = \sqrt{2m^* E_F}/\hbar$ and $v_F = \hbar k_F / m^*$. The radii of the nanotubes are $R_1 = 11$ Å, $R_2 = 15$ Å. The values of the impact parameters ρ_0 are (a) 0 Å, (b) 10 Å. We chose $\varepsilon_b = 2.4$, the electron effective mass $m^* = 0.25 m_e$ where m_e is the bare electron mass.

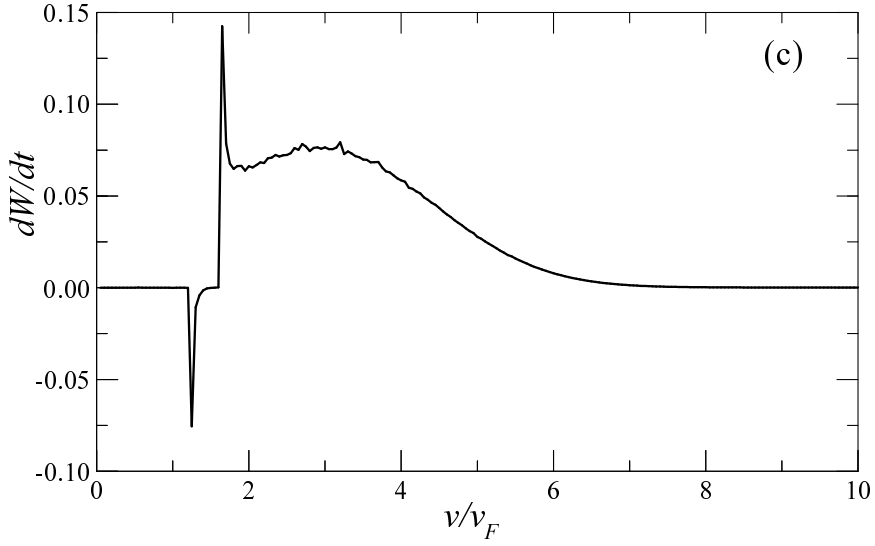

Figure 4.3: (c) The same as before but for impact parameter 17 Å.

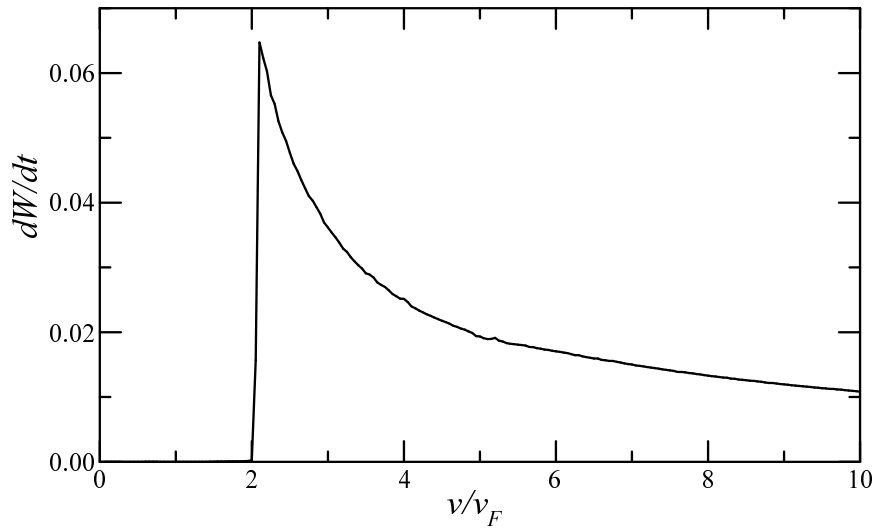

Figure 4.4: The rate of energy transfer when $L = 1$ due to plasmons as a function of the charged particle velocity parallel to the axis of the double-wall nanotube when $\rho_0 = 15$ Å.

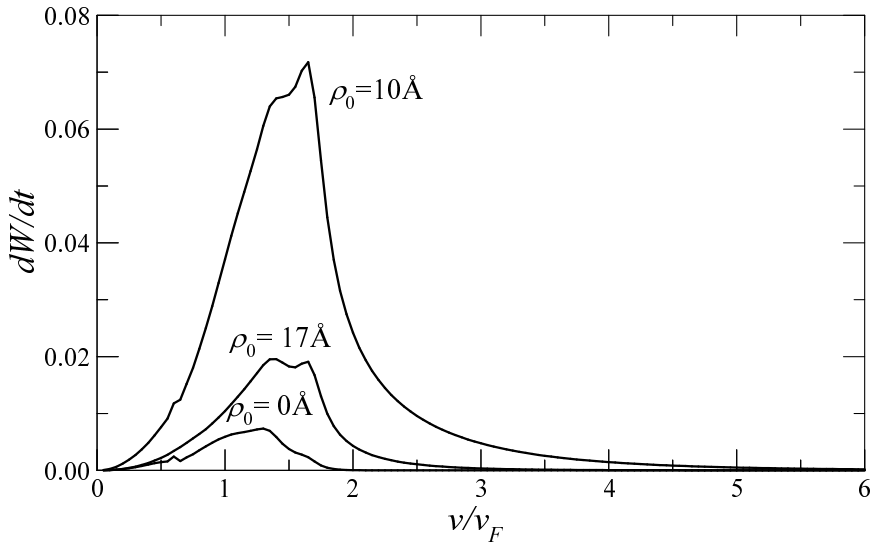

Figure 4.5: The rate of loss of energy from single-particle excitations within the $L = 0$ subband for a pair of coaxial tubules of radius $R_1 = 11$ Å and $R_2 = 15$ Å. All other material parameters for the background dielectric and electron effective mass are the same as in Fig. 4.3. The values for the impact parameter ρ_0 are indicated on the plots.

branch, the slope of this straight line corresponds to the resonance velocity in dW/dt. Furthermore, as the gradient of this straight line increases further, there is a range of values of particle velocity when the line sweeps through a plasmon branch. The height of the peak or depth of the dip depends on the impact parameter but its location on the velocity axis is independent of ρ_0. In Fig. 4.4 we plotted the energy loss to plasmons of $|L| = 1$ when $\rho_0 = 10$ Å. We see that this has the same form as in the case of one tubule (see Fig. 3.3(b)), and it does not have any instability dip. In contrast to the results in Fig. 4.3, Fig. 4.5 shows that irrespective of the impact parameter, the energy loss spectrum for single-particle excitations is always positive. The single-particle continuum corresponds to the peak positions which are also unchanged as the impact parameter is varied. However, the heights of the peaks depend on ρ_0. We further investigate the resonance

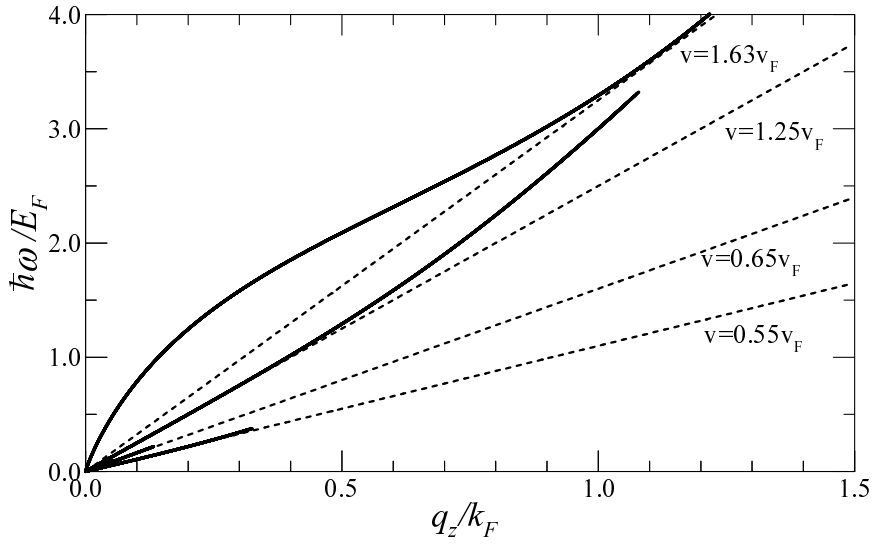

Figure 4.6: The $L = 0$ plasmon dispersion for the pair of coaxial nanotubes in Fig. 4.3. The straight lines $\omega = vq_z$ show when the plasmon branch contributes to dW/dt.

structure of Fig. 4.3. Except for the two most energetic plasmons, the branches of plasmon excitations lie within the gaps between single-particle excitations. In the long wavelength limit, the frequency of the second highest mode depends linearly on the wave number q_z (see Eq. (2.35)). On the other hand, instead of having a constant phase velocity, the highest mode has a phase velocity which exhibits a logarithmic dependence on wave number as we proved. Although some of the lower frequency modes have an almost constant phase velocity for small q_z, the second most energetic mode has the widest range over which the charged particle velocity could exactly coincide with its phase velocity. The dip occurs when the charged particle velocity lies in the range $1.00v_F$ to $1.50v_F$ which is shown in Fig. 4.6. Consequently, we must be investigate the plasmon excitations whose frequencies lie in the region bounded by straight lines having slopes equal to these two velocities. The first step we have taken in this direction was to redo the calculation for dW/dt by excluding the contributions from the two plasmon

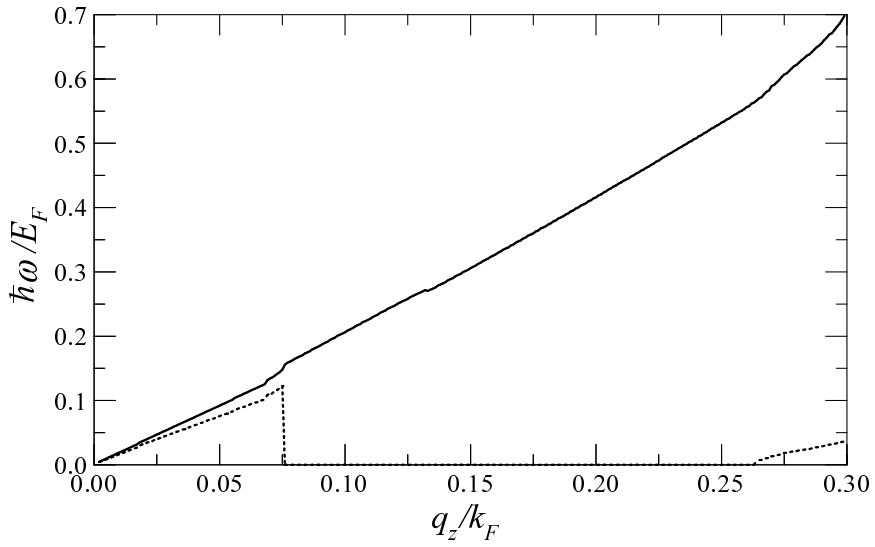

Figure 4.7: The real (solid line) and imaginary (dotted line) parts of the plasmon branch with the higher frequency in the instability region in Fig. 4.6.

branches determining this region. The resulting plot showed that there was no dip. This indicates that these branches are responsible for the observed feature. The peaks in Figs. 4.3(a)-(c) are like those we obtained for a single-wall nanotube in Figs. 3.1 and 3.2. Therefore, the physical meaning of the dip is that the plasmon branches with phase velocity in this region decay after being excited, not because they are Landau damped but by some other mechanism. Thus, the second step in our investigation was to solve the dispersion equation for complex plasmon frequencies. We obtained solutions for the frequencies whose real part lies in the bounded region $1.00v_Fq_z$ to $1.50v_Fq_z$. However, there were no such solutions outside this region. This means that the dip corresponds to a region of instability for excitations within the system and which does not include the particle-hole continuum. In Fig. 4.7, we plot the real and imaginary parts of the plasmon branch with the higher frequency in the instability region in Fig. 4.6. These results were obtained when we solved the dispersion equation in the complex frequency plane. The real part of the plasmon frequency in Fig. 4.7 differs

slightly from the second highest branch in Fig. 4.6. Also, the imaginary part of this frequency is much smaller than its real part. The imaginary part increases monotonically with wave vector before rapidly decreasing around $q_z \approx 0.075\ k_F$. There is an increase in the imaginary part near $q_z \approx 0.25\ k_F$. The inverse of the imaginary part of this complex frequency yields the lifetime of the collective excitation. Thus, it is only for some ranges of wave vector where the lifetime of the plasmon excitation is "finite". As we mentioned in Sec. 4.1 a positive complex part in the plasmon frequency is responsible for the exponential growth of the mode and the creation of instability. In Fig. 4.8, we plot the $L = 0$ plasmon contribution to the rate of transfer of energy for a pair of parallel single-wall nanotubes each of radius 11 Å and separation $a = 25$ Å. We chose the impact parameter as $\rho_0 = 0$. There are two dips in Fig. 4.8. These again correspond to plasmon excitations which become unstable after being excited by the charged particle. In Fig. 4.9, we present the plasmon excitation spectrum for the pair of parallel nanotubes used in Fig. 4.8 (the values of ε_b,R,E_F and m^* are the same as before). The tangent lines to the plasmon branches in Fig. 4.9 indicate the velocities where the energy loss spectrum has a dip or a peak. The path of the charged particle was chosen along the axis of one of the two nanotubes and the separation $a = 25$ Å. We can explain the dips and peaks of this figure in the same way as in the case of concentric nanotubes.

We found in Sec. 3.1 that for a charged particle moving parallel to one tubule, the only direction for which the energy can be transferred is along the z-axis. When there are though two tubules (concentric or parallel) the charged particle excites plasmons on one of them and then the energy can be transferred to the plasmon excitations in the other through electrostatic coupling. As a result of this the charged particle can gain energy, as we show in the present section. This gives rise to an increase of its energy (the dip in the energy loss spectrum).

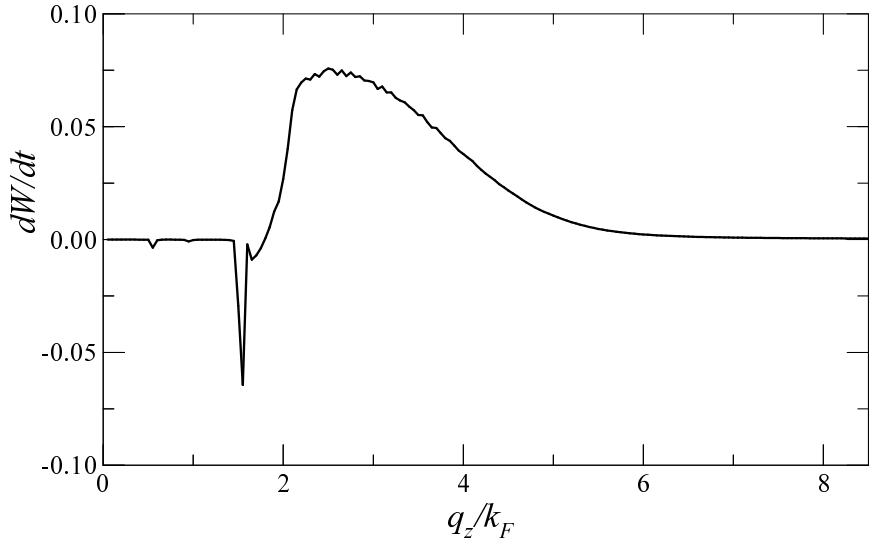

Figure 4.8: The plasmon contributions to the rate of energy transfer (in units of $e^2k_F^2v_F$) for subband transitions with $L = 0$ for two parallel nanotubes each of radius $R = 11$ Å with separation $a = 25$ Å between them.

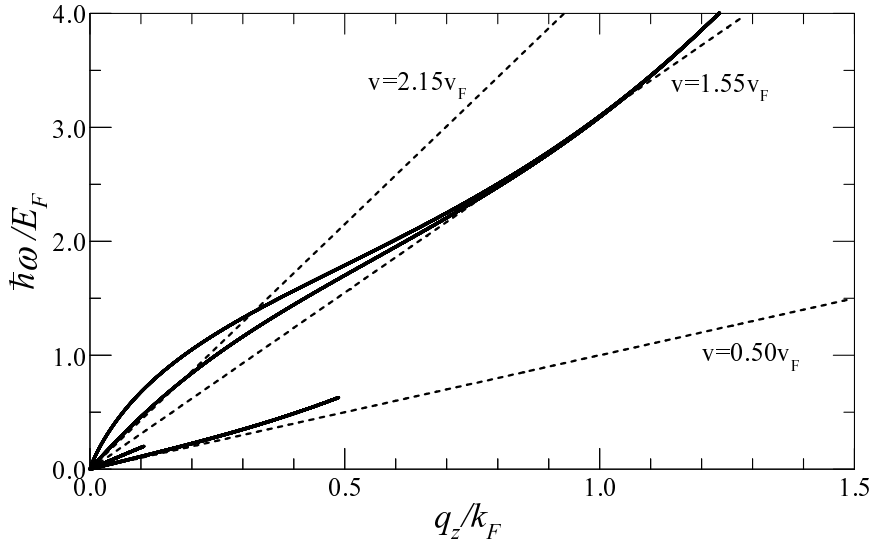

Figure 4.9: The $L = 0$ plasmon dispersion for the pair of parallel nanotubes of Fig. 4.8. The straight lines $\omega = vq_z$ show when the plasmon branch contributes to dW/dt.

Chapter 5

THE IMAGE POTENTIAL

In recent years, there have been several papers [43, 68] investigating the image potential due to a point source in relation to nanotubes, following the work of Granger, et al [58]. In that paper, it was shown that if a single-wall carbon nanotube is assumed to be a solid metallic rod [69] surrounded by vacuum, then image potential states can be supported outside the nanotube [58] depending on the value of the angular momentum of the orbiting charged particle. We confirm this result for the case of a hollow nanotube, embedded in a medium with background dielectric constant ε_b, on which an electron gas is confined. We include polarization effects due to the dynamic perturbation of the electrons on the surface of the tubule. The total effective potential is obtained by combining the image potential and the centrifugal interaction. The bound states we discuss are located several nanometers away from either inner or outer tubule. Consequently, the detailed behavior of the image potential at the surface of the cylinder should not affect our conclusions. We extend our calculations as well as those in [58] to show that for a double-wall nanotube the outer surface can increase the confinement of the charged particle. Furthermore, we also demonstrate that if there is a bound state for a chosen value of the angular momentum for a single-wall

nanotube , it may not exist when the second tubule is introduced.

5.1 Image potential for a single-wall nanotube

Consider a stationary external point charge located outside the single wall nanotube of Sec. 2.1 at $\mathbf{r}_0 = (\rho_0, \phi_0, 0)$. The external charged particle polarizes the surface charge and becomes attracted to its "image charge" residing on the other side of the surface. This gives rise to a spatially extended state. The induced potential outside the nanotube for this case is given by Eq. (3.21), where we use $\phi_0 = 0$ for convenience, with $v = 0$. The electrostatic potential energy of the interaction of the charged particle with the induced surface charge, or image potential, for $\rho_0 > R$ is defined by

$$U_{\rm im}(\rho_0) = \frac{1}{2} Q \Phi^{>}_{\rm ind}(\rho_0, \phi_0, 0) = -\frac{Q^2}{2\pi\varepsilon_2} \sum_{L=-\infty}^{\infty} \int_{-\infty}^{\infty} dq K_L^2(q_z\rho_0) I_L(q_z R) \times \left[\frac{1}{K_L(q_z R)} \frac{a_L(q_z, \omega=0)}{1 + a_L(q_z, \omega=0)} + q_z R(\varepsilon_1 - \varepsilon_2) \frac{I'_L(q_z R)}{D_L(q_z, \omega=0)} \right] , \quad (5.1)$$

where $a_L(q_z, \omega)$ and $D_L(q_z, \omega)$ are given by Eqs. (3.20) and (3.18) respectively. For $\rho_0 < R$ using Eq. (D.1) of Appendix D the image potential is given by

$$U_{\rm im}(\rho_0) = -\frac{Q^2}{2\pi\varepsilon_1} \sum_{L=-\infty}^{\infty} \int_{-\infty}^{\infty} dq I_L^2(q_z\rho_0) K_L(q_z R) \times \left[\frac{1}{I_L(q_z R)} \frac{a_L(q_z, \omega=0)}{1 + a_L(q_z, \omega=0)} + q_z R(\varepsilon_1 - \varepsilon_2) \frac{K'_L(q_z R)}{D_L(q_z, \omega=0)} \right] , \quad (5.2)$$

and $U_{\rm im}(\rho_0) \to -\infty$ as $\rho_0 \to R$ either from above or from below. In Ref. [58], the model used was a solid metallic cylinder. This corresponds to setting $\varepsilon_1 = \infty$ in Eq. (5.1) in which case we obtain the expression for $U_{\rm im}(\rho_0)$ used in Ref. [58]. The image potential in Ref. [58] can also be obtained in the limit when $a_L \to \infty$, but with finite background dielectric constant. In this limit, only the first term contributes. The same term is the only contribution to Eq. (5.1) in the model that we use when $\varepsilon_1 = \varepsilon_2 = \varepsilon_b$. We would like to determine whether

the polarization of the electron gas gives rise to bound states as described in Ref. [58]. For this reason we calculated the effective potential consisting of the negative image potential and the centrifugal potential, i.e.,

$$V_{\text{eff}}(\rho_0) = U_{\text{im}}(\rho_0) + \frac{\hbar^2(l_0^2 - \frac{1}{4})}{2M\rho_0^2}, \tag{5.3}$$

where M is the mass of the charged particle in an orbital state with angular momentum quantum number l_0. We calculated $V_{\text{eff}}(\rho_0)$ in Eq. (5.3) for a range of values of the ratio of the potential energy $Q^2/4\pi\varepsilon_0 R$ to the kinetic energy $\hbar^2/2MR^2$ which can be written as $\lambda = 2R/a_B^*$ in terms of an effective Bohr radius $a_B^* = \hbar^2/Me^2$. Our calculation showed that for chosen l_0, the λ must be sufficiently large for $V_{\text{eff}}(\rho_0)$ to have a potential minimum. In Fig. 5.1 we plot $V_{\text{eff}}(\rho_0)$ as a function of ρ_0 for a hollow cylindrical nanotube with the same radius and background dielectric constant as before ($R = 11$ Å, $\varepsilon_b = 2.4$). We chose the angular momentum quantum number with $4 \leq l_0 \leq 8$ and the charged particle mass $M = m_e$. In our calculations for $\rho_0 \leq 120$ nm, we could not find that $V_{\text{eff}}(\rho_0)$ has a minimum when $r_0 > R$ for $l_0 > 12$. The effective potential is negative as $r_0 \to R$ either from inside or outside the cylinder. Our calculations show that the main difference in $V_{\text{eff}}(\rho_0 > R)$ between the results for a perfectly conducting solid metal rod and the hollow cylinder arises when $\rho_0 \approx R$. The potential minima show that the effective potential for a hollow cylindrical nanotube embedded in a dielectric medium supports image states which are bound to the surface of the cylinder for $\rho_0 > R$ and the bound states with larger l_0 have weaker binding energies. We have also calculated $U_{\text{im}}(\rho_0)$ from Eq. (5.2) for $\rho_0 < R$. The image potential is always negative and decreases as ρ_0 increases from $\rho_0 = 0$ with $U_{\text{im}} \to -\infty$ as $\rho_0 \to R^-$. For $l_0 = 0$, the centrifugal term is negative definite, yielding a local maximum in V_{eff} at $\rho_0 < R$. For $l_0 > 0$, the centrifugal term is positive and does not yield a minimum in $V_{\text{eff}}(\rho_0)$ for $\rho_0 < R$ for any l_0. Consequently, all bound states for the nanotube occur for $\rho_0 > R$ only.

Recently, Höfer *et al.* [70] applied two-photon photoemission techniques to populate the coherent wave packets of image states close to a Cu(100) surface. The states observed in these experiments had $l_0 \sim 7$ and binding energies of 15-40 meV. These surface states collapsed onto the Cu surface with lifetimes of a few picoseconds. The states with larger l_0 have longer lifetimes [71]. Making use of the model described in the present dissertation, we can investigate how the band structure affects the image potential of semiconducting and semimetallic nanotubes. Consequently, we can obtain the lifetimes of the surface states of these two types of nanotubes and which has longer lifetimes.

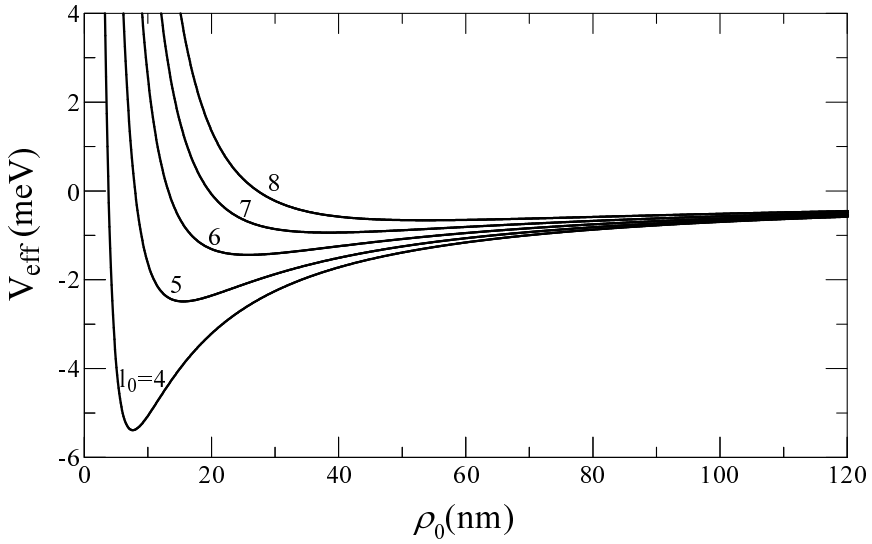

Figure 5.1: The effective potential for a charged particle with angular momentum quantum number $4 \leq l_0 \leq 8$.

5.2 Image potential for a double-wall nanotube

We now consider two co-axial cylinders of radii R_1 and R_2 whose axes are along the z-axis (Fig. 5.2). The background dielectric constant is ε_1 for $0 < \rho < R_1$, ε_2 for $R_1 < \rho < R_2$, and ε_3 for $\rho > R_2$. An electron gas is confined to the surface

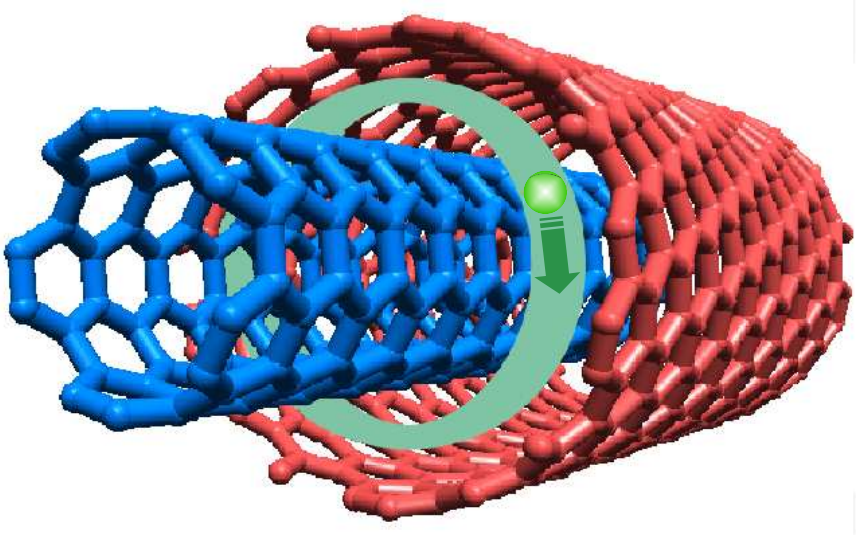

Figure 5.2: Schematic of coaxial cylindrical nanotubes and an orbiting point charge between the two surfaces. The inner cylinder has radius R_1 and the outer cylinder has radius R_2.

of each nanotube. If a charge Q is located at (ρ_0, ϕ_0, z_0), then for $\rho_0 > R_2$, the electrostatic potential is given by

$$\Phi(\rho, \phi, z) = \frac{Q}{\pi} \sum_{L=-\infty}^{\infty} e^{iL(\phi-\phi_0)} \int_{-\infty}^{\infty} dq_z e^{iq_z(z-z_0)} \Phi_L(\rho, q_z) \ , \tag{5.4}$$

where the Fourier coefficients are given by

$$\Phi_L(\rho, q_z) = \begin{cases} C_1^{(1)} I_L(q_z\rho) \ , & 0 < \rho < R_1 \\ C_{21}^{(1)} I_L(q_z\rho) + C_{22}^{(1)} K_L(q_z\rho) \ , & R_1 < \rho < R_2 \\ \dfrac{1}{\varepsilon_3} I_L(q_z\rho_<) K_L(q_z\rho_>) + C_3^{(1)} K_L(q_z\rho) \ , & \rho > R_2 \end{cases} \ , \tag{5.5}$$

with $\rho_<$ ($\rho_>$) denoting the smaller (greater) of the radial coordinates ρ and ρ_0. In addition, $C_1^{(1)}, C_{21}^{(1)}, C_{22}^{(1)}, C_3^{(1)}$ are determined through the continuity of the potential as well as the discontinuity of the displacement vector across each cylinder surface due to the induced charge density.

The wave functions for electrons confined on the surfaces of the two tubules are

given by Eq. (2.18) with $j = 1, 2$ and $\nu = \{k_z, l\}$. Using them in Eqs. (2.8), (2.9) and Fourier expanding the induced charge density as (in our case since we deal with a static charge we have that $\omega = 0$)

$$\rho_{\rm e}(\mathbf{r}, \omega) = \sum_L e^{iL(\phi - \phi_0)} \int \frac{dq_z}{2\pi} e^{iq_z z} \delta n_L(\rho, q_z, \omega) \ , \tag{5.6}$$

we find (since $\rho_{\rm e}(\mathbf{r}, \omega) = \sigma(\mathbf{r}, \omega)\delta(r - R)$) that the induced surface charge density on the j-th tubule is given by

$$\sigma_L(\rho = R_j, q_z, \omega) = -\frac{2e^2 Q}{R_j} \chi_{j,L}(q_z, \omega) \Phi_L(\rho = R_j, q_z, \omega) \ , \tag{5.7}$$

where $\Phi_L(\rho = R_j, q_z, \omega) = \Phi_L(\rho = R_j, q_z)\delta(\omega - q_z v)$. The coefficients $C_1^{(1)}, C_{21}^{(1)}$, $C_{22}^{(1)}, C_3^{(1)}$ are determined through the continuity of the electrostatic potential as well as the discontinuity of the displacement vector across the surface of each cylinder due to the induced charge density. We have

$$\begin{aligned}
&\Phi_L^{(1)}(\rho = R_1, q_z, \omega) = \Phi_L^{(2)}(\rho = R_1, q_z, \omega) \ , \\
&\Phi_L^{(2)}(\rho = R_2, q_z, \omega) = \Phi_L^{(3)}(\rho = R_2, q_z, \omega) \ , \\
&\varepsilon_1 \frac{\partial \Phi_L^{(1)}}{\partial \rho} - \varepsilon_2 \frac{\partial \Phi_L^{(2)}}{\partial \rho}\bigg|_{\rho = R_1} = 4\pi \sigma_L(\rho = R_1, q_z, \omega), \\
&\varepsilon_2 \frac{\partial \Phi_L^{(2)}}{\partial \rho} - \varepsilon_3 \frac{\partial \Phi_L^{(3)}}{\partial \rho}\bigg|_{\rho = R_2} = 4\pi \sigma_L(\rho = R_2, q_z, \omega),
\end{aligned} \tag{5.8}$$

with $\sigma_L(\rho, q_z, \omega)$ given by Eq. (5.7). The resulting set of linear simultaneous equations determining the coefficients are

$$\overleftrightarrow{\mathbf{D}}\,(q, \omega = 0) \begin{pmatrix} C_1^{(1)} \\ C_{21}^{(1)} \\ C_{22}^{(1)} \\ C_3^{(1)} \end{pmatrix} = \begin{pmatrix} I_L(q_z R_2) K_L(q_z \rho_0)/\varepsilon_3 \\ 0 \\ I_L'(q_z R_2) K_L(q_z \rho_0) \\ 0 \end{pmatrix} \ , \tag{5.9}$$

where the coefficient matrix $\overleftrightarrow{\mathbf{D}}$ is given by

$$\overleftrightarrow{\mathbf{D}}\,(q_z,\omega) = \begin{pmatrix} 0 & I_L(q_zR_2) & K_L(q_zR_2) & -K_L(q_zR_2) \\ -I_L(q_zR_1) & I_L(q_zR_1) & K_L(q_zR_1) & 0 \\ 0 & D_{32}(q_z,\omega) & D_{33}(q_z,\omega) & -\epsilon_3 K'_L(q_zR_2) \\ D_{41}(q_z,\omega) & -\epsilon_2 I'_L(q_zR_1) & -\epsilon_2 K'_L(q_zR_1) & 0 \end{pmatrix} , \tag{5.10}$$

and wherein the matrix elements are defined by

$$\begin{aligned} D_{32}(q_z,\omega) &= \frac{2e^2}{q_zR_2} I_L(q_zR_2)\chi_{2,L}(q_z,\omega) + \varepsilon_2 I'_L(q_zR_2) \ , \\ D_{33}(q_z,\omega) &= \frac{2e^2}{q_zR_2} K_L(q_zR_2)\chi_{2,L}(q_z,\omega) + \varepsilon_2 K'_L(q_zR_2) \ , \\ D_{41}(q_z,\omega) &= \frac{2e^2}{q_zR_1} I_L(q_zR_1)\chi_{1,L}(q_z,\omega) + \varepsilon_1 I'_L(q_zR_1) \ . \end{aligned} \tag{5.11}$$

The zeros of the determinant of the matrix $\overleftrightarrow{\mathbf{D}}\,(q,\omega)$ correspond to normal mode frequencies of the plasma excitations on the surfaces of the two coupled cylinders. The determinant of the matrix $\overleftrightarrow{\mathbf{D}}\,(q,\omega)$ may be written in the form

$$\det \overleftrightarrow{\mathbf{D}}\,(q_z,\omega) = \varepsilon_L^{(1)}(q_z,\omega)\,\varepsilon_L^{(2)}(q_z,\omega) + \varepsilon_L^{(1,2)}(q_z,\omega) \ , \tag{5.12}$$

where

$$\begin{aligned} \varepsilon_L^{(1)}(q_z,\omega) &= \varepsilon_2 I_L(q_zR_1)K'_L(q_zR_1) - \varepsilon_1 K_L(q_zR_1)I'_L(q_zR_1) \\ &\quad - \frac{e^2}{2\pi\varepsilon_0 q_zR_1} I_L(q_zR_1)K_L(q_zR_1)\chi_{1,L}(q_z,\omega) \ , \end{aligned} \tag{5.13}$$

$$\begin{aligned} \varepsilon_L^{(2)}(q_z,\omega) &= \epsilon_2 K_L(q_zR_2)I'_L(q_zR_2) - \epsilon_3 I_L(q_zR_2)K'_L(q_zR_2) \\ &\quad + \frac{e^2}{2\pi\epsilon_0 q_zR_2} I_L(q_zR_2)K_L(q_zR_2)\chi_{2,L}(q_z,\omega) \ , \end{aligned} \tag{5.14}$$

$$\begin{aligned} \varepsilon_L^{(1,2)}(q_z,\omega) &= \frac{e^2}{2\pi\epsilon_0 qR_2} I_L(qR_1)K_L^2(qR_2)\chi_{2,L}(q_z,\omega) \\ &\quad \times \left[\frac{e^2}{2\pi\epsilon_0 qR_1} I_L(q_zR_1)\chi_{1,L}(q_z,\omega) + (\epsilon_1-\epsilon_2)I'_L(q_zR_1)\right] \\ &\quad + (\epsilon_2-\epsilon_3)K_L(q_zR_2)I_L(q_zR_1)K'_L(q_zR_2) \\ &\quad \times \left[\frac{e^2}{2\pi\epsilon_0 q_zR_1} I_L(q_zR_1)\chi_{1,L}(q_z,\omega) + (\epsilon_1-\epsilon_2)I'_L(q_zR_1)\right] \ . \end{aligned} \tag{5.15}$$

Here, $\varepsilon_L^{(j)}(q_z,\omega) = 0$ is the dispersion equation for plasma excitations on the tubule of radius R_j $(j = 1, 2)$. The coupling between these plasma excitations is taken into account through the term $\varepsilon_L^{(1,2)}(q_z,\omega)$.

To calculate the induced potential outside the two cylinders, we obtain $C_3^{(1)}$ from Eq. (5.9) and then we substitute this expression into the third row on the right-hand side of Eq. (5.5). When the point charge Q is between the two cylinders, i.e., $R_1 < \rho_0 < R_2$, the electrostatic potential is given by Eq. (5.4) but with Φ_L now re-expressed as

$$\Phi_L(\rho,q_z) = \begin{cases} C_1^{(2)} I_L(q_z\rho)\ , & 0<\rho<R_1 \\ \dfrac{I_L(q_z\rho_<)K_L(q_z\rho_>)}{\varepsilon_2} + C_{21}^{(2)} I_L(q_z\rho) + C_{22}^{(2)} K_L(q_z\rho)\ , & R_1<\rho<R_2 \\ C_3^{(2)} K_L(q_z\rho)\ , & \rho>R_2 \end{cases} \tag{5.16}$$

where

$$\begin{aligned} &\overleftrightarrow{\mathbf{D}}\,(q_z,\omega) \begin{pmatrix} C_1^{(2)} \\ C_{21}^{(2)} \\ C_{22}^{(2)} \\ C_3^{(2)} \end{pmatrix} \\ &= \begin{pmatrix} -I_L(q_z\rho_0)K_L(q_zR_2)/\varepsilon_2 \\ -I_L(q_zR_1)K_L(q_z\rho_0)/\varepsilon_2 \\ -I_L(q_z\rho_0)K_L'(q_zR_2) - \dfrac{2e^2}{q_zR_2} I_L(q_z\rho_0)K_L(q_zR_2)\chi_L^{(2)}(q_z,\omega) \\ K_L'(q_z\rho_0)I_L(q_zR_1) \end{pmatrix}\ , \end{aligned} \tag{5.17}$$

with the coefficient matrix $\overleftrightarrow{\mathbf{D}}$ still given by Eq. (5.10). We then obtain the potential between the two cylinders by solving Eq. (5.17) for $C_{21}^{(2)}$ and $C_{22}^{(2)}$ and then substituting the results into the second line on the right-hand side of Eq. (5.16). The image potential is obtained by setting $\rho = \rho_0$ in Eq. (5.4) and exploiting the results in Eqs. (5.5) through (5.17). The effective potential is the sum of the image potential and the centrifugal term and is given by (see also the papers by Wendler and Grigoryan [72, 73] for additional explanations of the image potential

in cylindrical geometries) Eq. (5.3). In Figs. 5.3(a)-5.3(c) , we calculated $V_{\text{eff}}(\rho_0)$ as a function of ρ_0 and chose $l_0 = 2, 4, 5, 6$. We chose for the background dielectric constant $\varepsilon_1 = \varepsilon_2 = \varepsilon_3 = \varepsilon_b$ and we used for ε_b, m^* and E_F the same values as before. The orbiting particle effective mass is $M = m_e$.

The plots demonstrate the influence on the effective potential and hence the bound state due to the presence of the outer cylinder. We only present numerical results for $V_{\text{eff}}(\rho_0)$ between the two cylinders, i.e., for $R_1 \leq \rho_0 \leq R_2$. Our reason for concentrating on this region is that the bound state has been demonstrated to exist outside the surface of a cylinder in previous works [58] and in the last section where we studied the case of a single-walled nanotube. In Figs. 5.3(a)-5.3(c), the bound states for $V_{\text{eff}}(\rho_0)$ depend on the separation between the two cylinders as well as the value of the orbital quantum number l_0. Specifically, for fixed inner cylinder radius $R_1 = 11$ Å, we have bound state for $l_0 = 4$ when $R_2 = 880$ Å and $R_2 = 1100$ Å but there are no bound states when $R_2 = 440$ Å. Thus the image potential due to the two cylinders on the charged single particle may be too large for the centrifugal term to produce a bound state in the effective potential. For the other values of l_0 shown in Figs. 5.3(a)-5.3(c), there are no bound states for $R_1 \leq \rho_0 \leq R_2$. Furthermore, the potential minimum in Fig. 5.3(b) is lower than that in Fig. 5.3(c). Therefore, by suitably adjusting R_1 and R_2, one can vary the lifetime of the orbiting charged particle between the two cylinders.

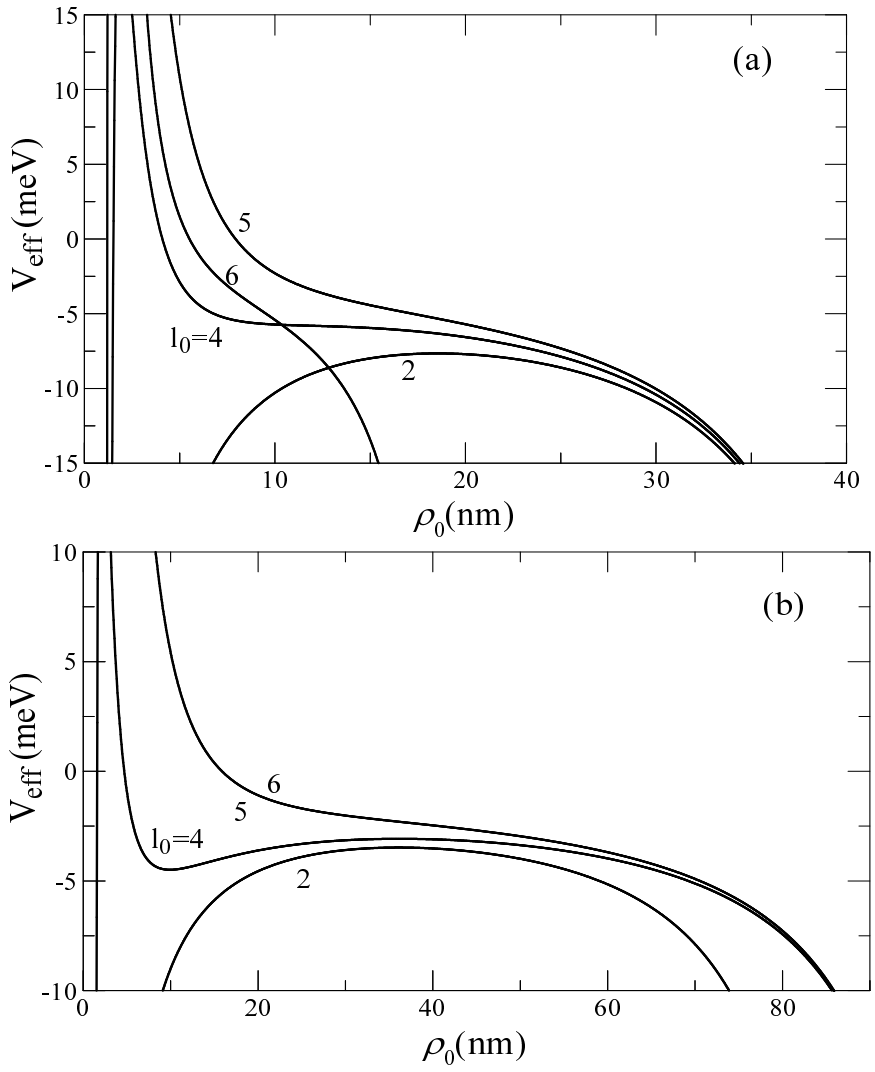

Figure 5.3: The effective potential between the cylinders for a charged particle with angular momentum quantum number l_0 when the radius of the outer cylinder is (a) $R_2 = 44$ nm, (b) $R_2 = 88$ nm.

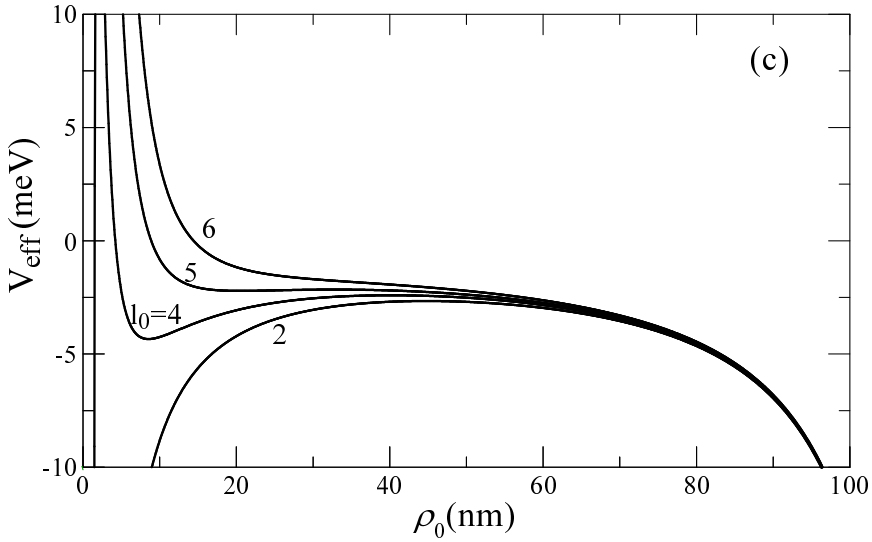

Figure 5.3: (c) The same as in the last figure but for $R_2 = 1100$ nm.

Chapter 6

CONCLUDING REMARKS

In summary, we presented a formalism for calculating the energy transfer from charged particles to cylindrical nanotubes. Experimentalists have used EELS over the years to investigate the spectroscopic properties of condensed matter surfaces. This tool has been complimentary to light scattering techniques which requires the calculation of the absorption coefficient in a theoretical investigation. The method we used in our calculations was suitable for examining both the particle-hole and plasmon excitations for single, coaxial and parallel tubules. The contributions of these modes to the energy transfer depend on the impact parameter of the charged particle. This means that one can adjust the way in which these two types of modes play a role in the energy loss of charged particles.

Plasmon instabilities for a pair of electrostatically coupled tubules arise when the drift velocity of a charged particle lies within a range which is determined by the phase velocity for the plasmon modes. These results show that since the instability occurs over a range of frequencies in the terahertz regime, potential applications may be to detectors. Furthermore, due to the durability of carbon nanotubes, these devices may be of use in space or in electronics in satellites. In general, plasmon phenomenology may be of practical importance in sensors

and detectors based on the use of radiative plasmon decay in tunable solid state sources of far-infrared electromagnetic radiation (terahertz oscillator). Current-driven infrared emission from layered semiconductors, due to thermal plasmon generation or Smith-Purcell effect, have already been detected [74]-[76]. Terahertz optics is an emerging field with promising applications including material characterization, tomographic imaging, as well as chemical and biological sensing [77, 78].

The model we used to describe the energy bands was simplified so that we could do some tractable analytical calculations. However, the results we have obtained are expected to be consistent with more realistic models. For example, our results for the image potential for one tubule reduce to those by Granger, et al [58].

Future work on extending the above calculations could focus on obtaining the modification to our model by the use of non-equilibrium electron distribution functions. These would be obtained from Boltzmann's equation. Also, the use of a tight-binding model instead of a a free-electron model would be another step in generalizing our formalism. In this dissertation, we did not investigate magnetic field effects. Some preliminary results have been reported by Gumbs, Shew and Balassis [79]. However, further calculations need to be carried out when the magnetic field is applied perpendicular to the axis of the nanotube.

Appendix A

Linear response theory

We consider a Hamiltonian of the form $\hat{H} = \hat{H}_0 + \hat{H}_1(\mathbf{r}, t)$, where $\hat{H}_0|\nu> = \epsilon_\nu|\nu>$ describes the unperturbed system (in our study the non-interacting electron gas) and $\hat{H}_1(\mathbf{r}, t)$ is a perturbation. The density matrix operator $\hat{\varrho} = e^{-\beta\hat{H}}$ depends on time and therefore the average value of any observable $\hat{A}$ depends on time too through the equation

$$< \hat{A}(t) >= Tr\left[\hat{\varrho}(t)\hat{A}\right] \ , \tag{A.1}$$

where we assumed that $Tr\left[\hat{\varrho}(t)\right] = 1$.

The time evolution of the density matrix operator is given by the von Neumann equation which in Schrodinger picture is

$$i\hbar\frac{\partial\hat{\varrho}}{\partial t} = \left[\hat{H}, \hat{\varrho}\right] = \left[\hat{H}_0, \hat{\varrho}\right] + \left[\hat{H}_1, \hat{\varrho}\right]. \tag{A.2}$$

We express $\hat{\varrho}$ for small perturbations as $\hat{\varrho} = \hat{\varrho}_0 + \hat{\varrho}_1$ where $\hat{\varrho}_0$ is the equilibrium density operator and $\hat{\varrho}_1$ is the perturbation. Equation (A.2) then becomes to lowest order

$$i\hbar\frac{\partial\hat{\varrho}_1}{\partial t} = \left[\hat{H}_0, \hat{\varrho}_1\right] + \left[\hat{H}_1, \hat{\varrho}_0\right] \ , \tag{A.3}$$

where we used $i\hbar(\partial\hat{\varrho}_0/\partial t) = [\hat{H}_0, \hat{\varrho}_0]$ and we neglected the higher order correction $[\hat{H}_1, \hat{\varrho}_1]$. Using the $\{|\nu>\}$ basis we can express Eq.(A.3) in matrix form as

$$i\hbar < \nu|\frac{\partial\hat{\varrho}_1}{\partial t}|\nu' >=< \nu|\left[\hat{H}_0, \hat{\varrho}_1\right]|\nu' > + < \nu|\left[\hat{H}_1, \hat{\varrho}_0\right]|\nu' > . \tag{A.4}$$

It holds $\hat{\varrho}_0|\nu >= 2f_0(\epsilon_\nu)|\nu >$, where $f_0(\epsilon_\nu)$ is the equilibrium Fermi-Dirac distribution function, and the last equation becomes

$$i\hbar < \nu|\frac{\partial\hat{\varrho}_1}{\partial t}|\nu' >= (\epsilon_\nu - \epsilon_{\nu'}) < \nu|\hat{\varrho}_1|\nu' > +2\left[f_0(\epsilon_{\nu'}) - f_0(\epsilon_\nu)\right] < \nu|\hat{H}_1|\nu' > , \tag{A.5}$$

or after we Fourier transform with respect to time

$$< \nu|\hat{\varrho}_1(\mathbf{r},\omega)|\nu' >= 2\frac{f_0(\epsilon_{\nu'}) - f_0(\epsilon_\nu)}{\hbar\omega + \epsilon_{\nu'} - \epsilon_\nu + i0^+} < \nu|\hat{H}_1(\mathbf{r},\omega)|\nu' > \ . \tag{A.6}$$

The particle density $n(\mathbf{r},\omega)$ at point $\mathbf{r}$ is given by the mean value of the operator $\hat{n}(\mathbf{r}) = \hat{\psi}^\dagger(\mathbf{r})\hat{\psi}(\mathbf{r})$

$$n(\mathbf{r},\omega) =< \hat{n}(\mathbf{r}) >= Tr\left[\hat{\varrho}(\omega)\hat{\psi}^\dagger(\mathbf{r})\hat{\psi}(\mathbf{r})\right] \ , \tag{A.7}$$

and the particle density perturbation (or induced particle density) $\rho(\mathbf{r},\omega)$ is given by

$$\rho(\mathbf{r},\omega) = Tr\left[\hat{\varrho}_1(\mathbf{r},\omega)\hat{\psi}^\dagger(\mathbf{r})\hat{\psi}(\mathbf{r})\right] \ . \tag{A.8}$$

We use the unperturbed states $|\nu>$ to calculate the trace

$$\begin{aligned}\rho(\mathbf{r},\omega) &= \sum_{\nu,\nu'} < \nu|\hat{\varrho}_1(\omega)|\nu' >< \nu'|\hat{\psi}^\dagger(\mathbf{r})\hat{\psi}(\mathbf{r})|\nu > \\ &= \sum_{\nu,\nu'} < \nu|\hat{\varrho}_1(\omega)|\nu' > \phi^*_{\nu'}(\mathbf{r})\phi_\nu(\mathbf{r}) \ ,\end{aligned} \tag{A.9}$$

or using Eq.(A.6) along with the completeness $\int d\mathbf{r}'|\mathbf{r}' >< \mathbf{r}'|$

$$\rho(\mathbf{r},\omega) = \int d\mathbf{r}'\chi_0(\mathbf{r},\mathbf{r}',\omega)\hat{H}_1(\mathbf{r}',\omega) \ . \tag{A.10}$$

In this notation

$$\chi_0(\mathbf{r},\mathbf{r}',\omega) = 2\sum_{\nu,\nu'}\frac{f_0(\epsilon_{\nu'}) - f_0(\epsilon_\nu)}{\hbar\omega + \epsilon_{\nu'} - \epsilon_\nu + i0^+}\psi_\nu(\mathbf{r})\psi^*_{\nu'}(\mathbf{r})\psi^*_\nu(\mathbf{r}')\psi_{\nu'}(\mathbf{r}') \ , \tag{A.11}$$

is the RPA, or Lindhard, polarization function. For the induced particle density of an interacting electron gas, we have in linear response theory an equation similar to (A.10)

$$\rho(\mathbf{r},\omega) = \int d\mathbf{r}'\chi(\mathbf{r},\mathbf{r}',\omega)\hat{H}_1(\mathbf{r}',\omega) \ , \tag{A.12}$$

where $\chi(\mathbf{r},\mathbf{r}',\omega)$ is the polarization function which includes the electron-electron interaction, and $\hat{H}_1(\mathbf{r}',\omega)$ is the external perturbation. In our study the perturbation comes from a scalar potential Φ.

In the case of the non-interacting electron gas, $\hat{H}_1(\mathbf{r},\omega)$ in Eq. (A.10) can describe only an externally applied scalar potential Φ_{ext}, so

$$\hat{H}_1(\mathbf{r},\omega) = -e\Phi_{\text{ext}}(\mathbf{r},\omega) \ . \tag{A.13}$$

The same equation though can describe the interacting electron gas, if in the perturbation Hamiltonian $\hat{H}_1(\mathbf{r},\omega)$ we include not only the external scalar potential, but in addition the scalar potential created by the induced electron density, therefore

$$\hat{H}_1(\mathbf{r},\omega) = -e\left[\Phi_{\text{ext}}(\mathbf{r},\omega) + \Phi_{\text{ind}}(\mathbf{r},\omega)\right] = U(\mathbf{r},\omega) + V_{\text{ind}}(\mathbf{r},\omega). \tag{A.14}$$

Equation (A.10) with $\hat{H}_1(\mathbf{r},\omega)$ given by Eq. (A.13) is exactly the same result that we found in the introduction, Eq. (1.23), using the Martin-Schwinger formalism. It is a self consistent field equation since the induced potential $\Phi_{\text{ind}}(\mathbf{r},\omega)$ can be found through Poisson's equation

$$\nabla^2\Phi_{\text{ind}}(\mathbf{r},\omega) = \frac{4\pi e}{\varepsilon_b}\rho(\mathbf{r},\omega) \ . \tag{A.15}$$

Using Eqs. (A.10), (A.12), (A.14) and (A.15) one can calculate the RPA equation for the polarization function of the interacting electron gas

$$\chi(\mathbf{q},\omega) = \frac{\chi_0(\mathbf{q},\omega)}{\tilde{\varepsilon}(\mathbf{q},\omega)} \ , \tag{A.16}$$

where $\tilde{\varepsilon}(\mathbf{q},\omega) = 1 - \dfrac{1}{\varepsilon_b}\chi_0(\mathbf{q},\omega)v(\mathbf{q},\omega)$.

Appendix B

The polarization function

We will often encounter in our study the 1D Fourier transform of the polarization function, defined as

$$\chi_L(q_z,\omega) = 2\lim_{\alpha\to 0^+}\sum_{l=-\infty}^{\infty}\int_{-\infty}^{\infty}\frac{dk_z}{2\pi}\frac{f_0(\epsilon_{k_z,l})-f_0(\epsilon_{k_z+q_z,l+L})}{\epsilon_{k_z+q_z,l+L}-\epsilon_{k_z,l}-\hbar\omega-i\hbar\alpha}\ , \tag{B.1}$$

where $f_0(\epsilon_{k_z,l})$ is the equilibrium Fermi-Dirac distribution function and $\epsilon_{k_z,l} = \frac{\hbar^2 k_z^2}{2m^*} + \frac{\hbar^2 l^2}{2m^*}$ are the energy eigenstates of the electron confined to move on the surface of a nanotube of radius R. We note that if we replace $k_z \to k_z - q_z$, $l \to l - L$ we obtain

$$\chi_L(q_z,\omega) = 2\lim_{\alpha\to 0^+}\sum_{l=-\infty}^{\infty}\int_{-\infty}^{\infty}\frac{dk_z}{2\pi}\frac{f_0(\epsilon_{k_z,l})-f_0(\epsilon_{k_z-q_z,l-L})}{\epsilon_{k_z-q_z,l-L}-\epsilon_{k_z,l}+\hbar\omega+i\hbar\alpha}\ , \tag{B.2}$$

which is the expression used in our text.

We use Dirac's identity $\lim_{\alpha\to 0^+} 1/(x \pm i\alpha) = P(1/x) \mp i\pi\delta(x)$, where P stands for the principal value of the integral, to separate the real and imaginary parts of Eq. (B.1).

For the real part we have

$$\Re e\,\chi_L(q_z,\omega) = \sum_{l=-\infty}^{\infty} P\int_{-\infty}^{\infty}\frac{dk_z}{2\pi}\frac{f_0(\epsilon_{k_z,l})-f_0(\epsilon_{k_z+q_z,l+L})}{\epsilon_{k_z+q_z,l+L}-\epsilon_{k_z,l}-\hbar\omega}\ . \tag{B.3}$$

We set $k_z \to -k_z - q_z$ and $l \to -l - L$ in the second term of the right hand side of Eq. (B.3) to obtain

$$\chi_L(q,\omega) = \sum_{l=-\infty}^{\infty} P \int_{-\infty}^{\infty} \frac{dk_z}{2\pi} f_0(\epsilon_{k,l}) \left(\frac{1}{G - \hbar\omega} + \frac{1}{G + \hbar\omega} \right) , \tag{B.4}$$

where $G = \epsilon_{k_z+q_z,l+L} - \epsilon_{k_z,l}$. The integration can be performed analytically at $T = 0$ K, when the Fermi-Dirac distribution function is a step function, i.e, $f_0(\epsilon_{k_z,l}) = \theta(E_F - \epsilon_{k,l})$. The result for the real part is

$$\Re e\, \chi_L(q_z,\omega) = \frac{m^*}{\pi\hbar^2 q_z} \sum_{l=-S}^{S} \ln \left| \frac{\hbar^2\omega^2 - E_+^2(l,L,q_z,k_{Fl})}{\hbar^2\omega^2 - E_-^2(l,L,q_z,k_{Fl})} \right| , \tag{B.5}$$

where S is the number of occupied subbands ($|l| \leq k_F R$), $k_{F,l} = \sqrt{k_F^2 - (l/R)^2}$ is the magnitude of the wave vector of the lth subband, and $E_\pm(l,L,q_z,k_{F,l})$ is given by

$$E_\pm(l,L,q_z,k_{F,l}) = \frac{\hbar^2}{2m^*}(q^2 + 2q_z k_{F,l}) + \frac{\hbar^2}{2m^* R^2}(L^2 + 2Ll) . \tag{B.6}$$

For the imaginary part we obtain

$$\Im m\, \chi_L(q,\omega) = \sum_{l=-\infty}^{\infty} \int_{-\infty}^{\infty} dk_z \left[f_0(\epsilon_{k_z,l}) - f_0(\epsilon_{k_z+q_z,l+L}) \right] \delta(\epsilon_{k_z+q_z,l+L} - \epsilon_{k_z,l} - \hbar\omega) , \tag{B.7}$$

which at $T = 0$ K gives

$$\begin{aligned} \Im m\, \chi_L(q,\omega) = & \sum_{l=-\infty}^{\infty} \int_{-\infty}^{\infty} dk_z \left[\theta(E_F - \epsilon_{k_z,l}) - \theta(E_F - \epsilon_{k_z+q_z,l+L}) \right] \\ & \times \delta(\epsilon_{k_z+q_z,l+L} - \epsilon_{k_z,l} - \hbar\omega) . \end{aligned} \tag{B.8}$$

We note that we have a non-zero result only in two cases

(i) $E_F < \epsilon_{k_z,l}$ and $\epsilon_{k_z+q_z,l+L} < E_F$ which combined give: $\epsilon_{k_z+q_z,l+L} - \epsilon_{k_z,l} < 0$ and from the delta function we see that $\omega < 0$,

(ii) $E_F > \epsilon_{k,l}$ and $\epsilon_{k_z+q_z,l+L} > E_F$ which combined give: $\epsilon_{k_z+q_z,l+L} - \epsilon_{k_z,l} > 0$ and from the delta function we see that $\omega > 0$.

The result of the integration is

$$\Im m\,\chi_L(q_z,\omega) = \sum_{l=-S}^{S} \begin{cases} \frac{m^*}{\hbar^2 q_z}\ , & \text{if } |E_-(l,L,q_z,k_{Fl})| < \hbar\omega < |E_+(l,L,q_z,k_{Fl})| \\ -\frac{m^*}{\hbar^2 q_z}\ , & \text{if } |E_+(l,L,q_z,k_{Fl})| < \hbar\omega < |E_-(l,L,q_z,k_{Fl})| \\ 0, & \text{otherwise} \end{cases} . \tag{B.9}$$

We can prove using the definition of the polarization function Eq. (B.1), or equivalently Eqs. (B.5) and (B.9) the following useful symmetry properties

$$\begin{aligned} \chi_L(q_z,\omega) &= \chi_{-L}(q_z,\omega) \\ \Re e\,\chi_L(q_z,\omega) &= \Re e\,\chi_L(-q_z,\omega) \\ -\Im m\,\chi_L(q_z,\omega) &= \Im m\,\chi_L(q_z,-\omega)\ . \end{aligned} \tag{B.10}$$

Appendix C

The polarization function in the long wavelength limit

We replace $k_z \to -k_z - q_z$, $l \to -l - L$ in the second term of Eq. (B.1) and we obtain

$$\chi_L(q_z,\omega) = 4 \lim_{\alpha\to 0^+} \sum_{l=-\infty}^{\infty} \int_{-\infty}^{\infty} \frac{dk_z}{2\pi} f_0(\epsilon_{k_z,l}) \frac{\epsilon_{k_z+q_z,l+L} - \epsilon_{k_z,l}}{\left(\epsilon_{k_z+q_z,l+L} - \epsilon_{k_z,l}\right)^2 - (\hbar\omega + i\hbar\alpha)^2} \ . \tag{C.1}$$

We look at the case that $L = 0$, then $\epsilon_{k_z+q_z,l+L} - \epsilon_{k,l} = \frac{\hbar^2}{2m^*}(q_z^2 + 2k_z q_z) \to 0$ for $q \to 0$. In this case we can expand the fraction in Eq.(C.1) in Taylor series using:

$$g(x) = \frac{x}{x^2 - a^2} = -\frac{x}{a^2} - \frac{x^3}{a^4} - \frac{x^5}{a^6} - \ldots, \quad x < 1 \tag{C.2}$$

and we obtain

$$\begin{aligned} &\chi_{L=0}(q_z,\omega) \\ &= -4 \lim_{\alpha\to 0^+} \sum_{l=-\infty}^{\infty} \int_{-\infty}^{\infty} \frac{dk_z}{2\pi} f_0(\epsilon_{k_z,l}) \left[\frac{\epsilon_{k_z+q_z,l} - \epsilon_{k_z,l}}{(\hbar\omega + i\hbar\alpha)^2} + \frac{(\epsilon_{k_z+q_z,l} - \epsilon_{k_z,l})^3}{(\hbar\omega + i\hbar\alpha)^4} + \ldots \right] , \end{aligned} \tag{C.3}$$

where $f_0(\epsilon_{k_z,l}) = \theta(E_F - \epsilon_{k_z,l})$ at $T = 0$ K. Keeping only the lowest order term in $\epsilon_{k_z+q_z,l} - \epsilon_{k_z,l}$ in the last expansion we find

$$\chi_{L=0}(q_z,\omega) \simeq -\frac{n q_z^2}{m^* \omega^2} \ , \tag{C.4}$$

where $n = N/L_z$ is the linear density of the electrons on the nanotube. This result is a good approximation for the polarization function in the case that $\epsilon_{k_z+q_z,l} - \epsilon_{k_z,l} \ll \hbar\omega$, i.e, if $\hbar^2(q_z^2 + 2k_z q_z)/2m^* \ll \hbar\omega$ for any k_z. Since $|k_z| < k_{F,l}$ we find that the result given by Eq.(C.4) holds if $\hbar\omega \gg E_{\pm}(q_z, k_F)$.

Appendix D

Induced potential and energy loss for a particle moving inside a single-wall nanotube

In this appendix, we quote the results for the induced potential and the rate of loss of energy for a charged particle Q moving with velocity v at distance $\rho_0 < R$ from the axis of the cylinder. For $\rho < R$ we have

$$\Phi^{<}_{\rm ind}(\mathbf{r},t) = -\frac{Q}{\pi\varepsilon_1}\sum_{L=-\infty}^{\infty} e^{iL(\phi-\phi_o)}\int_{-\infty}^{\infty} dq_z e^{iq_z(z-vt)} I_L(q_z\rho) I_L(q_z\rho_0) K_L(q_z R) \times \left[\frac{1}{I_L(q_z R)}\frac{\alpha_L(q_z,\omega)}{1+\alpha_L(q_z,\omega)} + q_z R(\varepsilon_1-\varepsilon_2)\frac{K'_L(q_z R)}{D_L(q_z,\omega)}\right]_{\omega=q_z v}, \quad \text{(D.1)}$$

while for $\rho > R$ we have

$$\Phi^{>}_{\rm ind}(\mathbf{r},t) = \frac{Q}{\pi}\sum_{L=-\infty}^{\infty} e^{iL(\phi-\phi_0)}\int_{-\infty}^{\infty} dq_z e^{iq_z(z-vt)}\frac{K_L(q_z\rho) I_L(q_z\rho_0)}{D_L(q_z,\omega=q_z v)}\,. \quad \text{(D.2)}$$

where $D_L(q_z,\omega)$ is defined in Eq.(3.19).

The rate of loss of energy for the charged particle is

$$\frac{dW}{dt} = \frac{Q^2}{\pi} v \sum_{L=-\infty}^{+\infty}\int_{-\infty}^{+\infty} dq_z q_z I_L^2(q_z\rho_0)\frac{K_L(q_z R)}{I_L(q_z R)} \times \frac{1}{\varepsilon_1 + q_z R(\varepsilon_1-\varepsilon_2) I_L(q_z R) K'_L(q_z R)}\,\Im m\left[\frac{1}{\varepsilon_L(q_z,\omega=q_z v)}\right]. \quad \text{(D.3)}$$

Bibliography

[1] S. Iijima, Nature **354**, 56 (1991).

[2] R. Saito, G. Dresselhaus, and M.S. Dresselhaus, *Physical Properties of Carbon Nanotubes*, (Imperial College Press, 1998).

[3] L.D. Landau, Sov. Phys. JETP **3**, 920 (1957).

[4] D. Bohm and D. Pines, Phys. Rev. **92**, 609 (1953).

[5] P. Martin and J. Schwinger, Phys. Rev. **115**, 1342 (1959).

[6] G. Rickayzen, *Green's Functions and Condensed Matter*, (Academic Press, London, 1980).

[7] L. P. Kadanoff and G. Baym, *Quantum Statistical Mechanics*, (W. A. Benjamin, New York, 1963).

[8] H. Bruus and K. Flensberg, *Many-body Quantum Theory in Condensed Matter Physics*, (Oxford University Press, New York, 2004).

[9] M. F. Lin and Kenneth W.-K. Shung, Phys. Rev. B **47**, 6617 (1993).

[10] G. Gumbs and G. R. Aizin, Phys. Rev. B **65**, 195407 (2002).

[11] W. Que, J. Phys.: Condens. Matter **14**, 5239 (2002).

[12] P. Longe and S.M. Bose, Phys. Rev. B **48**, 18239 (1993).

[13] Osamu Sato, Yukio Tanaka, Michisuke Kobayashi, and Akira Hasegawa, Phys. Rev. B **48**, 1947 (1993).

[14] P.S. Davids, L. Wang, A. Saxena, and A.R. Bishop, Phys. Rev. B **49**, 5682 (1994).

[15] P.J. Lin-Chung and A.K. Rajagopal, Phys. Rev. B **49**, 8454 (1994).

[16] C. Yannouleas, E.N. Bogacheck, and U. Landman, Phys. Rev. B **50**, 7977 (1994).

[17] P.S. Davids, L. Wang, A. Saxena, and A.R. Bishop, Phys. Rev. B **51**, 4557 (1995).

[18] M.F. Lin, D.S. Chuu, C.S. Huang, Y.K. Lin, K.W.K. Shung, Phys. Rev. B **53**, 15493 (1996).

[19] See, for example, G.F. Bertsch and R.A. Broglia, *Oscillations in Finite Quantum Systems*, (Cambridge University Press, New York, 1994).

[20] R.A. Broglia, F. Alasia, P. Arcagni, G. Coló, F. Ghielmetti, C. Milani, H.E. Roman, Z. Phys. D**40**, 240 (1997).

[21] K. Yabana and G.F. Bertsch, Z. Phys. D**42**, 219 (1997).

[22] M. Bianchetti, P.F. Buonsante, F. Ginelli, H.E. Roman, R.A. Broglia, and F. Alasia, Physics Reports **357**, 459 (2002).

[23] B. N. J. Persson, Solid State Commun. **52**, 811 (1984).

[24] N. R. Arista, Phys. Rev. A **64**, 032901 (2001).

[25] J.D. Jackson, *Classical Electrodynamics*, Third Edition, John Wiley & Sons Inc., New York (1998).

[26] F. Stern, Phys. Rev. Lett. **18**, 546 (1967).

[27] Q. P. Li and S. Das Sarma, Phys. Rev. B **43**, 11 768 (1991).

[28] A.Erdélyi, *Tables of Integral Transforms*, Vol.II (McGraw-Hill, New York, 1954) p. 54, # 41.

[29] R. H. Ritchie, Phys. Rev. **106**, 874 (1957).

[30] F. J. Garcia de Abajo and A. Howie, Phys. Rev. B **65**, 115418 (2002).

[31] G. Gumbs and N. J. M. Horing, Phys. Rev. B **43**, 2119 (1991).

[32] J. B. Pendry and L. M. Moreno, Phys. Rev. B **50** 5062 (1994); J. M. Pitarke, J. B. Pendry, and P. M. Echenique, *ibid.* **55**, 9550 (1997).

[33] P. M. Echenique and J. B. Pendry, J. Phys. C **8**, 2936 (1975).

[34] N. Zabala, E. Ogando, A. Rivacoba, and F. J. Garcia de Abajo, Phys. Rev. B **64**, 205410 (2001).

[35] A. Garcia-Lekue and J. M. Pitarke, Phys. Rev. B **64**, 035423 (2001).

[36] K. L. Aminov and J. B. Pedersen, Phys. Rev. B **63**, 125412 (2001).

[37] T. L. Ferrel, P.M. Echenique, and R.H. Ritchie, Solid State Commun. **32**, 419 (1979).

[38] N. J. M. Horing, H. C. Tso, and G. Gumbs, Phys. Rev. B **36**, 1588 (1987).

[39] G. F. Bertsch, H. Esbensen, and B. W. Reed, Phys. Rev. B **58**, 14031 (1998).

[40] J. L. Gervasoni and N. R. Arista, Phys. Rev. B **68**, 235302 (2003).

[41] Y. N. Wang and Z. L. Miskovic, Phys. Rev. A **66**, 042904 (2002).

[42] O. Stephan, D. Taverna, M. Kociak, K. Suenaga, L. Henrard, and C. Colliex, Phys. Rev. B **66**, 155422 (2002).

[43] J. M. Pitarke and F. J. Garcia-Vidal, Phys. Rev. B **63**, 073404 (2001).

[44] A. Rivacoba and F. J. Garcia de Abajo, Phys. Rev. B **67**, 085414 (2003).

[45] N. R. Arista and M. A. Fuentes, Phys. Rev. B **63**, 165401 (2001).

[46] A.B. Mikhailovskii, *Theory of Plasma Instabilities* (Consultants Bureau, New York, 1974).

[47] K. Kempa, Appl. Phys. Lett. **50**, 1185 (1987).

[48] P. Bakshi, J. Cen, and K. Kempa, J. Appl. Phys. **64**, 2243 (1988).

[49] J. Cen, K. Kempa, and P. Bakshi, Phys. Rev. B **38**, 10051 (1988).

[50] K. Kempa, P. Bakshi, J. Cen, and H. Xie, Phys. Rev. B **43**, 9273 (1991).

[51] V.I. Talyanskii, J. Phys.: Condens. Matter **48**, 10533 (1996).

[52] A.S. Bhatti, D. Richards, H.P. Hughes, and D.A. Ritchie, Phys. Rev. B **53**, 11016 (1996).

[53] M.V. Krasheninnikov and A.V. Chaplik, Zh. ksp. Teor. Fiz. **79**, 555 (1980) [Sov. Phys. JETP **52**, 279 (1980)].

[54] G.R. Aĭzin, N.J.M. Horing, and L.G. Mourokh, Phys. Rev. B **65**, 241311 (2002).

[55] M.I. Dyakonov and M.S. Shur, Phys. Rev. Lett. **71**, 2465 (1993).

[56] S.A. Mikhailov, Phys. Rev. B **58**, 1517 (1998).

[57] P. Bakshi and K. Kempa, Condensed Matter Theories **12**, 399 (1997).

[58] Brian E. Granger, Petr Král, H. R. Sadeghpour, and Moshe Shapiro, Phys. Rev. Lett. **89**, 135506 (2002).

[59] Dvira Segal et al., J. Chem. Phys. **122**, 134705 (2005).

[60] Trygve Ristroph, Anne Goodsell, J. A. Golovchenko, and Lene Vestergaard Hau, Phys. Rev. Lett. **94**, 066102 (2005).

[61] Dvira Segal, Brian E. Granger, H. R. Sadeghpour, Petr Krl and Moshe Shapiro, Phys. Rev. Lett. **94**, 016402 (2005).

[62] L. Tian and P. Zoller, Phys. Rev. Lett. **93**, 266403 (2004).

[63] Patrick Rinke, Kris Delaney, P. Garca-González, and R. W. Godby, Phys. Rev. A **70**, 063201 (2004).

[64] D. J. Mowbray, L. Mikovi, F. O. Goodman, and You-Nian Wang, Phys. Rev. B **70**, 195418 (2004).

[65] M. Zamkov, H. S. Chakraborty, A. Habib, N. Woody, U. Thumm, and P. Richard, Phys. Rev. Lett. **93**, 156803 (2004).

[66] Da-Peng Zhou, You-Nian Wang, Li Wei, and Z.L. Miskovic, Phys. Rev. A **72**, 023202 (2005).

[67] M. Zamkov, H.S. Chakraborty, A. Habib, N. Woody, U. Thumm, and P. Richard, Phys. Rev. B **70**, 115419 (2004).

[68] Dvira Segal, Petr Král, and Moshe Shapiro, Phys. Rev. B **69**, 153405 (2004).

[69] L. Lou, P. Nordlander, and R. E. Smalley, Phys. Rev. B **52**, 1429 (1995).

[70] U. Höfer, I. L. Shumay, Ch. Reuß, U. Thomann, W. Wallauer, and Th. Fauster, Science **277**, 1480 (1997).

[71] P. M. Echenique and J. B. Pendry, Prog. Surf. Sci. **32**, 111 (1989).

[72] L. Wendler and V. G. Grigoryan, Phys. Status Solidi B **181**, 133 (1994).

[73] L. Wendler and V. G. Grigoryan, Phys. Rev. B **49**, 14531 (1994).

[74] D. C. Tsui, E. Gornik and R. A. Logan, Solid State Commun. **35**, 875 (1080).

[75] E. Gornik, R. Christanell, R. Lassnig, W. Beinstingl and K. BertholdG. Weimann, Solid State Electron. **31**, 751 (1988).

[76] C. Wirner, C. Kiener, W. Boxleitner, M. Witzany, E. Gornik, P. Vogl, G. Bhm, and G. Weimann, Phys. Rev. Lett. **70**, 2609 (1993).

[77] B. Ferguson and X.-C. Zhang, Nat. Mater **1**, 26 (2002).

[78] D. Dragoman and M. Dragoman, Prog. Quantum Electron. **28**, 1 (2004).

[79] G. Gumbs, A. Balassis and C.-Y. Shew, Europhys. Lett., **64** (2), pp. 225-231 (2003).